Doctoral theses at NTNU, 2023:120

Yu Ding

Atomic Insights into Hydrogen-Grain Boundary Interactions

Doctoral thesis

NTNU
Norwegian University of Science and Technology
Thesis for the Degree of
Philosophiae Doctor
Faculty of Engineering
Department of Structural Engineering

NTNU
Norwegian University of
Science and Technology

Yu Ding

Atomic Insights into Hydrogen-Grain Boundary Interactions

Thesis for the Degree of Philosophiae Doctor

Trondheim, April 2023

Norwegian University of Science and Technology
Faculty of Engineering
Department of Structural Engineering

NTNU
Norwegian University of
Science and Technology

NTNU
Norwegian University of Science and Technology

Thesis for the Degree of Philosophiae Doctor

Faculty of Engineering
Department of Structural Engineering

ISBN 978-82-326-5886-2 (printed ver.)
ISBN 978-82-326-5314-0 (electronic ver.)
ISSN 1503-8181 (printed ver.)
ISSN 2703-8084 (online ver.)

IMT-report 2023:120

Doctoral theses at NTNU, 2023:120

Printed by NTNU Grafisk senter

There is only one heroism in the world: to see the world as it is, and to love it.

Preface

This thesis is submitted to the Norwegian University of Science and Technology (NTNU) for partial fulfilment of the requirements for the degree of philosophiae doctor.

The thesis comprises an introductory section, and 4 journal papers (two published and two submitted).

This doctoral work has been conducted in the period between August 2019 and January 2023 under the supervision of Professor Zhiliang Zhang, Professor Jianying He and Professor Haiyang Yu. The main simulation work was carried out at NTNU Nanomechanical Lab, Department of Structural Engineering (KT), Faculty of Engineering (IV), Norwegian University of Science and Technology (NTNU), Trondheim, Norway.

The thesis was financially supported by the Research Council of Norway and three industrial partners, Aker Solutions, Equinor and voestalpine High Performance Metals Norway via the M-HEAT project (Multiscale Hydrogen Embrittlement Assessment for Subsea Conditions), Grant No. 294689. All the simulations were carried out on the Fram and Betzy high-performance computer clusters under Grant No. NN9110K, No. NN9391K.

Abstract

Derived from the most abundant element in the universe, hydrogen is the smallest element and, at the same time, a clean, mobile, and efficient energy carrier. Nowadays, hydrogen is regarded as the fuel of future and could help the world transform into a zero-emissions scenario. However, the popularity of hydrogen-based energy economy has also put the problems associated with hydrogen storage and transport to the forefront. Hydrogen embrittlement (HE), the phenomenon where dissolved hydrogen in metals causes dramatic degradation of mechanical properties leading to sudden and catastrophic failure, was first observed in 1875. However, even after one-century research, the fundamental mechanisms of HE are still in the dark forest mainly due to the lacking of effective methodology for tracking hydrogen experimentally. In this thesis, the HE phenomenon is studied in a substituted way, by using atomistic simulations, to get a comprehensive understanding of the nanoscale mechanism.

Essentially, HE is all things about the interactions between hydrogen atoms and multiple types of microstructures in material, including vacancies, dislocations, grain boundaries (GBs) and crack tips. Of them, GB is the interface separating differently oriented crystallites and plays a central role in deformation and fracture mechanisms. In polycrystalline materials, the HE is often accompanied by a transition from transgranular to intergranular fracture. However, the nanoscale interactions between hydrogen and GB largely remain illusive. And there is a large knowledge gap in the connection between the microscale hydrogen-GB interactions and macroscale observed fracture transition. Starting from this, uniaxial straining is applied to bi-crystalline Ni with a $\Sigma5(210)[001]$ GB and a transgranular to intergranular fracture transition facilitated by hydrogen is directly elucidated by atomistic modeling. Hydrogen is found to form a local atmosphere in the vicinity of GB, which induces a local stress concentration and inhibits the subsequent stress relaxation at the GB during deformation. It is this local stress concentration that promotes earlier dislocation emission and generation of additional vacancies that ultimately facilitate nanovoiding. The nucleation and growth of nanovoids finally lead to intergranular fracture at the GB, in contrast to the transgranular fracture of hydrogen-free sample. This hydrogen-controlled plasticity mechanism provides a rationale for macroscale fracture transition.

To further validate the universality of this mechanism under various conditions and quantify the hydrogen-induced fracture transition process, uniaxial straining is applied to Ni Σ5(210)[001] and Σ9(1-10)[22-1] GBs with various hydrogen concentrations and temperatures based on a large statistical repetition. Without hydrogen, vacancy generation at GB is limited and transgranular fracture mode dominates. When charged, hydrogen as a booster can enhance strain-induced vacancy generation by up to ten times. This leads to the superabundant vacancy stockpiling at the GB, which agglomerates and nucleates intergranular nanovoids. While hydrogen tends to persistently enhance vacancy concentration, temperature plays an intriguing dual role as either an enhancer or an inhibitor for vacancy stockpiling. These results show a good agreement with positron annihilation spectroscopy experiments. Importantly, an S-shaped quantitative correlation between the proportion of intergranular fracture and vacancy concentration was for the first time derived, highlighting the existence of a critical vacancy concentration, beyond which fracture mode will be completely intergranular.

Besides GB fracture, hydrogen could also influence the migration behavior of GBs. The effect of solute hydrogen on shear-coupled GB migration is investigated with the dislocation-array type Σ25(430)[001] GB and a dual role of hydrogen on GB mobility is unraveled. In the low temperature and high loading rate regime, where hydrogen diffusion is substantially slower than GB motion, GB breaks away from the hydrogen atmosphere and transforms into a new stable phase with highly enhanced mobility. In the reverse regime, hydrogen atoms move along with GB, exerting a drag force on GB and decreasing its mobility. This helps to understand the coexistence of hydrogen hardening and softening in experiments.

Finally, we make an attempt to extend the results in bicrystal to polycrystal model. The trapping and diffusion of hydrogen in polycrystal was analyzed by elucidating the hydrogen-GB segregation spectrum. The spectrum shows three peaks corresponding to GB core sites and hybrid GB surface-octahedron/ tetrahedron sites, respectively. The low migration energy inside GB core and high energy barrier between different types of sites indicate the coexistence of short-circuit diffusion and GB trapping. Various stress conditions are further applied to investigate their influence on the spectrum, where hydrostatic stress shows the predominating role in hydrogen trapping behavior.

Acknowledgments

Three years ago, I came to Norway and started my PhD journey. All the way here, I really appreciate all the living beings I met and all the cheerful and painful moments I experienced. It's you that made parts of my life.

First and foremost, I want to give my most sincere gratitude to my supervisor Prof. Zhiliang Zhang for giving me the opportunity to start my PhD study, for guiding me through a thorny road to be an independent researcher, for the freedom you gave me. The greatest 'one piece' I learned from you is your great passion and dedication toward your career. I still remember the frequent mail contacts for manuscript modification at midnight, you won't turn a blind eye to any small mistakes or disharmony. It makes me in awe and builds the model for me. You are the mentor for work as well as for life. I was blessed to be with you on the PhD journey.

I also would like to express my heartfelt gratitude to my co-supervisor Prof. Jianying He, not only for her thoughtful supervision but also for her kind support and assistance in daily life. My thanks are extended to Prof. Haiyang Yu for the fruitful discussion and detailed suggestions.

Besides the advisors, I wish to acknowledge the help in both research and life from Prof. Senbo Xiao. Special thanks go to my colleague Dr. Meichao Lin for her constant encouragement. Thanks are also given to Prof. Kai Zhao, Prof. Michael Ortiz and Prof. Alexey Vinogradov for their valuable comments on the manuscript.

Great thanks are also given to all the colleagues at NTNU especially at the Department of Structural Engineering: Prof. Kjell Magne Mathisen, Prof. Helge Kristiansen, Prof. Senbo Xiao, Prof. Xu Lu, Yang Li, Tong Li, Junchao Pan, Tianle Zhou, Zexin Chang, Susanne Sandell, Merete Falck, Øyvind Othar Aunet Persvik, Verner Håkonsen, Sigrid Rønneberg, Ingrid Snustad, Yizhi Zhuo, Feng Wang, Sandra Sæther, Li Sun, Yuequn Fu, Siqi Liu, Tengjiao Jiang, Mingjie Zhang, Thorstein Wang, Xu Wang, Meichao Lin, Yuanhao Chang, Rui Ma, Jing He, Paul Rübsamen-von Döhren, Håvard Mo Fagersand, Chandrahaasan Soundararajan, Xinshu Zou, Yifan Zhang, Yuyu Liu, Jinhuan Hu, Mengnan Yu, Martha Seim Gunstad and Erling Velten Rothmund.

Particularly, I would like to thank my dear friends Jing He, Wei Pan, Lan Zhang and Lu Yan and my cute roommates Wenyu Zhou, Sida Yu, Viktor Fiskum and Cristian Baeza. Your existence made my life in Norway full of color.

Last but not least, I would like to express my gratitude to my parents for their unconditional understanding, support and love all those years.

List of Papers

The thesis is organized based on the following papers, which have all been published or under submission by the candidate:

1. **Yu Ding**, Haiyang Yu, Kai Zhao, Meichao Lin, Senbo Xiao, Michael Ortiz, Jianying He, and Zhiliang Zhang. "Hydrogen-induced transgranular to intergranular fracture transition in bi-crystalline nickel." *Scripta Materialia 204 (2021): 114122.*
2. **Yu Ding**, Haiyang Yu, Meichao Lin, Kai Zhao, Senbo Xiao, Alexey Vinogradov, Lijie Qiao, Michael Ortiz, Jianying He, and Zhiliang Zhang. "Hydrogen-enhanced grain boundary vacancy stockpiling causes transgranular to intergranular fracture transition." *Acta Materialia 239 (2022): 118279.*
3. **Yu Ding**, Kai Zhao, Meichao Lin, Haiyang Yu, Senbo Xiao, Jianying He, and Zhiliang Zhang. " The dual role of hydrogen in grain boundary mobility." *Journal of Applied Physics, 133(4), 045103.*
4. **Yu Ding**, Kai Zhao, Meichao Lin, Haiyang Yu, Senbo Xiao, Jianying He, and Zhiliang Zhang. " Hydrogen trapping and diffusion in polycrystalline nickel: the spectrum of grain boundary segregation." *To be submitted*

Besides the publication presented above, I have contributed to the following works related to hydrogen embrittlement:

1. Meichao Lin, Haiyang Yu, Xu Wang, Ruijun Wang, **Yu Ding**, Antonio Alvaro, Vigdis Olden, Jianying He, and Zhiliang Zhang. "A microstructure informed and mixed-mode cohesive zone approach to simulating hydrogen embrittlement." *International journal of hydrogen energy 47, no. 39 (2022): 17479-17493.*
2. Meichao Lin, Haiyang Yu, **Yu Ding**, Vigdis Olden, Antonio Alvaro, Jianying He, and Zhiliang Zhang. "Simulation of ductile-to-brittle transition combining complete Gurson model and CZM with application to hydrogen embrittlement." *Engineering Fracture Mechanics 268 (2022): 108511.*

3. Meichao Lin, Haiyang Yu, **Yu Ding**, Gang Wang, Vigdis Olden, Antonio Alvaro, Jianying He, and Zhiliang Zhang. "A predictive model unifying hydrogen enhanced plasticity and decohesion." *Scripta Materialia 215 (2022): 114707.*

The PhD candidate has also held oral presentations and poster presentations in the following international conferences/seminars:

1. **Yu Ding**, Jianying He and Zhiliang Zhang. “Atomic insights into hydrogen-induced transgranular to intergranular fracture transition”. NSCM-33 2021, Sweden. *Oral presentation*
2. **Yu Ding**, Haiyang Yu, Jianying He and Zhiliang Zhang. “Hydrogen-induced transgranular to intergranular fracture transition in bi-crystalline nickel”. ECCOMAS-8 2022, Norway. *Oral presentation*
3. **Yu Ding**, Meichao Lin, Haiyang Yu, Jianying He and Zhiliang Zhang. “Hydrogen-induced transgranular to intergranular fracture transition in bi-crystalline nickel”. ECF-23 2022, Portugal. *Oral presentation*
4. **Yu Ding**, Jianying He and Zhiliang Zhang. “Hydrogen-induced transgranular to intergranular fracture transition in bi-crystalline nickel”. ICMH-4 2022, Belgium. *Poster*

Contents

Chapter 1 Introduction

1.1 Background and Motivation

Renewable and low-carbon fuel is crucial for meeting the Paris Agreement goals to decarbonize the hard-to-abate sectors. Hydrogen as a flexible and efficient energy carrier with zero greenhouse gas emissions can be a perfect alternative to fossil fuels. According to DNV's forecast [1], hydrogen would need to meet around 15% of world energy demand by the mid-century. It means the usage of hydrogen energy will increase a hundredfold (**Figure 1.1**) and global spending on producing hydrogen for energy purposes till then will approach USD 6.8 trillion. The hydrogen economy as a sunrise industry will help the world transform into an environment-friendly community, as well as create more new jobs. However, developing a complete hydrogen economy is still facing many technical challenges during production, transportation, storage, and utilization. Of them, the most urgent task is the verification of the safety of large-scale hydrogen transportation systems [2], and the key to solving it lies in our understanding of the hydrogen embrittlement phenomenon.

Hydrogen embrittlement (HE) refers to the phenomenon where dissolved hydrogen in metals causes dramatic degradation of mechanical properties, including strength, ductility, and fracture toughness. It usually results in a premature and catastrophic failure, which is far below the yield stress and uneasy to predict. Due to its widespread presence, HE also brings a great challenge to a large number of industries, e.g., oil and gas companies. Since

first observed in 1875 [3], continued efforts from both industry and academia have been dedicated to studying this topic [4]. As shown in **Figure 1.2**, HE has attracted surging attention in the recent ten years due to the perspective of hydrogen economy. Despite this long history of study on HE, there is still a lot of blurry space as to the mechanism by which hydrogen degrades the mechanical response. Contributing to this situation is a lack of detailed information at the microstructural and atomistic scales. Even worse, hydrogen is notoriously tricky to detect by certain experimental techniques [5] and no direct observation of hydrogen atoms has been reported till now.

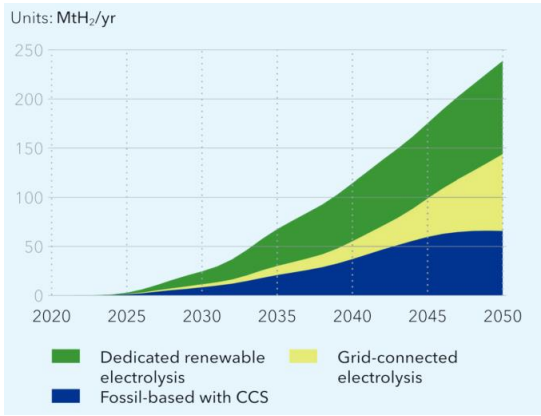

Figure 1.1. Global production of hydrogen and its derivatives for energy purposes by production route. The unit is million tonnes per year, CCS means carbon capture and storage, reprinted from Ref. [1].

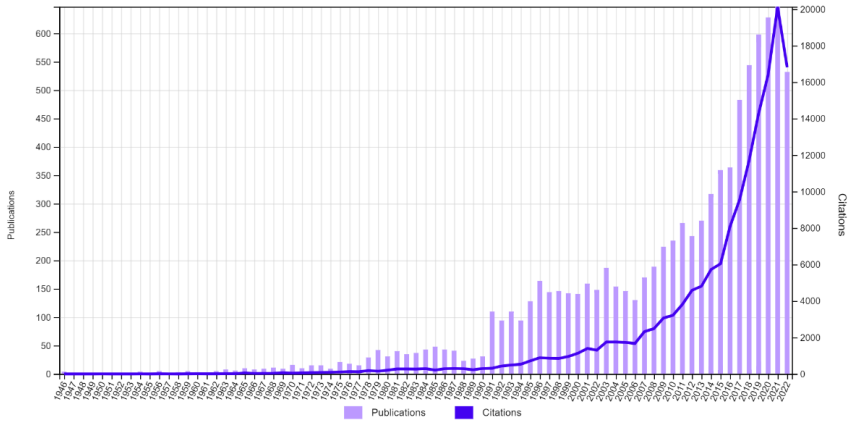

Figure 1.2. Publications and citations associated with 'Hydrogen embrittlement' from 1946 to now. The data is collected by Web of Science.

Conventionally, there are two strategies for solutions when HE is a concern. The first one is source control by designing HE-resisted material which has good resistance to HE or suppressing hydrogen uptake with surface coating. The second one is the development of predictive models based on physical mechanisms, facilitating the design and inspection during engineering applications. Over the years, data on the effect of hydrogen on mechanical properties of different metals and their alloys has been generated which makes the selection of relatively suitable materials possible. However, cost considerations will lead to more than 50% of hydrogen pipelines globally being repurposed from natural gas pipelines [1], and existing material may still fail prematurely when exposed to long-term permeation or the uncertainty of the environment. In this scenario, accurate prediction for HE is of immediate concern but failure prediction based on data in hand can be only viable in a narrow region. All the current limitations are due to the lack of a fundamental and universal understanding of the HE mechanisms.

To begin to address this problem, atomistic simulation is a good alternative pathway. Since the 1970s, with the dramatic increase in computer capacity and resources, computational material science has become increasingly important in promoting our understanding of the relationship between material properties and their fundamental structures. Atomistic simulation or molecular dynamics (MD) simulation [6] has been proved to be a powerful tool to capture the mechanical response of materials at the nanoscale. Thus, mainly by using atomistic simulations, we will explore the nanoscale HE mechanism in the thesis.

1.2 Research objectives

This PhD thesis study is part of the M-HEAT project, which aims to develop a model framework that investigates the atomic-scale HE mechanism and links it to mechanism-based hydrogen-induced failure criteria. Specifically, nickel will be the target material system with an emphasis on hydrogen-grain boundary interaction. These main objectives are described as following:

(1) To investigate the nanoscale hydrogen embrittlement mechanism by elucidating the microstructure evolution and effect of hydrogen during deformation in bicrystal.
(2) To examine the distinct roles and interactions of the existing mechanisms during the fracture mode transition and establish a mechanism-based predictive model.
(3) To extend the result from bicrystal to polycrystal.

1.3 Thesis outline

The thesis is composed of an introductory section and a collection of four peer-reviewed journal papers. The introductory section can be decomposed into four chapters. In **Chapter 1**, the background and motivation, and research objectives are stated. In **Chapter 2**, a literature review is presented. In **Chapter 3**, the main scientific results produced in this thesis are summarized. In **Chapter 4**, some perspectives are discussed.

Chapter 2 Literature review

2.1 Introduction

This Chapter will be unfolded in the same order as PhD learning process: In **2.2**, the current understanding in the hydrogen embrittlement community will be elucidated, with emphasis on several significant mechanisms and their representative work. In **2.3**, the current modeling methods for hydrogen embrittlement will be reviewed with a focus on atomistic simulations. In **2.4**, the previous study specific to hydrogen-grain boundary interaction will be introduced as a warm-up for our work.

2.2 Hydrogen embrittlement and its mechanisms

"After a few minutes' immersion (half a minute will sometimes suffice) in strong hydrochloric or dilute sulfuric acid—a piece breaking after being bent once on itself, while before immersion it would bear bending on itself and back again two or three times before breaking." This is the first demonstration of hydrogen-induced degradation in 1875 by Johnson who launched the field of study of hydrogen embrittlement of metals [3]. Since then, people recognized that ductility can be markedly decreased upon the formation of interfacial chemical compounds of which hydrogen can be a by-product [7]. Hydrogen can then diffuse to the component bulk, producing a wealth of interactions at various scales with the microstructure including vacancies, dislocations, grain boundaries, phase boundaries, precipitates, and dislocation cells, which finally facilitate the formation and propagation of cracks [8, 9]. Hydrogen embrittlement has also been a significant

concern for industry associated with oil and gas facilities, aircraft engines, and marine exposed to long-time hydrogen permeation. Especially in light of the hydrogen economy, hydrogen embrittlement has become one of the burning technical concerns towards a complete hydrogen value chain (**Figure 2.1**).

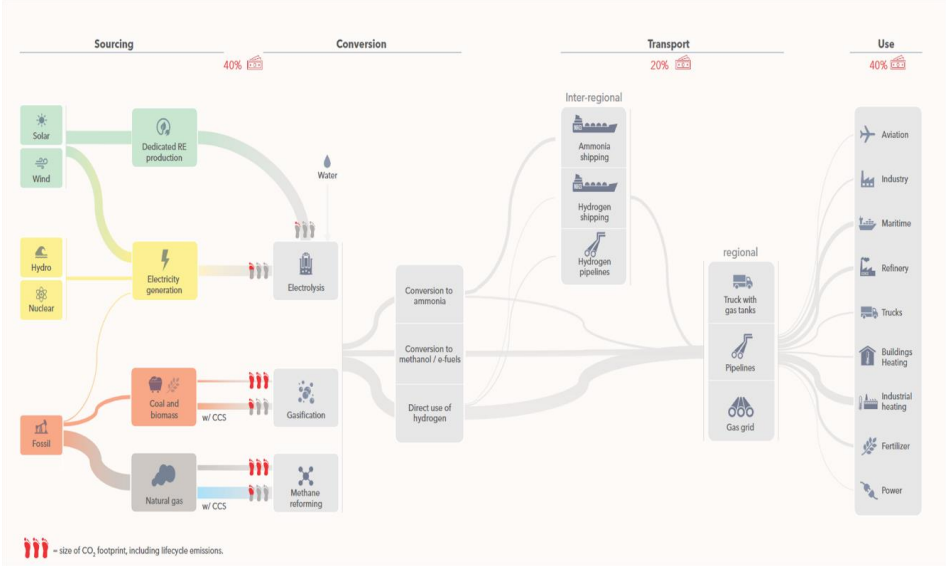

Figure 2.1. Forecasted hydrogen production and use in 2050, the thickness of the flow lines approximates the volume of each flow indicating major production routes and end uses. Reprinted from Ref. [1].

The discovery of the underlying fundamental mechanisms of hydrogen embrittlement is a complex multi-faceted challenge that requires knowledge of hydrogen source, hydrogen surface chemical interaction, hydrogen diffusion and hydrogen trapping, and importantly, how hydrogen modify the mechanical properties causing the observed ductile, "quasi-cleavage," and intergranular fracture modes [9]. With continuous efforts for nearly one and a half centuries [10, 11], several hydrogen embrittlement mechanisms are proposed, with the most commonly invoked being: hydrogen-enhanced decohesion (HEDE), hydrogen-enhanced localized plasticity (HELP), hydrogen-enhanced strain-induced vacancy mechanism (HESIV), adsorption-induced dislocation emission (AIDE), defactants theory, and hydride formation et al. Each of these mechanisms claim support from both theoretical and experimental results, but the multi-faceted nature of hydrogen-induced degradation, as well as the likelihood of mechanism synergy, complicates the

universal application of any one paradigm. However, a consistent theme amongst the proposed mechanisms is the assumption that hydrogen-induced degradation is principally driven by a localized hydrogen-microstructure interaction [12]. The myriad of possible hydrogen-microstructure interactions is illustrated in **Figure 2.2**, where atomic hydrogen (H+) ingress is followed by interactions with dislocations (⊥), promoting transgranular and intergranular cracks, leading to the formation of voids or twins, while interacting with phases such as austenite and precipitates. Of them, particular attention has been paid to hydrogen-induced intergranular fracture [13-16], eg. the hydrogen-GB interaction, which will also be the main results in this thesis.

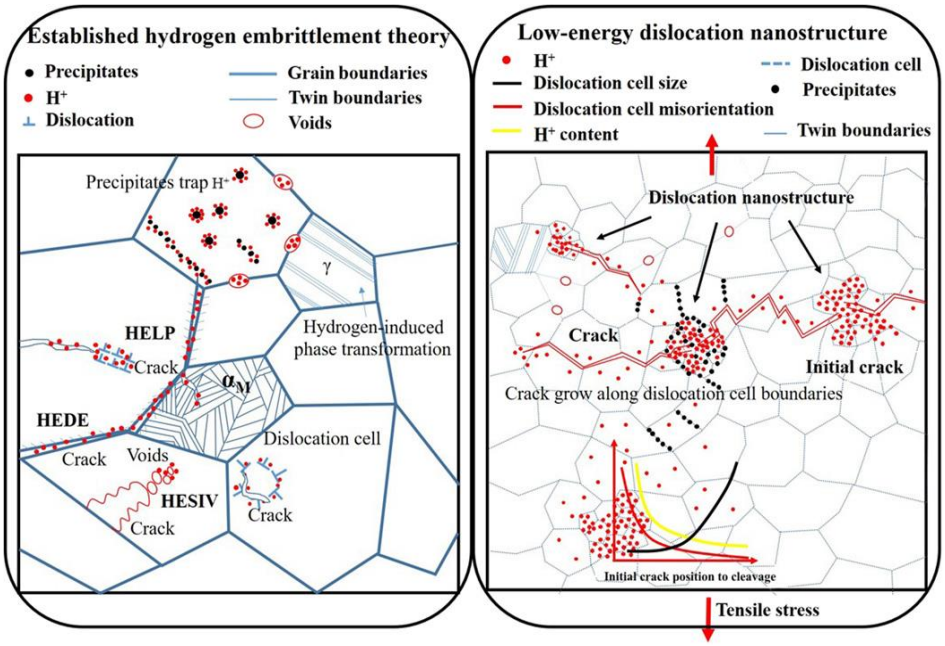

Figure 2.2. Multiscale depiction of HE. (Left) Accepted theories of HELP (hydrogen-enhanced localized plasticity), with strong interaction with dislocations at crack tips; HESIV (hydrogen-enhanced strain-induced vacancy formation), forming clusters of vacancies (voids) at the tips; and HEDE (hydrogen-enhanced decohesion), promoting decohesion. (Right) Hydrogen diffuses to crack tips, where its concentration increases, promoting dislocation cell formation, which, upon reaching a critical level, causes failure. Reprinted from Ref. [12].

2.2.1 Hydrogen-Enhanced Decohesion (HEDE)

The hydrogen-enhanced decohesion (HEDE) mechanism has the closest origin to "embrittlement". The decohesion concept was first proposed in 1926 by Pfeil [17], who proposed that " hydrogen decreased the cohesion across cubic cleavage planes " (and GBs). Troiano [18] suggested that the entry of 1s electron of hydrogen atom into the unfilled d-band of transition metals would elevate the interatomic repulsive force, thus decreasing the lattice cohesion. However, the existence of HE in the aluminum alloys with filled d-band suggests that the transfer of 1s electron is not the only factor to decrease the atomic bonding [19, 20]. Then the HEDE mechanism describing that the atomic bonding is weakened due to the presence of hydrogen atoms in solid solution was quantitatively developed by Oriani [21] and others [22-24], illustrated in **Figure 2.3**.

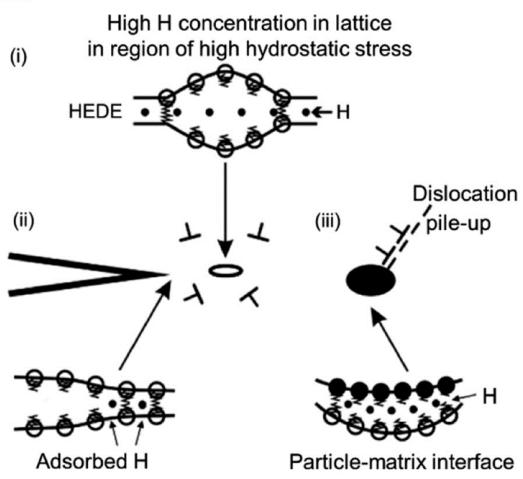

Figure 2.3. Schematic diagrams illustrating the HEDE mechanism involving tensile separation of atoms owing to weakening of interatomic bonds by (i) hydrogen in the lattice or segregated at grain boundaries ahead of crack tips, (ii) hydrogen adsorbed at crack tips, and (iii) hydrogen segregated at particle-matrix interfaces ahead of cracks. Crack growth could involve decohesion at one or more sites, and could occur in conjunction with other mechanisms. Reprinted from Ref. [10].

Decohesion is usually envisaged as a simple, sequential tensile separation of atoms when a critical crack-tip-opening displacement (CTOD) is reached. However, the separation of atoms at crack tips is constrained by surrounding atoms and, hence, the separation process could be more complex and involve incipient shear movement of

atoms to enable a critical CTOD (around half lattice constant) to be achieved. Brittle fracture associated could occur with very high concentrations of hydrogen, commonly at (i) sharp crack tips (ii) several tens of nanometres ahead of cracks where dislocation-shielding effects result in a tensile-stress maximum, (iii) positions of maximum hydrostatic stress and (iv) particle-matrix interfaces ahead of cracks. Decohesion could also happen at GB ahead of a crack given GB works as the preferred trapping site for hydrogen. To be noted, the simulation setups in the attached **Paper1** and **Paper2** mimic hydrogen-GB interaction in the high hydrostatic stress state region tens of nanometres ahead of crack tips.

Direct evidence of HEDE is difficult to obtain because there are no experimental techniques for directly observing hydrogen-crack interaction events on the atomic scale. But from the featureless fracture surface (without void or obvious dislocation trace) observed by scanning electron microscopy (SEM), researchers could still judge that decohesion has occurred [16, 25]. And recently, by using atom probe tomography (APT), Chen et al. [26] and Zhao et al. [20] have observed hydrogen accumulation at dislocations, GBs, and precipitates where the HEDE mechanism could work given the high density of local hydrogen clusters (**Figure 2.4**). Besides, numerous quantum mechanical calculations supported the decohesion concept where hydrogen-induced weakening of interatomic bonds leads to HEDE, especially in the case where common slip systems are not supported for crack propagation [27]. Previous calculations have covered many systems including Fe [28-30], Ni [31-33], and Al [19, 28, 31] and those could be utilized to quantitatively predict the hydrogen-caused fracture energy reduction. However, discrepancies also exist. When the fracture surface is examined at high-resolution SEM or transmission electron microscopy (TEM), the direct observation of nanoscale dimples on the surface [34] and dislocation cells underneath the surface [13] is beyond what HEDE could explain. Tehranchi et al. [35] studied the hydrogen-assisted intergranular fracture of Ni by atomistic simulations and concluded the presence of hydrogen creates no ductile-to-brittle transition for several types of GB cracks. Wang et. al [14] performed first-principle calculations for hydrogen-assisted intergranular fracture in Fe and found that decohesion alone could not account for the cohesive energy reduction and plasticity should play a role.

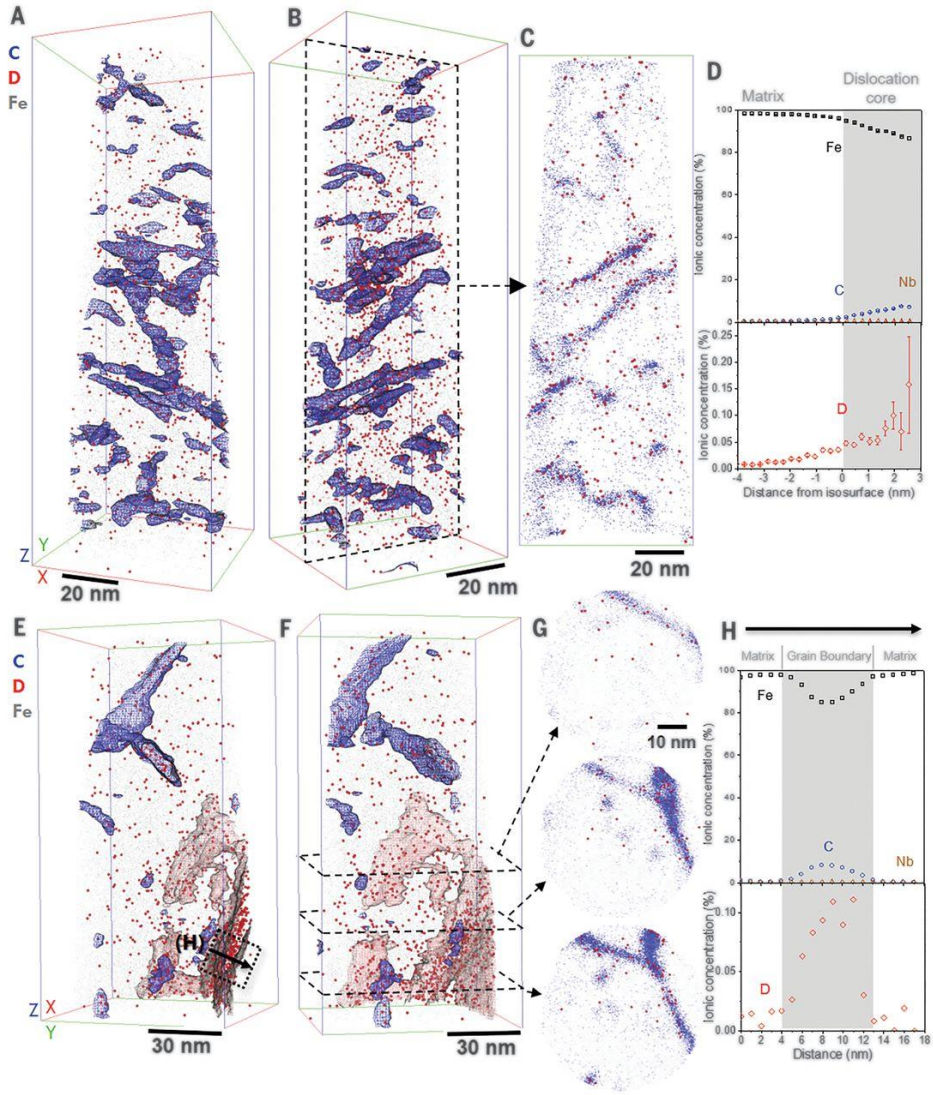

Figure 2.4. APT analyses of deuterium-charged martensitic steel samples containing GBs and dislocations. (A and B) Views at two different angles of a reconstructed atom map showing deuterium (red), iron (gray), and 2% carbon isosurfaces in blue. This sample contains a high density of linear, carbon-decorated dislocations. (C) Slice, 5 nm thick, from the center of the dataset shown in (B) (indicated with the black dashed rectangle) with carbon atoms (blue) and deuterium atoms (red) showing the spatial correlation between the two elements. (D) Collective proxigram analysis of the 70 dislocations and carbon isosurfaces contained in (A), showing that the dislocations have carbon and deuterium at their cores but little niobium. (E and F) Two views of a different dataset from the same sample. Again, features are highlighted by 2%

carbon isosurfaces, with one of these surfaces that encompasses a GB region highlighted by a transparent red isosurface. (G) z Axis, 5-nm-thick slices from the GB region, indicated in (F). (H) 1D composition profile with a 1-nm step size from a volume of 20 nm by 20 nm by 18 nm across the GB marked in (E). Reprinted from Ref. [26].

2.2.2 Hydrogen-Enhanced Localized Plasticity (HELP)

The concept of hydrogen-enhanced localized plasticity was first proposed by Beachem in 1972 [36], partly based on fractographic observations where hydrogen-assisted cracking is assumed to be a result of hydrogen facilitating the movement of dislocations. This idea was subsequently expanded by Birnbaum and coworkers [37-42] into a broad universe. The premise of the mechanism is that hydrogen assists the deformation processes, but only locally where hydrogen is present in sufficient concentrations, leading to fracture which is macroscopically brittle in appearance and behavior.

Hydrogen is strongly bound to dislocation, most likely trapped at the core [43, 44], as well as attracted by the elastic field surrounding the dislocation. Based on the observed hydrogen-related softening in FCC, BCC and HCP systems, including in pure metals, solid solutions and in precipitation hardened systems, Birnbaum and Sofronis proposed an analytical model for the hydrogen shielding effect on elastic stress field. As shown in **Figure. 2.5**, The net shear stress, τ_H, induced by the hydrogen atmospheres is found by the integration of the stress contributions of each of the hydrogen dilatation lines over the entire area S occupied by the atmosphere. In polar coordinates, the shear stress on dislocation 2 due to the hydrogen atmospheres is given by the following equation:

$$\tau_H = -\frac{\mu}{2\pi(1-v)}\frac{V_H}{N_A}\int_0^{2\pi} C(r,\phi)\frac{sin2\phi}{r}drd\phi \tag{2.1}$$

where μ and v are the shear modulus and Poisson's ratio respectively, r and ϕ are the polar coordinates as measured from the dislocation core and slip plane, and C is the local hydrogen concentration per unit volume. **Eq. (2.1)** indicates that the stress field of a hydrogen dilatation line decays as $1/r^2$ with distance r, and is associated with the volumetric strain produced by the introduction of hydrogen into the lattice (volumetric swelling), and the hydrogen-induced changes in the constitutive moduli (modulus effect). It is important to note that this shielding effect of hydrogen will result in several important

changes in dislocation behavior. The mobility of the dislocations is usually increased, with 2–10 fold increases having been recorded, depending upon the material [45, 46], and with the effect being more pronounced in solute-strengthened materials, which will accelerate the subsequent plastic deformation. Additionally, the dislocations will tend to pack closer together in pile-ups [41] and form stacking faults easily [47], but the cross-slip will be suppressed [48].

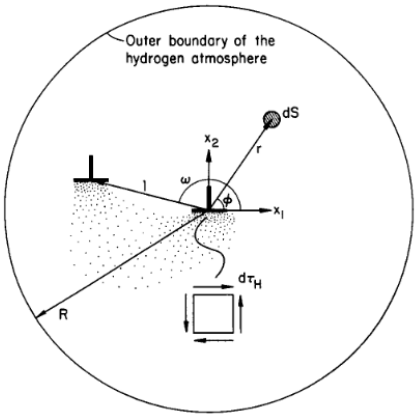

Figure 2.5. Schematic showing the coordinates of the interacting dislocations and the hydrogen atmospheres. The shear stress, $d\tau_H$ is the shear stress due to the hydrogen atmosphere in the area dS located at position (r, ϕ). The extent of the outer radius of the hydrogen atmosphere, R, is determined by convergence of the full elastic solutions. Reprinted from Ref. [37].

Besides the direct hydrogen-dislocation interactions, a bunch of recent work has been focusing on the role of HELP in hydrogen-induced intergranular fracture. One notable example is the mechanical evaluation of near-fracture surface microstructure in hydrogen-charged Fe and Ni using a combinatory transmission electron microscopy (TEM)/focused ion beam (FIB) technique [13, 49-51]. Martin et.al [52] found despite the different hydrogen and mechanical loading configurations, Fe and Ni both failed intergranularly due to the presence of hydrogen with little evidence of plasticity on the fracture surface (Ni shown in **Figure 2.6a**). The slip traces on the surface would suggest some plasticity, but being limited and of a planar character. However, in both cases, dislocation cells were found immediately beneath the fracture surface (**Figure 2.6b**) and the size of the dislocation cells was suggestive of a plastic strain nearly three times what

the sample actually experienced macroscopically. In fact, in the Ni case, this dislocation distribution was found to extend to over 3 mm from the fracture surface [57] (**Figure 2.6c**), suggesting that the structures extend throughout the gage length and were formed prior to crack initiation. They further concluded that hydrogen-induced intergranular fracture ultimately proceeds via decohesion of GBs due to the attainment of a critical localized stress and hydrogen concentration combination (i.e. HEDE), which is primarily driven by the interaction between hydrogen and dislocations (i.e. HELP).

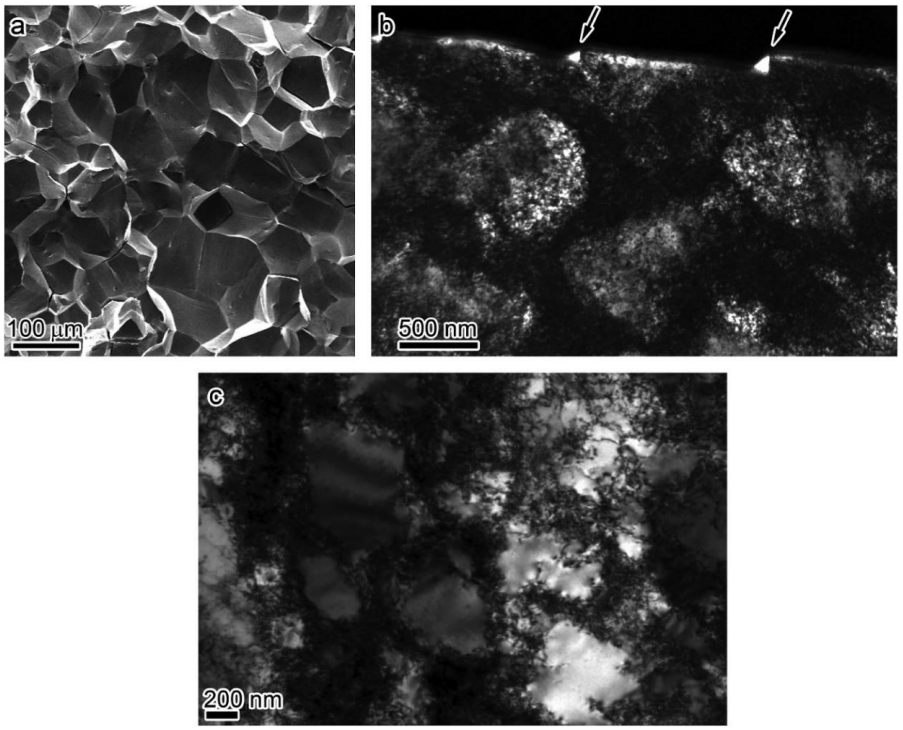

Figure 2.6. Hydrogen-induced intergranular failure of nickel. Uniaxial tensile tests were conducted on pre-charged tensile bars. a) SEM micrograph showing intergranular failure of fracture surface. b) TEM micrograph showing microstructure immediately underneath the fracture surface, comprising of dislocation cells. Arrows mark steps on the surface, usually labeled as slip traces. c) TEM micrograph showing microstructure 3–6 mm away from the fracture surface (i.e. bulk microstructure after loading). Note that cell structure still remains. Adapted from Refs. [13, 53].

Nevertheless, many debates or mysteries about HELP mechanism still exist. First, the reason for hydrogen atmospheres accelerating dislocation motion unlike other Cottrell atmospheres that have a solute drag effect is unclear. By checking the dislocation gliding

behavior in α-Fe over a wide range of hydrogen concentrations using atomistic simulations, Song and Curtin [54] found that the Cottrell atmospheres follow the moving dislocations, leading to a resistance to dislocation motion which is consistent with solute drag theory and reduces the dislocation mobility (**Figure 2.7**). Furthermore, once motion stops and a pile-up is established, the hydrogen Cottrell atmospheres do not affect the equilibrium spacing of dislocations in the pile-up; thus, the hydrogen atmosphere provides no "shielding" of dislocation–dislocation interactions. Furthermore, Xie et.al pointed out that the experimental set-up [41, 42, 55] to prove the shielding effect may not guarantee that the applied 'constant strain' or 'constant stress' was truly constant when tens of torrs of hydrogen gas flooded the TEM chamber, as fresh dislocations were seen to be generated in the 'constant strain' stage. By quantitative mechanical tests in an environmental TEM, they even found mobile dislocations can lose mobility with activating stress more than doubled, after exposing Al to hydrogen. Second, how enhanced dislocation slip in an atomic bond-switching manner (HELP) can lead to fracture in a bond-breaking manner (HEDE) is not known [56, 57]. Even HELP supporters insisted that HELP mechanism only works at a very specific material-dependent temperature and strain-rate range and establishes the necessary conditions for final HEDE, less is known for the quantitative contribution of mobile hydrogen-deformation interaction in determining the conditions required for HEDE, or more specifically, intergranular fracture. By interrupting the results from tensile tests conducted at cryogenic temperatures (77 K), where mobile H-deformation interactions are effectively precluded, and at room temperature, where the HELP mechanism should work, Harris [16] concluded that mobile hydrogen-deformation interactions are not an intrinsic requirement for H-induced intergranular fracture (**Figure 2.8**). Moreover, an evaluation of the true strain for intergranular microcrack initiation for testing conducted at room temperature and 77 K suggests that hydrogen which is segregated to GBs prior to the onset of straining dominates the hydrogen-induced fracture process for the prescribed hydrogen concentration of 4000 appm. More critical and detailed discussions about HELP are summarised by Lynch [58]. These contradictory results reflect the complexity of the interactions between plasticity and hydrogen when examined at different spatial and temporal scales and a more comprehensive understanding of HELP should be developed.

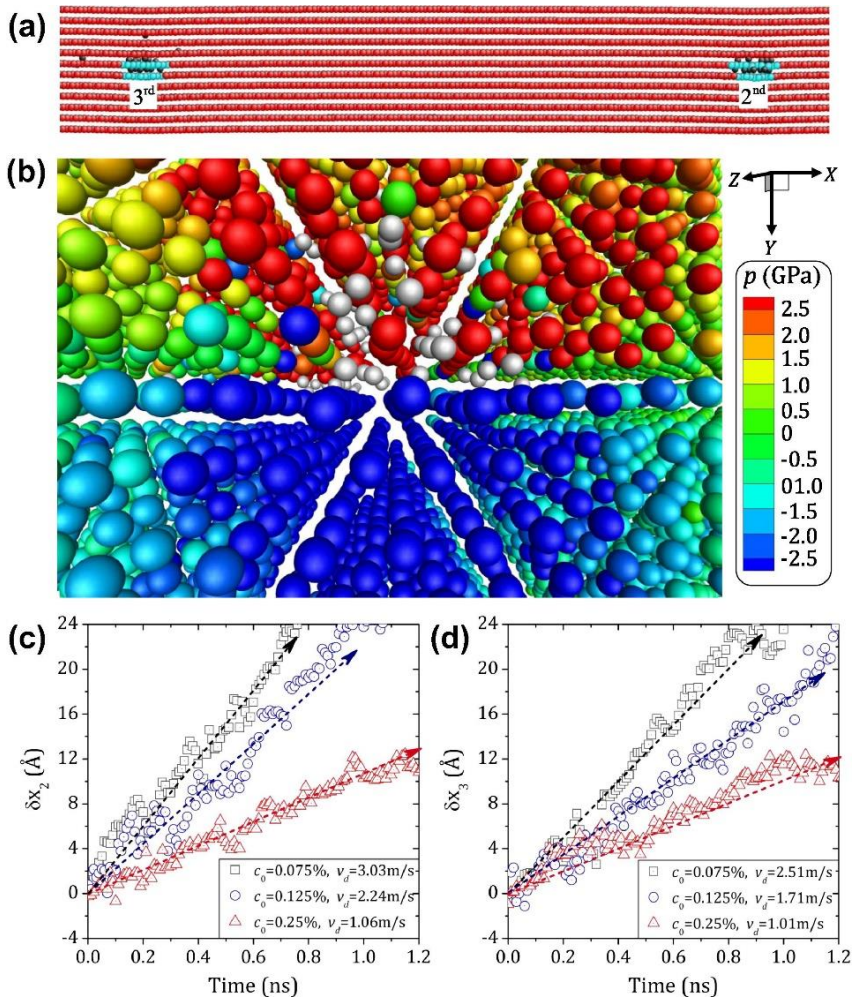

Figure 2.7. (a) Projected atomistic view (along the Z direction) of the second and third dislocation cores surrounded by clouds of H atoms (H atoms, black; Fe atoms in dislocation core, cyan; other Fe atoms, red). (b) Close-up perspective atomistic view of a dislocation core surrounded by the cloud of H atoms that form naturally in the simulation, at c_0 = 2% (H atoms, silver; Fe atoms colored via the pressure field p, with positive and negative values indicating tension and compression respectively). (c, d) Time evolution of the x-coordinate for the second and third dislocation cores within the first 1.2 ns after application of τ = 400 MPa, for materials with three representative H concentrations c0 as indicated. The corresponding dislocation velocities v_d (i.e. the slopes of curves) are also noted. Adapted from Ref. [54].

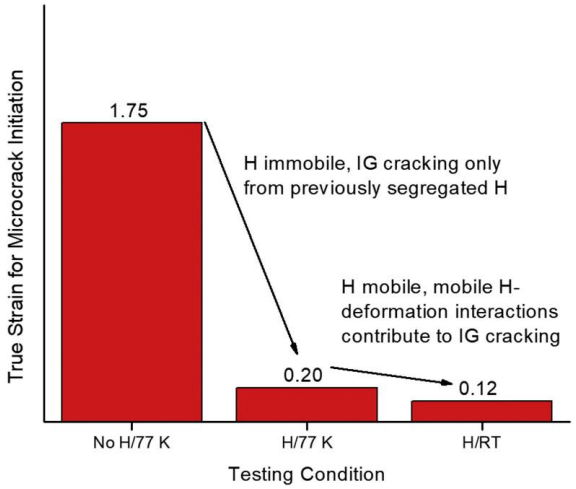

Figure 2.8. Effect of testing condition on true strain for H-induced intergranular (IG) microcrack initiation. The Adapted from Ref. [16].

2.2.3 Hydrogen-Enhanced Strain-Induced Vacancy (HESIV)

Dislocation is not the sole carrier of plasticity, vacancy could be generated by dislocation plasticity [59-61] and exert an influence through its interaction with hydrogen. Hydrogen has been experimentally found to facilitate the preservation of superabundant vacancies (SAVs) in a large variety of metals and alloys [62-65]. Based on these findings, Nagumo [66] first pointed out the predominant role of vacancies in premature fracture, which is referred to as hydrogen-enhanced strain-induced vacancies (HESIV) mechanism [67]. Takai et.al examined hydrogen-related failure in the Inconel 625 and iron by thermal desorption spectroscopy (TDS) and found annealing at 200 °C at the unloaded stage almost completely recovered the decrease in fracture strain. This result directly indicates the primary role of vacancies rather than hydrogen itself in hydrogen degradation. Similar charging-straining-annealing-TDS analysis processes were further applied to pure iron [68] with different annealing temperatures. Hydrogen absorbed in the weak trapping sites substantially increases with plastic strain, and continuous reduction in desorption in **Figure 2.9** with elevated annealing temperature implies the presence of vacancy clusters of different sizes. Positron annihilation spectroscopy (PAS) that efficiently and specifically discriminates vacancies from other traps like dislocations is also utilized to investigate hydrogen-induced vacancy generation where the mean positron lifetime was

substantially increased by tensile straining with charged hydrogen [69]. Lawrence further pointed out the role of GB in vacancy generation by PAS [70]. Besides experimental evidence, numerous first-principle calculations show that vacancy could be stabilized by forming hydrogen-vacancy (Va-H) complexes [71-75] and those Va-H complexes could influence the subsequent plastic deformation [76, 77]. Hydrogen adatoms on vacancy or nanovoid surfaces could also cause blistering at the surface [78, 79].

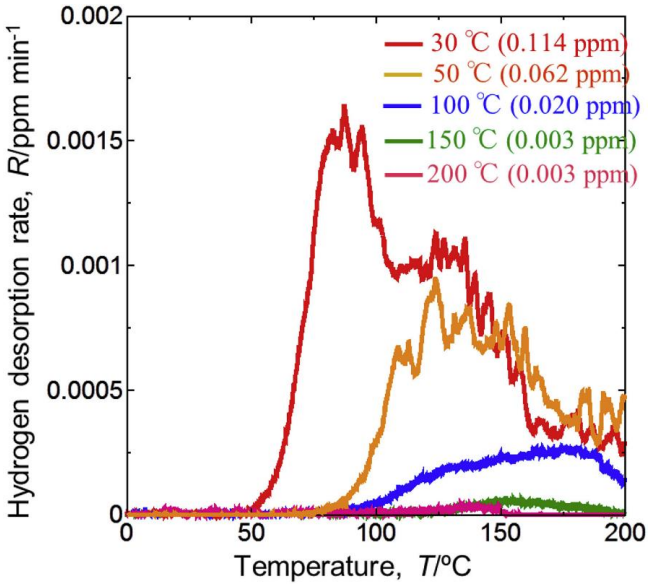

Figure 2.9. Low-temperature thermal desorption spectroscopy profiles of hydrogen introduced into iron specimens strained up to 25% with hydrogen precharging and successively annealed at various temperatures for 1 h at 303 K or 2 h at other annealing temperatures. The specimen thickness was 0.3 mm and tracer-hydrogen was introduced by cathodic electrolysis of a mild condition in 0.1 N NaOH + 5 g/l NH_4SCN aq at 100 A/m^2. Adapted from Ref. [68].

These SAVs generated by strain and hydrogen will further interact with other defects in the material, and importantly, agglomerate and nucleate the nanovoid. The nanovoid will further grow up, coalesce and cause crack propagation. One notable piece of evidence is the observation of significant dislocation plasticity and nanovoid beneath the fracture surfaces [80-82]. By carefully zooming into fracture surfaces in ferritic steels with TEM and conjugate analysis, Neeraj [34, 83] found the quasi-brittle fracture surfaces were covered with nanoscale dimples 5–20 nm wide and 1–5 nm deep (**Figure 2.10**). Most of the nanodimples appear to be "valley-on-valley" type, rather than"mound-on-valley" type,

indicating nanovoid nucleation and growth in the plastically flowing medium prior to ultimate failure. Based on these observations, an alternative scenario of plasticity-generated, hydrogen-stabilized vacancy damage accumulation and nanovoid coalescence mechanism is proposed as the failure pathway for HE (referred to as NVC mechanism in **Figure 2.11**). And this mechanism will be the inspiration for the attached **Paper2**.

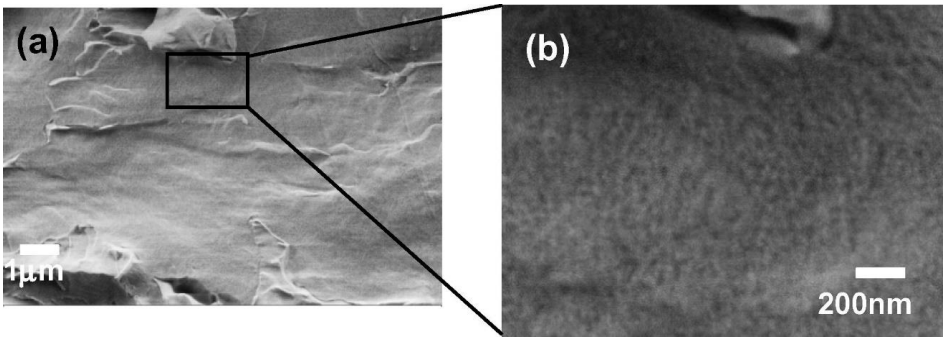

Figure 2.10. (a) Typical quasi-brittle fracture observed in X60 CT sample tested in 21 MPa hydrogen gas pressure. (b) Higher magnification view of a small region from (a). The fracture surface shows "mottled" contrast, indicating the presence of nanoscale dimples on hydrogen-embrittled quasi-brittle facets. This is similar to the observations in H pre-charged SENB samples. Adapted from Ref. [34].

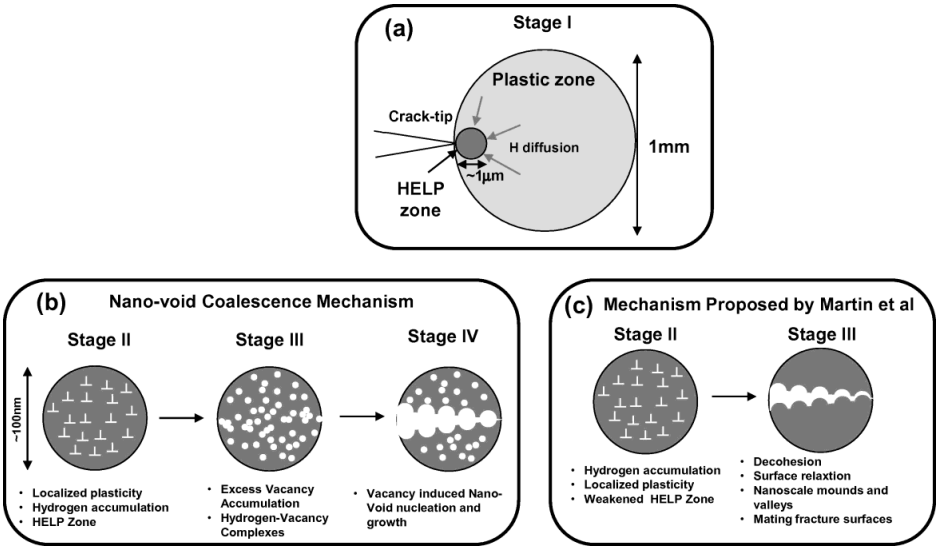

Figure 2.11. Schematic of NVC mechanism compared to HELP mechanism by Martin [56]. Adapted from Ref. [34].

2.2.4 Adsorption-Induced Dislocation Emission (AIDE)

The Adsorption-induced dislocation emission (AIDE) mechanism was first proposed by Lynch [84, 85]. As shown in **Figure 2.12**, the term "dislocation emission" encompasses both nucleation and subsequent movement of dislocations away from the crack tip, and it is the only nucleation stage that is critical and facilitated by adsorption. Once nucleated, dislocations can readily move away from the crack tip under the applied stress. The nucleation stage involves the simultaneous formation of a dislocation core and surface step by cooperative shearing of atoms (breaking and reforming of interatomic bonds) over several atomic distances. Thus, the weakening of interatomic bonds over several atomic distances by "adsorbed" hydrogen can facilitate the process.

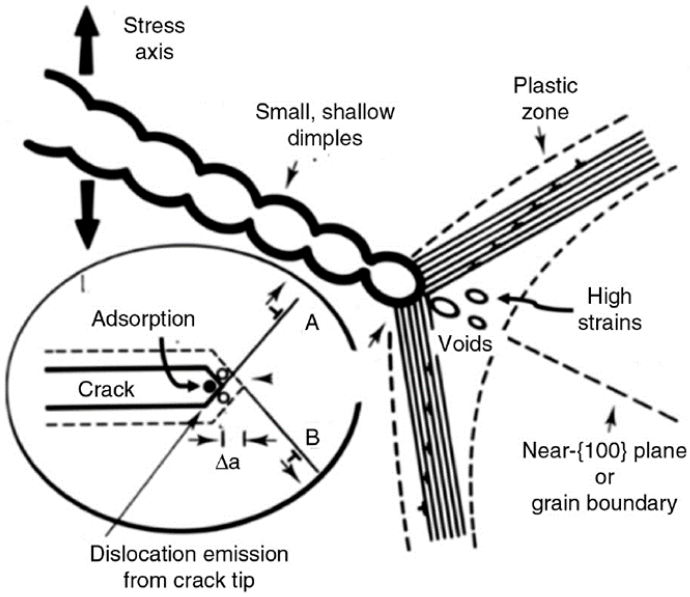

Figure 2.12. Schematic diagram illustrating the AIDE/void-coalescence mechanism for HE for some systems, resulting in small, shallow dimples on cleavage-like or intergranular fracture surfaces, which are often inclined to the stress axis. Note that voids may be extremely small (on the nanoscale) so that dimples on fracture surfaces may not be obvious (or obscured by films). Dislocation emission from crack tips (owing to adsorption-induced weakening of interatomic bonds) promotes the coalescence of the crack with voids formed in the plastic zone. The inset illustrates emission on plane A, and then on plane B resulting in an increment of crack opening and crack advance, Δa. For transgranular cracking, there is a tendency for equal amounts of slip to occur on slip planes on either side of cracks since back stresses from emitted dislocations on a more active slip plane would then favor emission on the other slip plane. Intergranular cracking can

occur in some cases owing to preferential adsorption at crack-tip/grain-boundary intersections. The stresses required for AIDE are sufficient for dislocation activity and void formation ahead of cracks, and some crack growth and blunting occur by egress of dislocations around crack tips, as well as dislocation emission from crack tips. The degree of embrittlement and deviations of crack planes away from low-index planes depends on the relative extent of dislocation emission from crack tips vis-à-vis dislocation activity from near-crack-tip sources adapted from Ref. [10].

In the AIDE model, crack growth occurs not only by dislocation emission from crack tips, nucleation and growth of microvoids (or nano-voids) ahead of crack tips also make a contribution, similar to the NVC model in **Figure 2.11**. Nucleation and growth of voids at second-phase particles, slip-band intersections, or other sites in the plastic zone ahead of cracks occurs because stresses required for dislocation emission are sufficiently high that some general dislocation activity occurs ahead of cracks. Void formation contributes to crack growth, and also serves to resharpen crack tips and result in small crack tip-opening angles. In summary, AIDE is a fundamentally complex model combining HEDE, HELP and HESIV where HEDE weakens the bonding energy, HELP accelerates crack growth and HESIV facilitates void growth and coalescence.

2.2.5 Defactants theory

"DEFect ACTing AgeNTS" commonly referred to as Defactants theory is introduced by Kirchheim [86-88], in analogy to the concept that the surface energy of water can be reduced by solute molecules known as surfactants (SURFace ACTing AgeNTS). Solute atoms segregating at defects with an excess Γ are called defactants because they lower the defect formation energy of defects γ, with μ as the chemical potential of the defactant we have the following equation:

$$d\gamma = -\Gamma d\mu \tag{2.2}$$

Excess defactant, Γ, given by **Eq. (2.2)** is positive, and defactants therefore reduce the defect energy γ. In other words, attractive interaction between solute atoms and defects leads to excess solute at the defect and a free energy gain. For the HE scenario, the segregation of hydrogen into defects, such as vacancies, dislocations, and stacking faults, can reduce the defect formation energy and therefore enhance their generation rate. The defactants theory rationalizes reduced fracture energy in HEDE and enhanced dislocation and vacancy generation in HELP and HESIV at the same time. In addition, it

is most useful to comprehend recent nanoindentation experiments which reveal a reduction of the dislocation line energy in the presence of hydrogen [89-91].

2.2.6 Hydride formation

A mechanism based on the formation and fracture of hydrides at crack tips was first proposed by Westlake in 1969 [92]. The basic mechanism is thought to involve repeated sequences of (i) hydrogen diffusion to regions of high hydrostatic stress ahead of cracks, (ii) nucleation and growth of a hydride phase, (iii) cleavage of the hydride when it reaches a critical size, and (iv) crack-arrest at the hydride matrix interface (**Figure 2.13**). This mechanism is more generally accepted but only available in certain materials such as V, Zr, Nb, Ta, and Ti [45, 93] where there is a strong thermodynamic driving force for brittle hydride formation.

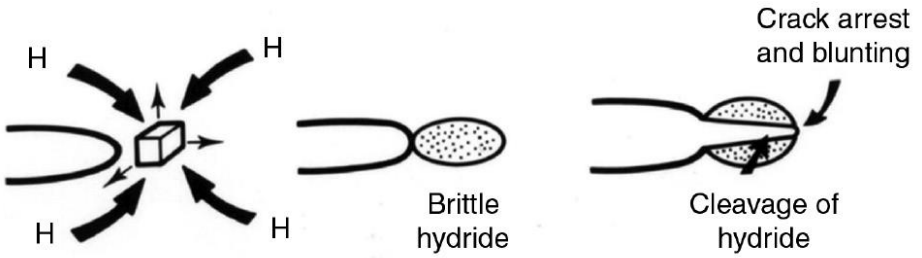

Figure 2.13. Schematic diagram illustrating sub-critical crack growth involving hydride formation. Adapted from Ref. [10].

In summary, the aforementioned mechanisms have captured certain characteristics in HE experiments but a universal mechanism still does not exist, due to the complex HE processes depending on various environmental conditions and local microstructures. However, those mechanisms are not necessarily mutually exclusive. For example, easier defect formation could be expected in HELP, HESIV and AIDE. A number of researchers have suggested the synergistic action of mixed mechanisms [94-96], where a crack forms under a single mechanism followed by propagation under an alternative one, or by a combination of both or several. Furthermore, the remaining puzzles about the mechanism for typical hydrogen-induced transgranular to intergranular fracture transition and the quantitative contributions of each mechanism to this process will be discussed in attached **Paper1** and **Paper2**.

2.3 Atomistic modeling for hydrogen embrittlement

In the recent 50 years, with the advance of computational capacity, the emerging multi-scale and multi-physics materials modeling methods help to bridge the wide range of time and length scales in a number of essential phenomena and processes in materials science and engineering. Typically, depending on the scale of systems, the methodology (**Figure 2.14**) could be divided into ab initio methods based on many-body electronic structure theory, density functional theory (DFT), quantum chemistry, atomistic simulations widely used as molecular dynamics (MD) or kinetic Monte Carlo models, mesoscopic modelings such as discrete dislocation dynamics and continuum mechanism-based simulation which could be polycrystalline plasticity or Finite element method.

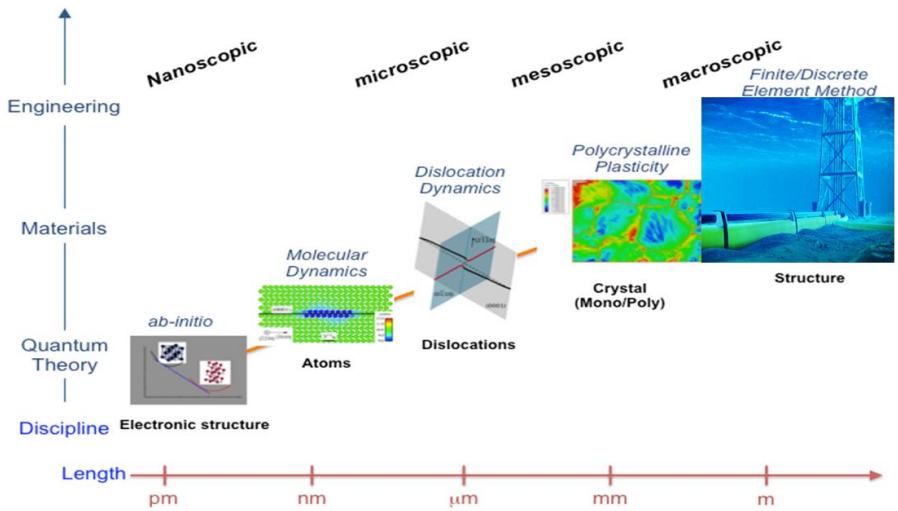

Figure 2.14. Illustration of the multiscale modeling in varying scales.

Depending on the purpose, different methods could provide valuable information for HE at different scales but with a tradeoff between accuracy and complexity. For example, the finite element method could be a very useful engineering tool to predict failure strain and sample lifespan in hydrogen environment, but it requires constitutive relations and associated parameters which are almost always obtained empirically. Dislocation dynamics could well describe the mesoscopic collective interaction between dislocations during plasticity under the premise of a correct understanding of the role of hydrogen and

dislocations. Molecular dynamics are particularly suited to understand kinetically dominated mechanisms including hydrogen diffusion, trapping and interaction with metal atoms based on the accurate atomic potential. Ab initio calculations give a precise description of the bonds and elementary excitations from which all material properties derive from, however, its system is limited to thousands of atoms due to the exponentially increased calculation complexity. As our motivation is to investigate the fundamental mechanisms and try to establish mechanism-based quantitative criteria, molecular dynamics is chosen as the main methodology which could provide direct hydrogen-metal interaction in a range of varying temperatures and stress conditions.

Plenty of previous work [33, 97-102] has proved atomistic simulations as a powerful tool for understanding nanoscale HE mechanisms and provided information on the local and global mechanical behavior in the presence and absence of hydrogen. Those atomistic studies of HE could be divided into several sub-processes, i.e., vacancy formation [19, 71, 74, 75, 103-106], dislocation dynamics [107-110], intergranular decohesion [111-113], and crack propagation [44, 54, 114-119]. Hydrogen is trapped by vacancy and forms Va-H complex [120-122], and Hou et.al [75] explicitly demonstrated sequential adsorption of hydrogen adatoms on Wigner–Seitz squares of nanovoids with distinct energy levels and found a pairwise power-law repulsion using DFT. Using MD and cluster dynamics simulations, Li et.al [123] revealed that, unlike a lattice vacancy, a Va-H complex is not absorbed by dislocations sweeping through the lattice (**Figure 2.15**). Additionally, this complex has lower lattice diffusivity; therefore, it has a lower probability of encountering and being absorbed by various lattice sinks. Hence, it can exist metastably for a rather long time and act as the embryo for the formation of proto nano-voids. Ping et.al [109] further pointed out that the main effect of hydrogen on dislocation is increasing the core radii and decreasing the core energies. Using DFT [110], Li et.al found at low hydrogen concentrations, dislocation maintains the intrinsic easy-core structure, and hydrogen atoms are attached to the “periphery” of dislocation to enhance dislocation motion. While at high concentration, dislocation transforms into a hard-core, metal hydride-like structure, as hydrogen atoms become the “body” of dislocation to significantly reduce the dislocation mobility. Besides, systematic work has been done by Tehranchi et.al [35, 124] to investigate the intergranular decohesion with a

set of GBs. Finally, crack propagation behavior has been widely studied by atomistic simulations. Using mode II loading, Taketomi et al. [125] showed hydrogen-enhanced (112)<111> edge dislocation emission is proportional to the hydrogen content around the crack tip. In the contrast, Song and Curtin [98] propose an atomic mechanism where the suppression of dislocation emission at the crack tip due to aggregation of hydrogen permits brittle-cleavage failure followed by slow crack growth with mode I loading (**Figure 2.16**).

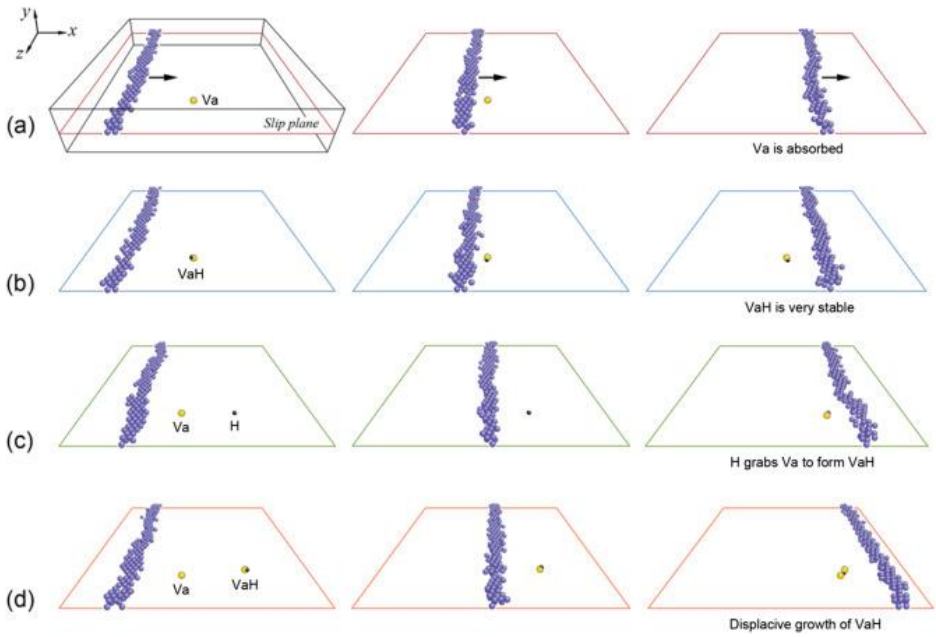

Figure 2.15. Four independent events illustrating the high stability of hydrogen-vacancy complex when interacting with dislocations in α-Fe. Crystals are oriented along x-[111], y-[-101], z-[1-21]. Spheres with blue, gold and black colors refer to iron atoms in dislocations, vacancies and hydrogen, respectively. The radius of vacancy and hydrogen are enlarged for clarity. (a) When a a/2<111>-type edge dislocation interacts with a vacancy in the slip plane, the dislocation absorbs the vacancy. (b) In contrast, the hydrogen-vacancy complex is very stable when colliding with an edge dislocation. (c) The stability of hydrogen-vacancy complex is further confirmed when lattice hydrogen grabs an absorbed vacancy from an edge dislocation and stabilizes it in the form of a hydrogen-vacancy complex. (d) The hydrogen-vacancy complex can even grow displacively by capturing more vacancies that were absorbed by edge dislocations. Adapted from Ref. [123].

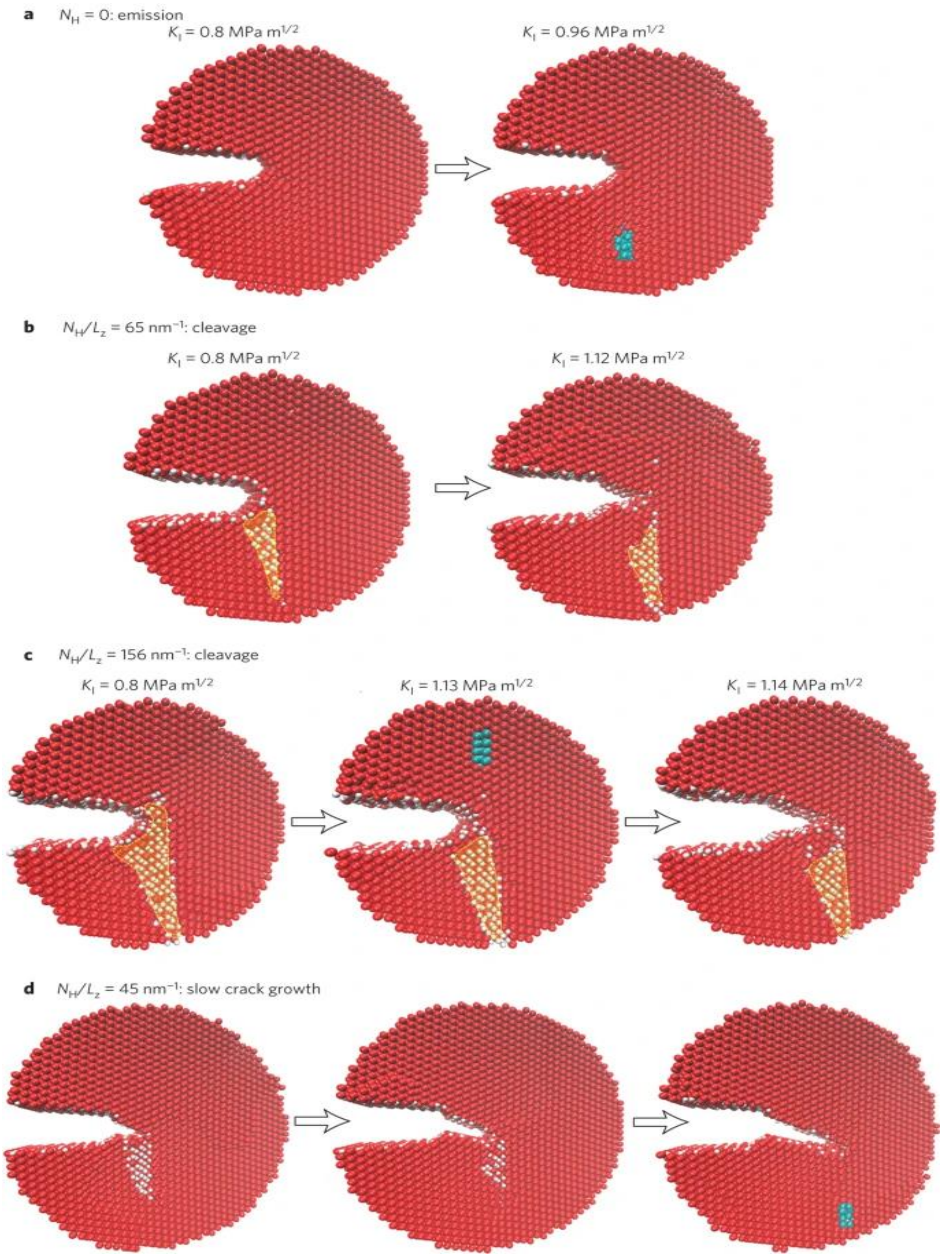

Figure 2.16. H atoms are colored white, and Fe atoms are colored red, except for those in a dislocation core colored cyan; shaded regions in b,c show areas of bcc→fcc phase transformation. a, For low amounts of H, H saturates the crack surfaces and the crack tip deforms through dislocation emission. b, For increased H, the H accumulates into a H-rich wedge-shaped region in the bulk near the crack tip, which evolves to induce

a bcc→fcc phase transformation that blocks dislocation emission, and leads to brittle cleavage. c, Increased H leads to further growth of the H-rich region, which intersects the crack front and leads to emission of a single full dislocation of Burgers vector [-1-1-1]/2 followed immediately by brittle cleavage. d, Loading beyond the onset of cleavage leads to slow crack growth, where the H-rich region moves with the crack tip through diffusion; with a fixed amount of H, the H-rich region shrinks as H atoms are depleted by surface segregation until eventually it becomes so small that dislocation emission resumes. Adapted from Ref. [98].

2.4 Hydrogen-grain boundary interaction

Grain boundaries (GBs) [126] are the interface between two grains or crystallites in a polycrystalline material. Most of them are preferred sites for solute segregation and onset of corrosion, including hydrogen embrittlement where the hydrogen-induced ductile to brittle transition is often accompanied by a transgranular to intergranular fracture transition. In metallic materials such as high-strength steels and nickel, etc., this embrittlement is manifested by a loss of cohesion primarily in the GBs (HEDE concept), leading to low-toughness intergranular fracture. Due to the energy-favorable trapping sites GBs, local accumulation of hydrogen is inevitable and it can result in intergranular fracture which is the most serious by inducing time-dependent subcritical cracking at low applied stresses and leading to unexpected catastrophic failures of structures. The associated hydrogen-GB interactions are thus extensively studied through previous experiments [25, 26, 40, 101, 127-133] or modelings [35, 101, 111, 124, 134-139], and multiple studies suggest the hydrogen diffusion, trapping and decohesion behavior depend highly on the GB types and local structures.

For instance, through permeation tests, Yao et al. [132, 140] discover that GB diffusivity of hydrogen is concentration-dependent. When the hydrogen concentration is extremely low, the grain boundary diffusion of hydrogen is virtually stopped. And the low-energy sites within GBs are postulated to be responsible for such retardation. Oudriss et al. [127, 129, 141] further illustrate the effects of random and special boundaries on the different defects and trapping sites stored in the GBs. The high-angle random boundaries are considered as disordered phase where the hydrogen diffusion is accelerated, while the special boundaries constitute a potential zone for hydrogen trapping due to the high density of trapping sites as dislocations and vacancies. Based on DFT calculations, Xiao et al. [137] found a transition between slow and fast hydrogen diffusion along the GB

with an abrupt change in hydrogen diffusivity. Low-angle GBs are shown to comprise isolated high-barrier regions to trap and inhibit H diffusion, while high-angle GBs are shown to provide interconnected low-barrier channels to facilitate H transport (**Figure 2.17**).

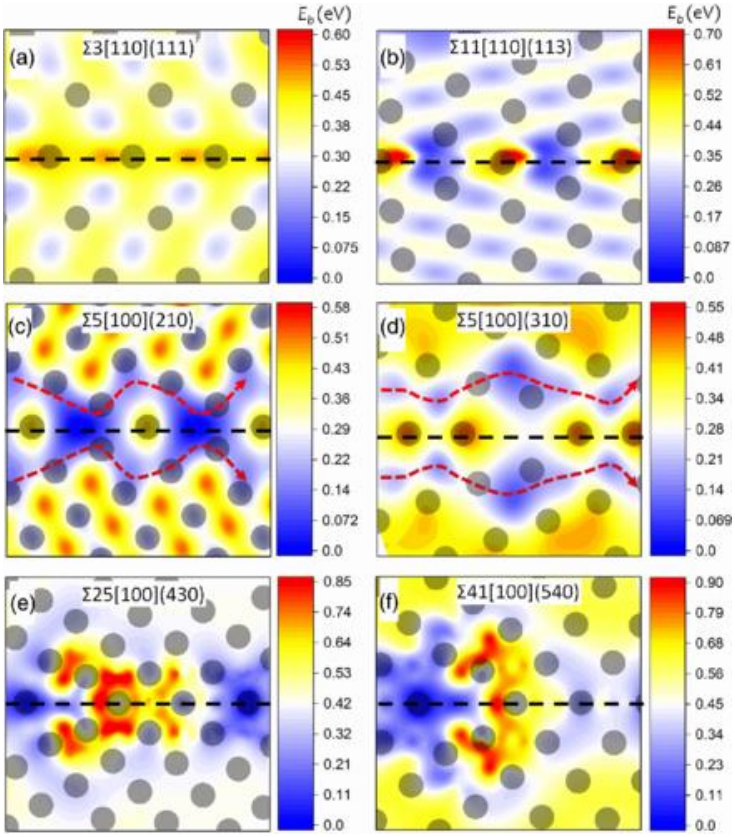

Figure 2.17. Contour mapping of the energy barrier Eb of H migration at representative GBs. (a) Σ3[110](111), (b) Σ11[110](113), (c) Σ5[100](210), (d) Σ5[100](310), (e) Σ25[100](430), (f) Σ41[100](540). Big gray spheres represent host Ni atoms. Adapted from Ref. [137].

As for hydrogen trapping behavior, by TDS, Wada et al. [25] found that hydrogen was trapped along GBs with a binding energy of $\approx$20 kJ/mol in polycrystalline Ni, and further true fracture stress analysis and fracture surface morphology examination showed hydrogen-induced intergranular fracture of pure Ni is controlled by the concentration of the GB trapped hydrogen, and not by the concentration of lattice hydrogen (**Figure 2.18**). Besides, Bechtle et al. [128] conducted experiments on GB-engineered Ni samples with

and without hydrogen, and the results showed that the susceptibility of HE can be drastically reduced at special GBs that are characterized by low excess free volumes and a high degree of atomic matching. Using DFT calculations on two typical GBs of Σ3[-110](111) with a close-packed interface structure and Σ5[001](210) with a less dense interface structure consisting of open structural units, Davide et al. [139] found these two GBs have a markedly different interaction behavior with atomic hydrogen that Σ3 GB neither traps hydrogen nor enhances its diffusion but Σ5 enhance the trapping and on-plane diffusion behavior. Xiao et al. [136] demonstrated the chemomechanical origin of hydrogen trapping at GBs. The GB excess volume was found to linearly determine the hydrogen trapping energy in a variety of face-centered cubic metals of Ni, Cu, γ-Fe, and Pd.

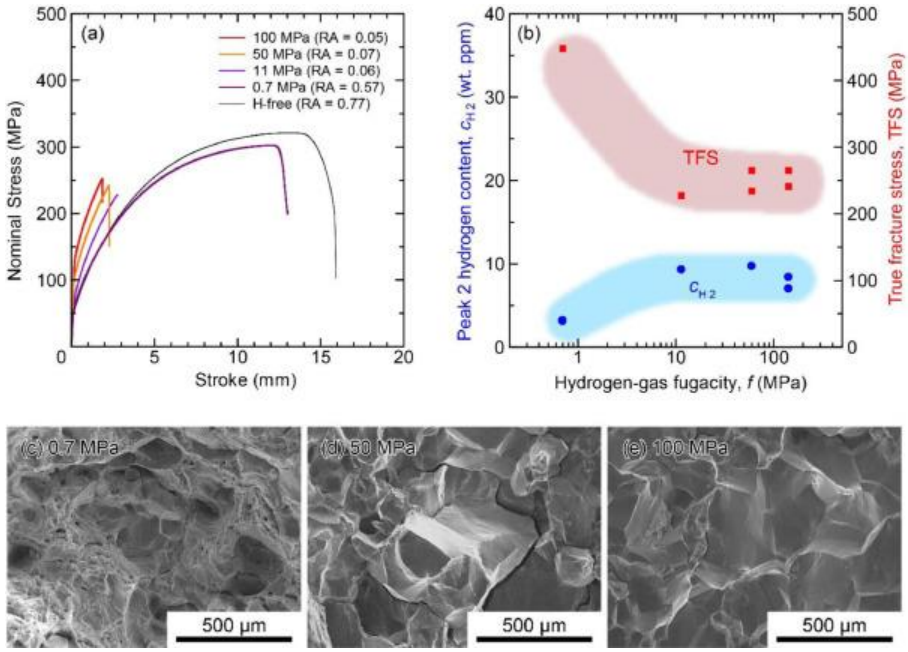

Figure 2.18. (a) Stress–stroke curves of H-free and H-charged pure Ni. (b) Peak 2 hydrogen content and true fracture stress as functions of hydrogen-gas fugacity. (c–e) Fracture surface morphologies of H-charged pure Ni in 0.7 MPa (c), 50 MPa (d) and 100 MPa (e) hydrogen gas. Adapted from Ref. [25].

To quantitatively predict decohesion behavior and fracture energy reduction caused by hydrogen, many theoretical studies combined with atomistic calculations have been done. Ali [35] calculated the binding energy of hydrogen atoms to various atomic sites and to

various surfaces created by separating these GBs into two possible fracture surfaces and found no tendency for hydrogen to cause a ductile-to-brittle transformation for cracks along most GBs. The experimental observations of cleavage-like failure are thus attributed to mechanisms involving H diffusion or dynamic crack growth. Shuai et al. [14] further calculated the reduction of the reversible work of separation of Fe GBs and found the reduction is lower than the experimental observations even at a level near the hydride formation limit. They posited that hydrogen-enhanced plasticity and attendant effects establish the local conditions responsible for the transition in fracture mode from transgranular to intergranular. The conclusion is reached that intergranular failure occurs by a reduction of the cohesive energy (HEDE) but with contributions from structural as well as compositional changes in the GB that are driven by hydrogen-enhanced plasticity (HELP) processes. However, the microscale detailed HELP-mediated HEDE mechanism is still not clear. Using MD simulations, Li et al. [142] and Zhu [143] et al.further examine the dynamics behaviors of GBs in the hydrogen environment with uniaxial tension, the dislocation nucleation stress was found to be decreased by hydrogen but intergranular fracture always happens even without hydrogen. Using atomistic modeling to investigate the mechanical response of GBs in alpha-iron with various hydrogen concentrations, Liang et al. [101] found that dislocations impingement and emission on the GB can provoke it to locally transform into an activated state with a more disordered atomistic structure, and introduce a local stress concentration. The activation of the GB segregated with hydrogen atoms can greatly facilitate decohesion of the GB, with the proposed model in **Figure 2.19**. In all, previous simulations has shown the reduced fracture toughness at GB by inserting hydrogen, but no transgranular to intergranular fracture transition corresponding to experiments was observed, which is due to their low stress triaxiality state setting and will be further analysed in the attached Paper1 and Paper2.

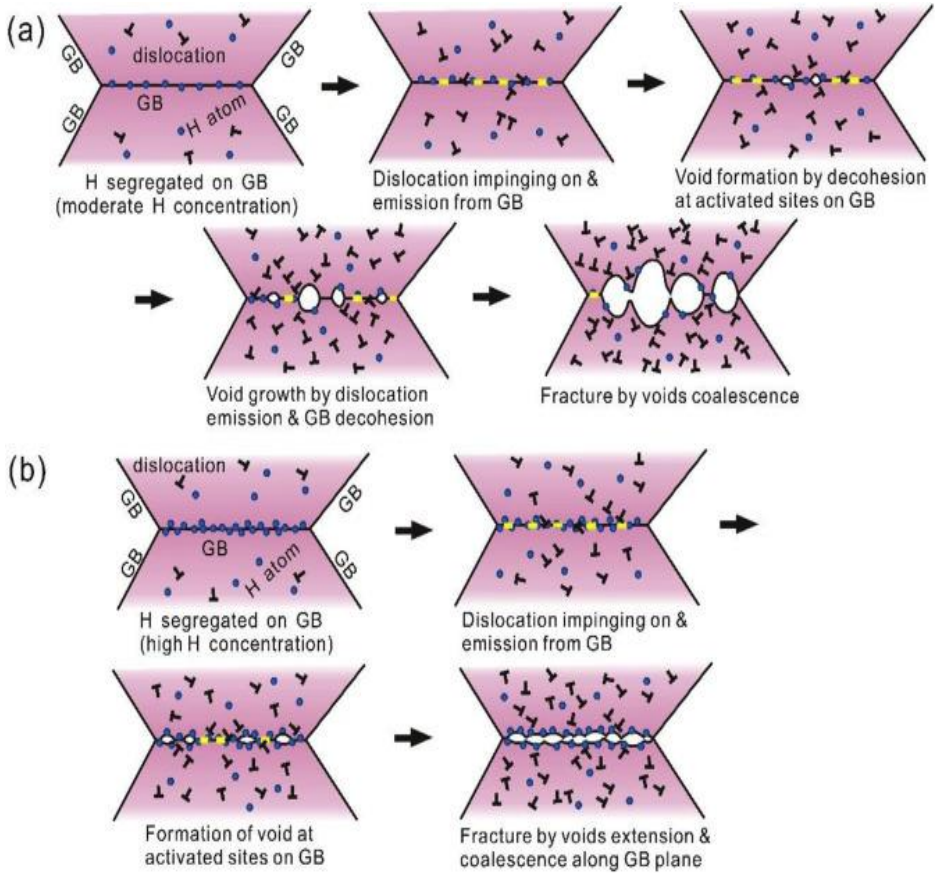

Figure 2.19. Schematic illustration of H embrittlement controlled by dislocation-GB reaction in metals. (a) Polycrystalline sample with moderate concentration of hydrogen mechanically failed with a quasi-cleavage fracture surface on which the traces of the original GBs can hardly be identified. (b) Intergranular fracture of a polycrystalline sample with fairly high hydrogen concentration for which the traces of original GBs are largely preserved on the fracture surface. The yellow strips on the GBs represent sites at which the reaction of GB with dislocations results in a locally activated state of the GB. Adapted from Ref. [101].

Chapter 3 Main results

Hydrogen embrittlement (HE) has been a long-standing issue for both academia and industry, however, the nanoscale HE mechanisms associated with a broad range of hydrogen-microstructure interactions are largely unknown. Of particular significance, the hydrogen-grain boundary (GB) interaction can make HE occur in its most severe form, i.e., intergranular fracture. Herein, aiming to understand the microscale mechanism of intergranular fracture and develop a mechanism-based predictive model, a set of atomistic simulations is designed and performed to obtain atomic insights into hydrogen-GB interactions.

Previous work focused on the decohesion effect of hydrogen at GB, but the critical timing for transgranular to intergranular fracture transition has not been recorded in the literature. By applying uniaxial straining to mimic the high-stress triaxiality state in the vicinity of crack tips, we first show a nanoscale transgranular to intergranular fracture transition facilitated by hydrogen at Ni Σ5(210)[001] GB. Hydrogen is found to form a local atmosphere in the GB region, which induces a local stress concentration and inhibits the subsequent stress relaxation at the GB during deformation. It is this local stress concentration that promotes earlier dislocation emission, twinning evolution, and generation of more vacancies that facilitate nanovoiding. The nucleation and growth of nanovoids finally leads to intergranular fracture at the GB, in contrast to the transgranular fracture of hydrogen-free sample. These observations revealed a specific hydrogen-induced plasticity-participated decohesion mechanism.

To universalize this mechanism to varying GBs and environmental conditions and develop a quantitative prediction, statistically reliable simulations on Ni Σ5(210)[001] and Σ9(1-10)[22-1] GBs with or without pre-charged hydrogen at various temperatures are carried out. Without hydrogen, vacancy generation at GB is limited and transgranular fracture mode dominates. When charged, hydrogen as a booster can enhance strain-induced vacancy generation by up to ten times. This leads to the superabundant vacancy stockpiling at the GB, which agglomerates and nucleates intergranular nanovoids eventually causing the intergranular fracture. Compared to the enhancement of vacancies, changes in dislocation quantities and behavior are negligible and not sensitive to intergranular fracture. While hydrogen tends to persistently enhance vacancy concentration, temperature plays an intriguing dual role as either an enhancer or an inhibitor for vacancy stockpiling. These results directly indicate the critical role of vacancy in the fracture mode transition and good agreement with recent positron annihilation spectroscopy experiments. An S-shaped quantitative correlation (Fig. 3.1) between the proportion of intergranular fracture and vacancy concentration was for the first time derived, highlighting the existence of a critical vacancy concentration, beyond which fracture mode will be completely intergranular. The relationship provides a robust tool to quantitatively predict the transgranular to intergranular fracture transition.

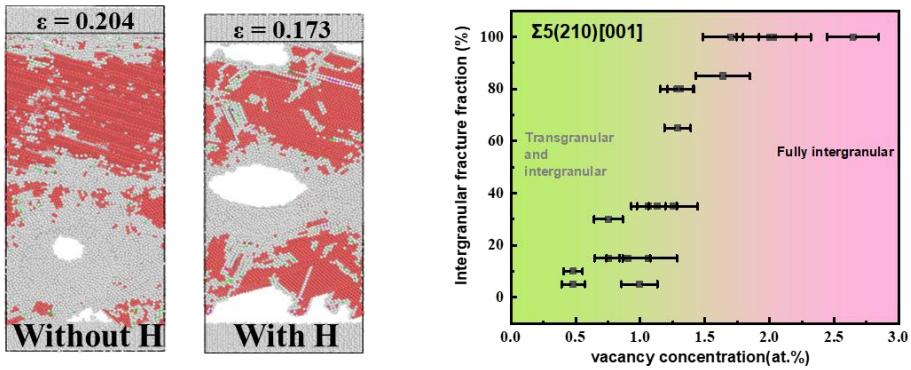

Figure 3.1. Left: Transgranular nanovoid formation in the absence of hydrogen and intergranular nanovoid formation in the presence of hydrogen. Right: Relationship between intergranular fracture fraction and vacancy concentration at GB.

Besides the decohesion effect on fracture behavior, hydrogen also influences the mobility of GB during the shear-coupled migration process. By inserting hydrogen as solute at the typical dislocation-array Σ25(430)[001] GB and applying shear deformation, the hydrogen-coupled GB migration is investigated and a dual role of hydrogen on GB mobility is unraveled. In the low temperature and high loading rate regime, where hydrogen diffusion is substantially slower than GB motion, GB breaks away from the hydrogen atmosphere and transforms into a new stable phase with highly enhanced mobility (Fig. 3.2). In the reverse regime, hydrogen atoms move along with GB, exerting a drag force on GB and decreasing its mobility. These findings provide rationale for the coexistence of hydrogen hardening and softening observed experimentally in polycrystalline materials.

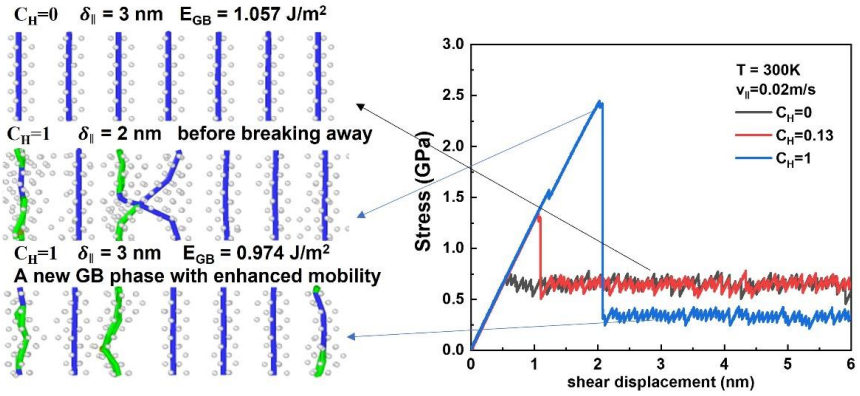

Figure 3.2. Left: GB core structure in the absence of hydrogen, in the presence of hydrogen before breaking away and in the presence of hydrogen after breaking away, respectively. Right: Stress-strain curve during GB migration.

Finally, to transfer the results from a certain special GB to a general GB, i.e, from bicrystal to polycrystal, we elucidate the hydrogen segregation energy spectrums at GBs of polycrystalline Ni by traversing all the geometrically favorable trapping sites. The spectrum is a statistical result from millions of local atomic motifs and it is found to be naturally captured by a three-peak Gaussian mixture distribution (Fig. 3.3). The first peak (-0.205eV) corresponds to GB core sites which account for the most favorable trapping sites and also contribute to the fast GB network diffusion with lower migration energy, while the second and third peaks correspond to hybrid GB surface-octahedron/

tetrahedron sites acting as an on-plane diffusion barrier. A thermodynamic model is further derived to describe the equilibrium hydrogen concentration at GB. Through mean squared displacement analysis, these general GBs in polycrystal show a higher diffusion coefficient by three orders of magnitude at GB compared to the fcc lattice.

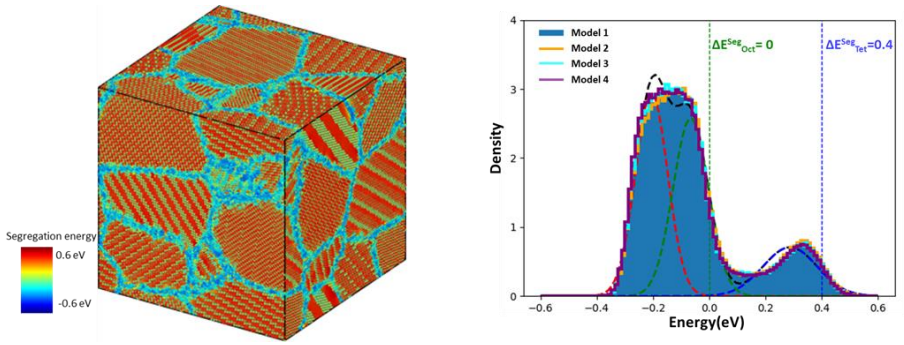

Figure 3.3. Left: Hydrogen trapping spectrum in polycrystal. Right: Density distribution of segregation energy for varying trapping sites.

Chapter 4 Perspectives

Hydrogen embrittlement has almost a history of 150 years, the remaining debates may originate from 1) hydrogen as the smallest element is still tricky to be detected, 2) the collective effect of small-scale interaction to macroscale is still unclear. To resolve these issues, new technology and interpretation are necessary. In this thesis, we could have a glance into the nanoscale HE with the help of atomistic modeling, however, limitation exists and potential further studies could be:

1) Atomistic simulation has its own limitation due to the constrained time and space scale. The slow hydrogen diffusion in reality may take several years to get fully saturated and the macroscale mechanical may depend on long-range plastic behavior across the whole sample, which makes the simulation condition oversimplified to the real situation. This gap may be mitigated by the advance of experimental techniques (atom probe tomography and high-resolution transmission electron microscopy) into a smaller scale and the revolution in computer hashrate (quantum computing). The accuracy of atomistic simulation highly depends on the atomic potential, more material systems and varying potential can be verified in the future. For instance, hydrogen in bcc iron could be a future target system where the diffusion is faster than typical fcc Ni. The

emerging machine-learning potential can be a good candidate for simulating multiple systems.

2) Nowadays, machine learning is coupled with powerful data processing and high prediction performance and is being widely used in multiple fields. Its previous success in pattern recognition, drug development, etc. can also be transferred to predict hydrogen embrittlement or design anti-hydrogen embrittlement materials based on a bunch of past data. For example, the component-properties relationship for high-entropy alloy could be derived by computer to design suitable material.
3) Specifically in this thesis, we explore hydrogen interaction with a range of GBs, however, the effect of pre-existing dislocation, precipitate and phase boundary are still not considered. More attention could be focused on their collective interaction with an accelerated kinetic hydrogen diffusion modeling methodology.

Bibliography

[1] DNV, Energy Transition Outlook — A Global and Regional Forecast to 2050. Available at:https://www.dnv.com/energy-transition-outlook/index.html, (2021).
[2] Y. Dou, L. Sun, J. Ren, L. Dong, Opportunities and future challenges in hydrogen economy for sustainable development, Hydrogen economy, Elsevier2017, pp. 277-305.
[3] W.H. Johnson, On some remarkable changes produced in iron and steel by the action of hydrogen and acids, Nature Publishing Group, 1875.
[4] R.P. Gangloff, B.P. Somerday, Gaseous hydrogen embrittlement of materials in energy technologies: mechanisms, modelling and future developments, Elsevier2012.
[5] Y.-S. Chen, D. Haley, S.S. Gerstl, A.J. London, F. Sweeney, R.A. Wepf, W.M. Rainforth, P.A. Bagot, M.P. Moody, Direct observation of individual hydrogen atoms at trapping sites in a ferritic steel, Science 355(6330) (2017) 1196-1199.
[6] D.C. Rapaport, D.C.R. Rapaport, The art of molecular dynamics simulation, Cambridge university press2004.
[7] G.S. Frankel, J.D. Vienna, J. Lian, J.R. Scully, S. Gin, J.V. Ryan, J. Wang, S.H. Kim, W. Windl, J. Du, A comparative review of the aqueous corrosion of glasses, crystalline ceramics, and metals, npj Materials Degradation 2(1) (2018) 1-17.
[8] J.P. Hanson, A. Bagri, J. Lind, P. Kenesei, R.M. Suter, S. Gradecak, M.J. Demkowicz, Crystallographic character of grain boundaries resistant to hydrogen-assisted fracture in Ni-base alloy 725, Nature Communications 9 (2018).
[9] H.C. Rogers, Hydrogen Embrittlement of Metals: Atomic hydrogen from a variety of sources reduces the ductility of many metals, Science 159(3819) (1968) 1057-1064.
[10] S. Lynch, Hydrogen embrittlement phenomena and mechanisms, Corrosion Reviews 30(3-4) (2012) 105-123.
[11] I.M. Robertson, P. Sofronis, A. Nagao, M.L. Martin, S. Wang, D.W. Gross, K.E. Nygren, Hydrogen Embrittlement Understood, Metallurgical and Materials Transactions B-Process Metallurgy and Materials Processing Science 46(3) (2015) 1085-1103.
[12] P. Gong, J. Nutter, P.E.J. Rivera-Diaz-Del-Castillo, W.M. Rainforth, Hydrogen embrittlement through the formation of low-energy dislocation nanostructures in nanoprecipitation-strengthened steels, Science Advances 6(46) (2020).
[13] M.L. Martin, B.P. Somerday, R.O. Ritchie, P. Sofronis, I.M. Robertson, Hydrogen-induced intergranular failure in nickel revisited, Acta Materialia 60(6-7) (2012) 2739-2745.
[14] S. Wang, M.L. Martin, I.M. Robertson, P. Sofronis, Effect of hydrogen environment on the separation of Fe grain boundaries, Acta Materialia 107 (2016) 279-288.
[15] E. Pouillier, A.F. Gourgues, D. Tanguy, E.P. Busso, A study of intergranular fracture in an aluminium alloy due to hydrogen embrittlement, International Journal of Plasticity 34 (2012) 139-153.
[16] Z.D. Harris, S.K. Lawrence, D.L. Medlin, G. Guetard, J.T. Burns, B.P. Somerday, Elucidating the contribution of mobile hydrogen-deformation interactions to hydrogen-induced intergranular cracking in polycrystalline nickel, Acta Materialia 158 (2018) 180-192.
[17] L.B. Pfeil, The effect of occluded hydrogen on the tensile strength of iron, Proceedings of the Royal Society of London. Series A, Containing Papers of a Mathematical and Physical Character 112(760) (1926) 182-195.
[18] A.R. Troiano, The Role of Hydrogen and Other Interstitials in the Mechanical Behavior of Metals (1959 Edward De Mille Campbell Memorial Lecture), Metallography Microstructure and Analysis 5(6) (2016) 557-569.

[19] G. Lu, E. Kaxiras, Hydrogen embrittlement of aluminum: The crucial role of vacancies, Physical Review Letters 94(15) (2005).
[20] H. Zhao, P. Chakraborty, D. Ponge, T. Hickel, B. Sun, C.-H. Wu, B. Gault, D. Raabe, Hydrogen trapping and embrittlement in high-strength Al-alloys, arXiv preprint arXiv:2201.04490 (2022).
[21] R.A. Oriani, Mechanistic Theory of Hydrogen Embrittlement of Steels, Berichte Der Bunsen-Gesellschaft Fur Physikalische Chemie 76(8) (1972) 848-&.
[22] J. Song, W.A. Curtin, Mechanisms of hydrogen-enhanced localized plasticity: An atomistic study using alpha-Fe as a model system, Acta Materialia 68 (2014) 61-69.
[23] C.J. McMahon, Hydrogen-induced intergranular fracture of steels, Engineering Fracture Mechanics 68(6) (2001) 773-788.
[24] W. Gerberich, P. Marsh, J. Hoehn, Hydrogen induced cracking mechanisms-are there critical experiments?, Proceedings of the 1994 5th International Conference on the Effect of Hydrogen on the Behavior of Materials, Minerals, Metals & Materials Soc (TMS), 1996, pp. 539-551.
[25] K. Wada, J. Yamabe, H. Matsunaga, Visualization of trapped hydrogen along grain boundaries and its quantitative contribution to hydrogen-induced intergranular fracture in pure nickel, Materialia 8 (2019).
[26] Y.S. Chen, H.Z. Lu, J.T. Liang, A. Rosenthal, H.W. Liu, G. Sneddon, I. McCarroll, Z.Z. Zhao, W. Li, A.M. Guo, J.M. Cairney, Observation of hydrogen trapping at dislocations, grain boundaries, and precipitates, Science 367(6474) (2020) 171-+.
[27] M.S. Daw, M.I. Baskes, Application of the embedded atom method to hydrogen embrittlement, Chemistry and physics of fracture, Springer1987, pp. 196-218.
[28] C.L. Fu, G.S. Painter, 1st Principles Investigation of Hydrogen Embrittlement in Feal, Journal of Materials Research 6(4) (1991) 719-723.
[29] M. Yamaguchi, J. Kameda, K.-I. Ebihara, M. Itakura, H. Kaburaki, Mobile effect of hydrogen on intergranular decohesion of iron: first-principles calculations, Philosophical Magazine 92(11) (2012) 1349-1368.
[30] M. Yamaguchi, First-principles study on the grain boundary embrittlement of metals by solute segregation: Part I. iron (Fe)-solute (B, C, P, and S) systems, Metallurgical and Materials Transactions A 42(2) (2011) 319-329.
[31] D.E. Jiang, E.A. Carter, First principles assessment of ideal fracture energies of materials with mobile impurities: implications for hydrogen embrittlement of metals, Acta Materialia 52(16) (2004) 4801-4807.
[32] F.H. Wang, C.Y. Wang, First-principles investigation of hydrogen embrittlement in polycrystalline Ni3Al, Physical Review B 57(1) (1998) 289-295.
[33] A. Tehranchi, X. Zhou, W.A. Curtin, A decohesion pathway for hydrogen embrittlement in nickel: Mechanism and quantitative prediction, Acta Materialia 185 (2020) 98-109.
[34] T. Neeraj, R. Srinivasan, J. Li, Hydrogen embrittlement of ferritic steels: Observations on deformation microstructure, nanoscale dimples and failure by nanovoiding, Acta Materialia 60(13-14) (2012) 5160-5171.
[35] A. Tehranchi, W.A. Curtin, Atomistic study of hydrogen embrittlement of grain boundaries in nickel: II. Decohesion, Modelling and Simulation in Materials Science and Engineering 25(7) (2017).
[36] C.D. Beachem, A new model for hydrogen-assisted cracking (hydrogen “embrittlement”), Metallurgical and Materials Transactions B 3(2) (1972) 441-455.
[37] H.K. Birnbaum, P. Sofronis, Hydrogen-enhanced localized plasticity—a mechanism for hydrogen-related fracture, Materials Science and Engineering: A 176(1-2) (1994) 191-202.

[38] I.M. Robertson, H.K. Birnbaum, An Hvem Study of Hydrogen Effects on the Deformation and Fracture of Nickel, Acta Metallurgica 34(3) (1986) 353-366.
[39] G. Bond, I. Robertson, H. Birnbaum, The influence of hydrogen on deformation and fracture processes in high-strength aluminum alloys, Acta Metallurgica 35(9) (1987) 2289-2296.
[40] I.M. Robertson, T. Tabata, W. Wei, F. Heubaum, H.K. Birnbaum, Hydrogen Embrittlement and Grain-Boundary Fracture, Scripta Metallurgica 18(8) (1984) 841-846.
[41] P.J. Ferreira, I.M. Robertson, H.K. Birnbaum, Hydrogen effects on the interaction between dislocations, Acta Materialia 46(5) (1998) 1749-1757.
[42] P.J. Ferreira, I.M. Robertson, H.K. Birnbaum, Hydrogen effects on the character of dislocations in high-purity aluminum, Acta Materialia 47(10) (1999) 2991-2998.
[43] S.M. Myers, M.I. Baskes, H.K. Birnbaum, J.W. Corbett, G.G. Deleo, S.K. Estreicher, E.E. Haller, P. Jena, N.M. Johnson, R. Kirchheim, S.J. Pearton, M.J. Stavola, Hydrogen Interactions with Defects in Crystalline Solids, Reviews of Modern Physics 64(2) (1992) 559-617.
[44] R. Matsumoto, S. Taketomi, S. Matsumoto, N. Miyazaki, Atomistic simulations of hydrogen embrittlement, International Journal of Hydrogen Energy 34(23) (2009) 9576-9584.
[45] H. Birnbaum, I. Robertson, P. Sofronis, D. Teter, Mechanisms of hydrogen related fracture--a review, Second International Conference on Corrosion-Deformation Interactions. CDI'96, 1996, pp. 172-195.
[46] D. Shih, I. Robertson, H. Birnbaum, Hydrogen embrittlement of α titanium: in situ TEM studies, Acta Metallurgica 36(1) (1988) 111-124.
[47] P. Ferreira, I.M. Robertson, H. Birnbaum, Influence of hydrogen on the stacking-fault energy of an austenitic stainless steel, Materials Science Forum, 1996.
[48] I.M. Robertson, The effect of hydrogen on dislocation dynamics, Engineering Fracture Mechanics 64(5) (1999) 649-673.
[49] S. Wang, M.L. Martin, P. Sofronis, S. Ohnuki, N. Hashimoto, I.M. Robertson, Hydrogen-induced intergranular failure of iron, Acta Materialia 69 (2014) 275-282.
[50] S. Wang, A. Nagao, K. Edalati, Z. Horita, I.M. Robertson, Influence of hydrogen on dislocation self-organization in Ni, Acta Materialia 135 (2017) 96-102.
[51] A. Nagao, C.D. Smith, M. Dadfarnia, P. Sofronis, I.M. Robertson, The role of hydrogen in hydrogen embrittlement fracture of lath martensitic steel, Acta Materialia 60(13-14) (2012) 5182-5189.
[52] M.L. Martin, M. Dadfarnia, A. Nagao, S. Wang, P. Sofronis, Enumeration of the hydrogen-enhanced localized plasticity mechanism for hydrogen embrittlement in structural materials, Acta Materialia 165 (2019) 734-750.
[53] M.L. Martin, A new approach to discovering the fundamental mechanisms of hydrogen failure, University of Illinois at Urbana-Champaign2013.
[54] J. Song, W. Curtin, Mechanisms of hydrogen-enhanced localized plasticity: an atomistic study using α-Fe as a model system, Acta Materialia 68 (2014) 61-69.
[55] G. Bond, I. Robertson, H. Birnbaum, Effects of hydrogen on deformation and fracture processes in high-ourity aluminium, Acta Metallurgica 36(8) (1988) 2193-2197.
[56] M.L. Martin, I.M. Robertson, P. Sofronis, Interpreting hydrogen-induced fracture surfaces in terms of deformation processes: A new approach, Acta Materialia 59(9) (2011) 3680-3687.
[57] S. Lynch, Interpreting hydrogen-induced fracture surfaces in terms of deformation processes: A new approach, Scripta Materialia 65(10) (2011) 851-854.
[58] S. Lynch, Discussion of some recent literature on hydrogen-embrittlement mechanisms: addressing common misunderstandings, Corrosion Reviews 37(5) (2019) 377-395.
[59] H. Wilsdorf, The ductile fracture of metals: a microstructural viewpoint, Materials Science and Engineering 59(1) (1983) 1-39.

[60] R. Lyles Jr, H. Wilsdorf, Microcrack nucleation and fracture in silver crystals, Acta Metallurgica 23(2) (1975) 269-277.
[61] H.G. Wilsdorf, The role of glide and twinning in the final separation of ruptured gold crystals, Acta Metallurgica 30(6) (1982) 1247-1258.
[62] Y. Fukai, N. Ōkuma, Formation of superabundant vacancies in Pd hydride under high hydrogen pressures, Physical review letters 73(12) (1994) 1640.
[63] Y. Fukai, The metal-hydrogen system: basic bulk properties, Springer Science & Business Media2006.
[64] C. Buckley, H. Birnbaum, J. Lin, S. Spooner, D. Bellmann, P. Staron, T. Udovic, E. Hollar, Characterization of H defects in the aluminium–hydrogen system using small-angle scattering techniques, Journal of applied crystallography 34(2) (2001) 119-129.
[65] Y. Fukai, Superabundant vacancies formed in metal–hydrogen alloys, Physica Scripta 2003(T103) (2003) 11.
[66] M. Nagumo, Hydrogen related failure of steels–a new aspect, Mater Sci Tech-Lond 20(8) (2004) 940-950.
[67] M. Nagumo, K. Takai, The predominant role of strain-induced vacancies in hydrogen embrittlement of steels: Overview, Acta Materialia 165 (2019) 722-733.
[68] A. Ikeda, H. Suzuki, K. Takai, Hydrogen desorption spectra of hydrogen-enhanced strain-induced vacancies in pure iron, CAMP ISIJ2017, p. 857.
[69] K. Sakaki, T. Kawase, M. Hirato, M. Mizuno, H. Araki, Y. Shirai, M. Nagumo, The effect of hydrogen on vacancy generation in iron by plastic deformation, Scripta materialia 55(11) (2006) 1031-1034.
[70] S.K. Lawrence, Y. Yagodzinskyy, H. Hanninen, E. Korhonen, F. Tuomisto, Z.D. Harris, B.P. Somerday, Effects of grain size and deformation temperature on hydrogen-enhanced vacancy formation in Ni alloys, Acta Materialia 128 (2017) 218-226.
[71] D. Tanguy, Y. Wang, D. Connetable, Stability of vacancy-hydrogen clusters in nickel from first-principles calculations, Acta Materialia 78 (2014) 135-143.
[72] R. Nazarov, T. Hickel, J. Neugebauer, First-principles study of the thermodynamics of hydrogen-vacancy interaction in fcc iron, Physical Review B 82(22) (2010) 224104.
[73] X.S. Kong, S. Wang, X. Wu, Y.W. You, C.S. Liu, Q.F. Fang, J.L. Chen, G.N. Luo, First-principles calculations of hydrogen solution and diffusion in tungsten: Temperature and defect-trapping effects, Acta Materialia 84 (2015) 426-435.
[74] W. Geng, L. Wan, J.-P. Du, A. Ishii, N. Ishikawa, H. Kimizuka, S. Ogata, Hydrogen bubble nucleation in α-iron, Scripta Materialia 134 (2017) 105-109.
[75] J. Hou, X.S. Kong, X.B. Wu, J. Song, C.S. Liu, Predictive model of hydrogen trapping and bubbling in nanovoids in bcc metals, Nature Materials 18(8) (2019) 833-+.
[76] S.Z. Li, Y.G. Li, Y.C. Lo, T. Neeraj, R. Srinivasan, X.D. Ding, J. Sun, L. Qi, P. Gumbsch, J. Li, The interaction of dislocations and hydrogen-vacancy complexes and its importance for deformation-induced proto nano-voids formation in alpha-Fe, International Journal of Plasticity 74 (2015) 175-191.
[77] Y.X. Zhu, Z.H. Li, M.S. Huang, H.D. Fan, Study on interactions of an edge dislocation with vacancy-H complex by atomistic modelling, International Journal of Plasticity 92 (2017) 31-44.
[78] D.-G. Xie, Z.-J. Wang, J. Sun, J. Li, E. Ma, Z.-W. Shan, In situ study of the initiation of hydrogen bubbles at the aluminium metal/oxide interface, Nature materials 14(9) (2015) 899-903.
[79] M.C. Tiegel, M.L. Martin, A.K. Lehmberg, M. Deutges, C. Borchers, R. Kirchheim, Crack and blister initiation and growth in purified iron due to hydrogen loading, Acta Materialia 115 (2016) 24-34.

[80] S. Jothi, S. Merzlikin, T. Croft, J. Andersson, S. Brown, An investigation of micro-mechanisms in hydrogen induced cracking in nickel-based superalloy 718, Journal of Alloys and Compounds 664 (2016) 664-681.
[81] D.M. Symons, A.W. Thompson, The effect of hydrogen on the fracture of alloy X-750, Metallurgical and Materials Transactions A 27(1) (1996) 101-110.
[82] T. Homma, T. Chiba, K. Takai, E. Akiyama, W. Oshikawa, M. Nagumo, Cracking Process in Delayed Fracture of High-Strength Steel after Long Atmospheric Exposure, ISIJ International (2022) ISIJINT-2021-238.
[83] T. Neeraj, R. Srinivasan, Hydrogen Embrittlement of Steels: Vacancy Induced Damage and Nano-Voiding Mechanisms, Corrosion 73(4) (2017) 437-447.
[84] S. Lynch, Environmentally assisted cracking: overview of evidence for an adsorption-induced localised-slip process, Acta Metallurgica 36(10) (1988) 2639-2661.
[85] S. Lynch, Metallographic contributions to understanding mechanisms of environmentally assisted cracking, Metallography 23(2) (1989) 147-171.
[86] R. Kirchheim, Revisiting hydrogen embrittlement models and hydrogen-induced homogeneous nucleation of dislocations, Scripta Materialia 62(2) (2010) 67-70.
[87] R. Kirchheim, Reducing grain boundary, dislocation line and vacancy formation energies by solute segregation. I. Theoretical background, Acta Materialia 55(15) (2007) 5129-5138.
[88] R. Kirchheim, Solubility, diffusivity and trapping of hydrogen in dilute alloys. Deformed and amorphous metals—II, Acta Metallurgica 30(6) (1982) 1069-1078.
[89] A. Barnoush, H. Vehoff, In situ electrochemical nanoindentation: A technique for local examination of hydrogen embrittlement, Corrosion Science 50(1) (2008) 259-267.
[90] A. Barnoush, H. Vehoff, Recent developments in the study of hydrogen embrittlement: Hydrogen effect on dislocation nucleation, Acta Materialia 58(16) (2010) 5274-5285.
[91] A. Barnoush, M. Asgari, R. Johnsen, Resolving the hydrogen effect on dislocation nucleation and mobility by electrochemical nanoindentation, Scripta Materialia 66(6) (2012) 414-417.
[92] D.G. Westlake, A Generalized Model for Hydrogen Embrittlement, Asm Transactions Quarterly 62(4) (1969) 1000-&.
[93] H.K. Birnbaum, Mechanisms of hydrogen related fracture of metals, ILLINOIS UNIV AT URBANA DEPT OF MATERIALS SCIENCE AND ENGINEERING, 1989.
[94] M.B. Djukic, G.M. Bakic, V.S. Zeravcic, A. Sedmak, B. Rajicic, The synergistic action and interplay of hydrogen embrittlement mechanisms in steels and iron: Localized plasticity and decohesion, Engineering Fracture Mechanics 216 (2019).
[95] M. Lin, H. Yu, Y. Ding, G. Wang, V. Olden, A. Alvaro, J. He, Z. Zhang, A predictive model unifying hydrogen enhanced plasticity and decohesion, Scripta Materialia 215 (2022) 114707.
[96] B. Sun, D. Wang, X. Lu, D. Wan, D. Ponge, X. Zhang, Current challenges and opportunities toward understanding hydrogen embrittlement mechanisms in advanced high-strength steels: a review, Acta Metallurgica Sinica (English Letters) 34(6) (2021) 741-754.
[97] J. Song, W.A. Curtin, A nanoscale mechanism of hydrogen embrittlement in metals, Acta Materialia 59(4) (2011) 1557-1569.
[98] J. Song, W.A. Curtin, Atomic mechanism and prediction of hydrogen embrittlement in iron, Nature Materials 12(2) (2013) 145-151.
[99] A. Tehranchi, W.A. Curtin, The role of atomistic simulations in probing hydrogen effects on plasticity and embrittlement in metals, Engineering Fracture Mechanics 216 (2019).
[100] D.G. Xie, S.Z. Li, M. Li, Z.J. Wang, P. Gumbsch, J. Sun, E. Ma, J. Li, Z.W. Shan, Hydrogenated vacancies lock dislocations in aluminium, Nature Communications 7 (2016).

[101] L. Wan, W.T. Geng, A. Ishii, J.P. Du, Q.S. Mei, N. Ishikawa, H. Kimizuka, S. Ogata, Hydrogen embrittlement controlled by reaction of dislocation with grain boundary in alpha-iron, International Journal of Plasticity 112 (2019) 206-219.
[102] S. Yin, G.M. Cheng, T.H. Chang, G. Richter, Y. Zhu, H.J. Gao, Hydrogen embrittlement in metallic nanowires, Nature Communications 10 (2019).
[103] Y.-W. You, X.-S. Kong, X.-B. Wu, Y.-C. Xu, Q. Fang, J. Chen, G.-N. Luo, C. Liu, B. Pan, Z. Wang, Dissolving, trapping and detrapping mechanisms of hydrogen in bcc and fcc transition metals, AIP advances 3(1) (2013) 012118.
[104] R. Nazarov, T. Hickel, J. Neugebauer, Ab initio study of H-vacancy interactions in fcc metals: Implications for the formation of superabundant vacancies, Physical Review B 89(14) (2014) 144108.
[105] X.-S. Kong, S. Wang, X. Wu, Y.-W. You, C. Liu, Q. Fang, J.-L. Chen, G.-N. Luo, First-principles calculations of hydrogen solution and diffusion in tungsten: Temperature and defect-trapping effects, Acta Materialia 84 (2015) 426-435.
[106] N. Fernandez, Y. Ferro, D. Kato, Hydrogen diffusion and vacancies formation in tungsten: Density Functional Theory calculations and statistical models, Acta Materialia 94 (2015) 307-318.
[107] S. Taketomi, R. Matsumoto, N. Miyazaki, Atomistic study of hydrogen distribution and diffusion around a {1 1 2}< 1 1 1> edge dislocation in alpha iron, Acta Mater 56(15) (2008) 3761-3769.
[108] J. Von Pezold, L. Lymperakis, J. Neugebeauer, Hydrogen-enhanced local plasticity at dilute bulk H concentrations: The role of H–H interactions and the formation of local hydrides, Acta Materialia 59(8) (2011) 2969-2980.
[109] P. Yu, Y.G. Cui, G.Z. Zhu, Y. Shen, M. Wen, The key role played by dislocation core radius and energy in hydrogen interaction with dislocations, Acta Materialia 185 (2020) 518-527.
[110] Y.-H. Li, H.-B. Zhou, F. Gao, G. Lu, G.-H. Lu, F. Liu, Hydrogen induced dislocation core reconstruction in bcc tungsten, Acta Materialia 226 (2022) 117622.
[111] B. Kuhr, D. Farkas, I.M. Robertson, Atomistic studies of hydrogen effects on grain boundary structure and deformation response in FCC Ni, Computational Materials Science 122 (2016) 92-101.
[112] K.N. Solanki, M.A. Tschopp, M.A. Bhatia, N.R. Rhodes, Atomistic Investigation of the Role of Grain Boundary Structure on Hydrogen Segregation and Embrittlement in alpha-Fe, Metall Mater Trans A 44a(3) (2013) 1365-1375.
[113] J. Li, C. Lu, L. Pei, C. Zhang, R. Wang, Atomistic investigation of hydrogen induced decohesion of Ni grain boundaries, Mechanics of Materials 150 (2020) 103586.
[114] A. Tehranchi, W. Curtin, Atomistic study of hydrogen embrittlement of grain boundaries in nickel: II. Decohesion, Modelling and Simulation in Materials Science and Engineering 25(7) (2017) 075013.
[115] J. Chen, S. Liang, Y. Zhu, L. Zhao, M. Huang, Z. Li, Studying crack propagation along symmetric tilt grain boundary with H segregation in Ni by MD simulation, Computational Materials Science 212 (2022) 111569.
[116] Z. Zhao, B. Safaei, Y. Wang, Y. Liu, F. Chu, Y. Wei, Atomistic scale behaviors of intergranular crack propagation along twist grain boundary in iron under dynamic loading, Engineering Fracture Mechanics 273 (2022) 108731.
[117] X. Xing, H. Zhang, G. Cui, J. Liu, Z. Li, Hydrogen inhibited phase transition near crack tip–An atomistic mechanism of hydrogen embrittlement, International Journal of Hydrogen Energy 44(31) (2019) 17146-17153.

[118] X. Xing, Y. Zhang, S. Wang, Z. Li, C. Yang, G. Cui, S. Zhang, J. Liu, J. Gou, H. Yu, Atomistic simulation of hydrogen-induced plastic zone compression during cyclic loading, International Journal of Hydrogen Energy 45(31) (2020) 15697-15709.
[119] R. Zamora, A. Nair, R. Hennig, D. Warner, Ab initio prediction of environmental embrittlement at a crack tip in aluminum, Physical Review B 86(6) (2012) 060101.
[120] Y.-L. Liu, Y. Zhang, H.-B. Zhou, G.-H. Lu, F. Liu, G.-N. Luo, Vacancy trapping mechanism for hydrogen bubble formation in metal, Physical Review B 79(17) (2009) 172103.
[121] W. Xing, X.-Q. Chen, Q. Xie, G. Lu, D. Li, Y. Li, Unified mechanism for hydrogen trapping at metal vacancies, international journal of hydrogen energy 39(21) (2014) 11321-11327.
[122] K. Ohsawa, J. Goto, M. Yamakami, M. Yamaguchi, M. Yagi, Trapping of multiple hydrogen atoms in a tungsten monovacancy from first principles, Physical Review B 82(18) (2010) 184117.
[123] S. Li, Y. Li, Y.-C. Lo, T. Neeraj, R. Srinivasan, X. Ding, J. Sun, L. Qi, P. Gumbsch, J. Li, The interaction of dislocations and hydrogen-vacancy complexes and its importance for deformation-induced proto nano-voids formation in α-Fe, International Journal of Plasticity 74 (2015) 175-191.
[124] A. Tehranchi, W.A. Curtin, Atomistic study of hydrogen embrittlement of grain boundaries in nickel: I. Fracture, Journal of the Mechanics and Physics of Solids 101 (2017) 150-165.
[125] S. Taketomi, R. Matsumoto, N. Miyazaki, Atomistic study of the effect of hydrogen on dislocation emission from a mode II crack tip in alpha iron, International Journal of Mechanical Sciences 52(2) (2010) 334-338.
[126] P.R. Cantwell, M. Tang, S.J. Dillon, J. Luo, G.S. Rohrer, M.P. Harmer, Grain boundary complexions, Acta Materialia 62 (2014) 1-48.
[127] A. Oudriss, J. Creus, J. Bouhattate, E. Conforto, C. Berziou, C. Savall, X. Feaugas, Grain size and grain-boundary effects on diffusion and trapping of hydrogen in pure nickel, Acta Materialia 60(19) (2012) 6814-6828.
[128] S. Bechtle, M. Kumar, B.P. Somerday, M.E. Launey, R.O. Ritchie, Grain-boundary engineering markedly reduces susceptibility to intergranular hydrogen embrittlement in metallic materials, Acta Materialia 57(14) (2009) 4148-4157.
[129] A. Oudriss, J. Creus, J. Bouhattate, C. Savall, B. Peraudeau, X. Feaugas, The diffusion and trapping of hydrogen along the grain boundaries in polycrystalline nickel, Scripta Materialia 66(1) (2012) 37-40.
[130] M. Koyama, D. Yamasaki, K. Tsuzaki, Reply to comments on the paper "In situ observations of silver-decoration evolution under hydrogen permeation: Effects of grain boundary misorientation on hydrogen flux in pure iron" by Gavriljuk and Teus, Scripta Materialia 140 (2017) 91-92.
[131] K. Wada, J. Yamabe, Y. Ogawa, O. Takakuwa, T. Iijima, H. Matsunaga, Comparative study of hydrogen-induced intergranular fracture behavior in Ni and Cu-Ni alloy at ambient and cryogenic temperatures, Mat Sci Eng a-Struct 766 (2019).
[132] J. Yao, C. Jr, Experimental Studies of Grain-Boundary Diffusion of Hydrogen in Metals, Acta Metallurgica Et Materialia 39(1) (1991) 119-126.
[133] P. Cotterill, The Hydrogen Embrittlement of Metals, Progress in Materials Science 9(4) (1961) 205-301.
[134] S. Jothi, T.N. Croft, S.G.R. Brown, Influence of grain boundary misorientation on hydrogen embrittlement in bi-crystal nickel, International Journal of Hydrogen Energy 39(35) (2014) 20671-20688.

[135] S. Huang, D.K. Chen, J. Song, D.L. McDowell, T. Zhu, Hydrogen embrittlement of grain boundaries in nickel: an atomistic study, Npj Computational Materials 3 (2017).
[136] X. Zhou, D. Marchand, D.L. McDowell, T. Zhu, J. Song, Chemomechanical Origin of Hydrogen Trapping at Grain Boundaries in fcc Metals, Physical Review Letters 116(7) (2016).
[137] X. Zhou, N. Mousseau, J. Song, Is Hydrogen Diffusion along Grain Boundaries Fast or Slow? Atomistic Origin and Mechanistic Modeling, Physical Review Letters 122(21) (2019).
[138] S. He, W. Ecker, R. Pippan, V.I. Razumovskiy, Hydrogen-enhanced decohesion mechanism of the special Σ5 (0 1 2)[1 0 0] grain boundary in Ni with Mo and C solutes, Computational Materials Science 167 (2019) 100-110.
[139] D. Di Stefano, M. Mrovec, C. Elsasser, First-principles investigation of hydrogen trapping and diffusion at grain boundaries in nickel, Acta Materialia 98 (2015) 306-312.
[140] J. Yao, J. Cahoon, Theoretical modeling of gain boundary diffusion of hydrogen and its effect on permeation curves, Acta metallurgica et materialia 39(1) (1991) 111-118.
[141] A. Oudriss, S. LeGuernic, Z. Wang, B.O. Hoch, J. Bouhattate, E. Conforto, Z. Zhu, D.S. Li, X. Feaugas, Meso-scale anisotropic hydrogen segregation near grain-boundaries in polycrystalline nickel characterized by EBSD/SIMS, Materials Letters 165 (2016) 217-222.
[142] J. Li, C. Lu, L. Pei, C. Zhang, R. Wang, K. Tieu, Influence of hydrogen environment on dislocation nucleation and fracture response of< 1 1 0> grain boundaries in nickel, Computational Materials Science 165 (2019) 40-50.
[143] Y. Zhu, Z. Li, M. Huang, Solute hydrogen effects on plastic deformation mechanisms of α-Fe with twist grain boundary, International Journal of Hydrogen Energy 43(22) (2018) 10481-10495.

Appendix A Appended Papers

A.1 Paper 1

Hydrogen-induced transgranular to intergranular fracture transition in bi-crystalline nickel

Authors: Yu Ding, Haiyang Yu, Kai Zhao, Meichao Lin, Senbo Xiao, Michael Ortiz, Jianying He, Zhiliang Zhang

Scripta Materialia 204 (2021): 114122.

Paper 1

Scripta Materialia 204 (2021) 114122

Contents lists available at ScienceDirect

Scripta Materialia

journal homepage: www.elsevier.com/locate/scriptamat

Hydrogen-induced transgranular to intergranular fracture transition in bi-crystalline nickel

Yu Ding[a], Haiyang Yu[b], Kai Zhao[c], Meichao Lin[a], Senbo Xiao[a], Michael Ortiz[d], Jianying He[a], Zhiliang Zhang[a,*]

[a] Department of Structural Engineering, Norwegian University of Science and Technology (NTNU), Trondheim 7491, Norway
[b] Division of Applied Mechanics, Department of Materials Science and Engineering, Uppsala University, Uppsala SE-75121, Sweden
[c] Jiangsu Key Laboratory of Advanced Food Manufacturing Equipment and Technology, Jiangnan University, Wuxi 214122, China
[d] Graduate Aerospace Laboratories, California Institute of Technology, 1200 E. California Blvd., Pasadena, CA 91125, United States

ARTICLE INFO

Article history:
Received 31 May 2021
Revised 28 June 2021
Accepted 28 June 2021

Keywords:
Hydrogen embrittlement
Fracture
Grain boundary
Molecular dynamics (MD)

ABSTRACT

It is known that hydrogen can influence the dislocation plasticity and fracture mode transition of metallic materials, however, the nanoscale interaction mechanism between hydrogen and grain boundary largely remains illusive. By uniaxial straining of bi-crystalline Ni with a $\Sigma5(210)[001]$ grain boundary, a transgranular to intergranular fracture transition facilitated by hydrogen is elucidated by atomistic modeling, and a specific hydrogen-controlled plasticity mechanism is revealed. Hydrogen is found to form a local atmosphere in the vicinity of grain boundary, which induces a local stress concentration and inhibits the subsequent stress relaxation at the grain boundary during deformation. It is this local stress concentration that promotes earlier dislocation emission, twinning evolution, and generation of more vacancies that facilitate nanovoiding. The nucleation and growth of nanovoids finally leads to intergranular fracture at the grain boundary, in contrast to the transgranular fracture of hydrogen-free sample.

As indicated by its name, a key feature of hydrogen embrittlement (HE) [1–3] is the transition from ductile to "brittle" fracture in the presence of hydrogen. For polycrystalline materials, this transition is usually attributed to hydrogen-induced transgranular to intergranular fracture at the microscopic scale, observed in a large number of *ex-situ* experiments [4–7]. All the studies [8–16] show that grain boundary (GB) plays an important role in HE and the hydrogen-GB interactions hold the key to understanding the transgranular to intergranular fracture transition. Nowadays, it is well understood that the transition process may involve the synergistic action of several important HE mechanisms [11,17]. Three widely accepted mechanisms are hydrogen enhanced local plasticity (HELP), hydrogen enhanced decohesion (HEDE), and hydrogen enhanced strain-induced vacancy formation (HESIV). The theory of HELP [18–22] is based on the experimental evidence of enhanced dislocation mobility and well-evolved dislocation structures beneath the fracture surfaces of hydrogen-embrittled samples. However, there is still a large gap in the understanding of how this locally ductile behavior could lead to the eventual "brittle" fracture. HEDE [23–27] postulates that local accumulation of H at crack tips could contribute to the weakening of metal bonds resulting in fracture, but it does not make an explanation for the enhanced plasticity. HESIV [28–32] assumes that the vacancy clusters generated during plastic deformation are stabilized by forming H-vacancy complexes, which will further interact with the dislocations. However, the connection of those stabilized vacancies to embrittlement remains unexplained. All these mechanisms can be viable at the GBs, which is a material interface with intensive dislocation activity and high *H* trapping capacity [33]. The hydrogen-enhanced plasticity mediated failure mechanism [3] has been proposed as a connection between HELP and HEDE, trying to make a universal explanation to HE phenomena. It should be mentioned that the whole framework was established as a posteriori interpretation of evolved microstructures. The transition process of the fracture mode has not been directly demonstrated by *in-situ* experiment or simulation. Verification of this mechanism is one of the outstanding issues in HE research.

The interaction between hydrogen and grain boundary/material interface has been simulated both using the continuum approach [34] and the atomistic method [35]. Hydrogen segregation around GBs [36,37] and the influence of hydrogen on the propagation of an existing crack [38] have been elaborated. However, the direct transgranular to intergranular transition without an initial crack

* Corresponding author.
E-mail address: zhiliang.zhang@ntnu.no (Z. Zhang).

https://doi.org/10.1016/j.scriptamat.2021.114122

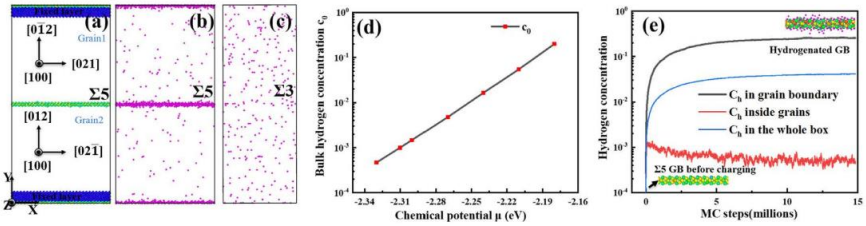

Fig. 1. (a) Equilibrium structures of perfect Σ5(210)[001] GB. (b, c) *H* distribution map for Σ5 GB and Σ3 CTB, respectively. (d) The relationship between Equilibrium bulk *H* concentration c_0 in perfect FCC Ni and chemical potential μ used in the charging process. (e) *H* concentration in the GB region (1 nm around GB), inside the grains, and in the whole box as a function of MC charging time.

has not been observed. Recent experimental studies [39–41] indicate that mobile H-deformation interaction is not an intrinsic requirement for H-induced intergranular fracture, implying that the initial *H* segregation on the GB is the key. But it is still unclear how the segregated *H* interacts with the GB. The present work zooms into the GB region with segregated *H* and probes the mechanisms behind H-induced intergranular fracture. A Σ5(210)[001] GB was created by constructing two separate crystals with desired crystallographic orientations and joining them along a plane normal to the Y-direction (Fig. 1a). The initial configuration was then modified by shifting the upper grain in the X-Z plane, deleting overlapping atoms, and applying the conjugate gradient method to equilibrate the system. The simulation box was divided into three regions: The vicinity ±1 nm to the GB as GB region, 1 nm thick region on the top of grain1 and bottom of grain2 as boundary layers to apply displacement controlled loading, and rest part as grains. Periodic boundary conditions were imposed along the *X* and *Z* directions while a free boundary condition was employed along the *Y* direction. After equilibrium in the isothermal–isobaric (NPT) ensemble at 300 K for 100 ps, the mixed grand canonical Monte Carlo (GCMC)/molecular dynamic (MD) method was utilized to obtain the dynamic trapping map around the GB. For the GCMC implementation, the system was kept at constant chemical potential μ, volume *V* and temperature *T*. There is a relationship between chemical potential μ and equilibrium bulk *H* concentration c_0 in perfect lattice: $\mu = kT\ln c_0 + \Delta E$, where ΔE is the segregation energy of one *H* atom and *k* is the Boltzmann constant. During the *H* charging process, each step of GCMC runs (insertion or deletion of one randomly chosen *H* atom) was followed by 50 steps of MD runs in canonical (NVT) ensemble until the *H* concentration fluctuates in a narrow range (±1% atomic ratio). The simulations were first performed for the perfect FCC Ni lattice without GB, to obtain the relationship between c_0 and μ (Fig. 1d). Then $\mu = -2.31$ eV was chosen as the charging parameters for all the subsequent study corresponding to $c_0 = 0.001$ in the bulk grain. The equilibrium hydrogenated GB after charging was regarded as the 100% saturation case with the 0, 13, 25, 40, 60% saturation cases as comparison. After charging, the system was relaxed in the NPT ensemble for 100 ps. To obtain a realistic stress state in front of a crack tip and avoid unphysical elongation, uniaxial straining in the NVT ensemble was carried out by moving the upper boundary layer at a constant velocity of 2 m/s along *Y* direction while the lower layer is kept stationary. The atomic stress during deformation was analyzed by Viral theory [42], illustrations of all simulation snapshots were achieved by the coordination number centrosymmetry parameter [43] and common neighbor analysis (CNA) [44], and dislocations were identified by Ovito [45].

The *H* distribution during charging is shown in Fig. 1e. The *H* concentration in the grains and GB reaches $c_0 = 0.001$ in the first 100,000 MC steps. *H* atoms continue to pump into the GB region due to the high trapping energy and excess volumes in the subsequent MC steps. However, the *H* concentration inside the grains is slightly reduced and kept around $c = 0.0008$, which is mainly caused by the attractive interaction between the formed *H* atmosphere around the GB and newly inserted H. Finally, the GB structure reaches an equilibrium at $c = 0.25$ after 15,000,000 MC steps in Fig. 1b. The locally high *H* concentration agrees well with the experimental results [33] and theoretical calculation [46], indicating that this type of Σ5 GB could be a preferred gathering site for H. For comparison, a Σ3 coherent twin boundary (CTB) is charged under the same conditions. The evenly distributed *H* in Fig. 1c implies that CTB has an inconsequential effect to trap *H* because of the compact structure and few trapping sites, indicating that CTBs have good resistance to HE [16,47].

Fig. 2a shows the stress (Syy)-strain curve in the *Y* direction with varying *H* concentrations during deformation. Fig. 2c–h are the snapshots of the elastic stage, plastic stage, and final fracture for the cases without *H* and with *H* in the 100% saturation case, respectively. Without *H*, the sample fractured ($\varepsilon = 0.208$) with nanovoid nucleation in the grains near the upper boundary layer due to the accumulation of high-density dislocations. With *H* in the 100% saturation case, the sample fractured ($\varepsilon = 0.173$) with nanovoid nucleation on the GB. This shift of nanovoid nucleation site from grain interior to the GB caused by *H* is manifested as H-induced transgranular to intergranular fracture transition. The sample deforms mainly through the nucleation and gliding of 1/6<112> Shockley dislocations (green pipelines) and leaves the twins (red stacking fault) on the path in which they have glided. At the first drop of stress (critical stress), the twins start to grow and soon get pinned by the top and bottom boundary. The inserted *H* could facilitate earlier twinning nucleation ($\varepsilon = 0.08$ without *H* and $\varepsilon = 0.062$ with H) and decrease the critical stress (Syy = 11.06 GPa without *H* and $\varepsilon = 9.55$ GPa with *H*) during this stage. Higher *H* concentration could amplify those effects. To release the stress caused by subsequent deformation, more dislocations nucleate, multiplicate and exit on the GB, which generates more twins. These twins interact with each other in the junctions, further increasing the dislocation density. As shown in Fig. 2b, the twins volume fraction evolution displays a zig-zag pattern until fracture, which is the main plasticity activity during deformation. It should be noted that hydrogen promoted deformation twinning, revealed in the MD simulation, has not been experimentally observed in typical Ni microstructures [39,48–50]. This is probably because the MD simulation assumes no pre-existing dislocations before deformation, so continued plasticity dominated by dislocation gliding was source-controlled and twinning was facilitated, this can be the case for nanocrystalline Ni [51,52]. Therefore, caution should be taken when applying hydrogen-induced twinning mechanism in Ni, since this is likely applicable to highly specialized cases instead of the typical coarse-grained microstructures.

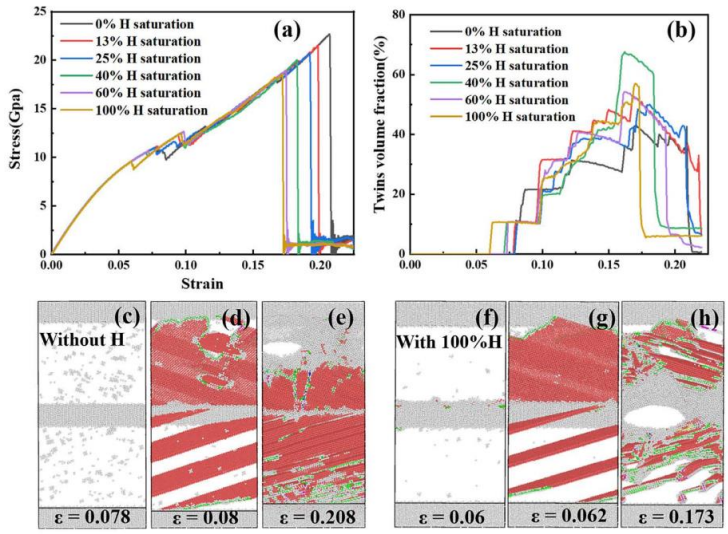

Fig. 2. (a) stress-strain curve in the *Y* direction for varying *H* concentrations. (b) Twins volume fraction as a function of strain with varying *H* concentration. (c–e) atomic structure without H at different strains. (f–h) atomic structure with 100% *H* at different strains. Only atoms in defect structure are colored, HCP atoms are marked red, white atoms indicate other type atoms, and green pipelines outline the 1/6<112> Shockley dislocations.

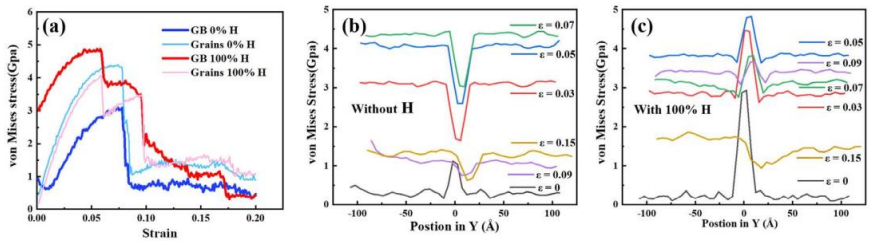

Fig. 3. (a) Average Von Mises stress-strain curve in different regions. (b, c) Average Von Mises stress distribution along the *Y* direction without or with *H*, respectively.

Nevertheless, this can still be a viable mechanism in a number of FCC alloys that undergo deformation twinning, such as in TWIP steels [53,54] or those with nanocrystalline grain structures. To better understand how *H* influences local plasticity, the average von Mises stress distribution along the *Y* direction in different regions is plotted in Fig. 3. It is interesting to note that in Fig. 3b the Σ5(210)[001] GB could release the initial stress and always keep its stress level lower than in the grains during deformation without H. This might be a good explanation for the huge amount of point defects in the grains without *H* (Fig. 2c) and the eventual transgranular fracture. The saturated *H* can increase the initial stress concentration in the GB region and more importantly inhibit the stress-releasing ability of the GB during deformation. The GB thus stays at an activated state [11] with a more disordered atomistic structure due to the higher stress level maintained at the GB than the grain interior, which induces the earlier twinning nucleation and void formation on the GB. Increased *H* concentration could increase the local stress concentration which induces more serious plastic deformation and earlier fracture.

Another important feature revealed in Fig. 2e,h is nanovoiding. In order to investigate the nanovoid formation mechanism, the process of vacancy formation, which could be the embryo of the final void [31], is analyzed in the GB region. The extremely distorted atoms are identified as vacancy cluster and the vacancy volume fraction-strain curve is plotted in Fig. 4a. It is found that there are few vacancies formed around the GB before twinning nucleation without *H*, but the fraction of vacancy volume comes to grow after more plasticity occurs around the GB. With *H*, the vacancy volume fraction comes to grow in the elastic stage which shows that the GB has entered a plasticity-activated state [33], and the vacancy volume fraction rises with increasing pre-charged *H* concentration. It indicates that *H* accelerates vacancy formation at early plasticity stage on the GB, possibly through lattice dislocation interaction and jog formation. Previous studies also show that vacancies could be stabilized by forming Va-H complexes [31,32], consistent with the high vacancy volume fraction observed in the *H* charged cases. Those Va-H complexes could be the reason for the earlier void formation with *H* in Fig. 4g.

In summary, by scrutinizing the tensile responses of Ni Σ5(210)[001] GB with varied hydrogen concentration using atomistic modeling, we demonstrate a transgranular to intergranular-fracture transition mechanism controlled by hydrogen-influenced

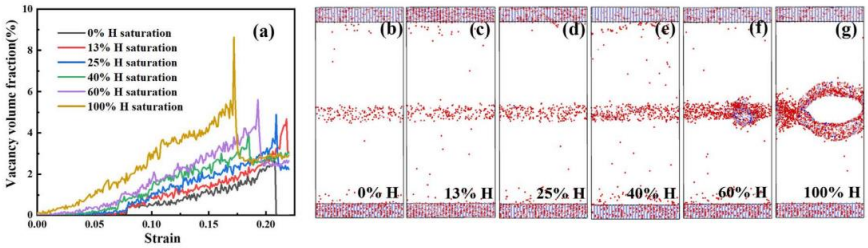

Fig. 4. (a) Vacancy volume fraction as a function of strain with varying H concentration. (b,–g) Snapshots of vacancy surface atoms at strain = 0.18 with varying *H* concentration. Only highly distorted atoms with coordination numbers less than 8 are colored.

plasticity. Compared with the Σ3 coherent twin GB which traps nearly no *H* atoms, *H* will form an atmosphere at the Σ5 GB due to the high trapping energy and excess volume and induce a higher initial local stress. In the case without *H*, less stress is built up at the Σ5 GB region during deformation, which leads to transgranular fracture. In contrast, *H* suppresses the stress-releasing ability of the Σ5 GB, which causes a local stress concentration and promotes local plasticity on the GB. This further leads to early dislocation emission, severe twinning evolution, increased number of vacancies and thus enhanced nanovoiding on the GB. The growth of nanovoids with *H* finally completes the transgranular to intergranular-fracture transition. This work reveals that hydrogen-grain boundary interaction and hydrogen enhanced vacancy formation are important factors in the hydrogen-induced intergranular fracture at room temperature. However, the influence of hydrogen on atomic bonds, i.e. the HEDE mechanism, was not examined here. According to Harris et al. [39], HEDE may play an important part in the process. Therefore, the transgranular to intergranular-fracture transition with hydrogen is likely due to the synergistic action of all the three mechanisms.

Declaration of Competing Interest

The authors declare that they have no known competing financial interests or personal relationships that could have appeared to influence the work reported in this paper.

Acknowledgments

Y.D. acknowledge the financial support provided by the Research Council of Norway under the M-HEAT project (Grant No. 294689). All simulations are carried out on the Fram (Grant No. NN9110K, NN9391K) high-performance computer clusters at NTNU, Trondheim, and Stallo at UiT, Tromsø.

Supplementary materials

Supplementary material associated with this article can be found, in the online version, at doi:10.1016/j.scriptamat.2021.114122.

References

[1] W.H. Johnson, W. Thomson, Proceedings of the Royal Society of London 23 (156–163) (1875) 168–179.
[2] R.P. Gangloff, B.P. Somerday, Gaseous Hydrogen Embrittlement of Materials in Energy Technologies: Mechanisms, Modelling and Future Developments, Elsevier, 2012.
[3] I.M. Robertson, P. Sofronis, A. Nagao, M.L. Martin, S. Wang, D.W. Gross, K.E. Nygren, Metall. Mater. Trans. B 46 (3) (2015) 1085–1103.
[4] S.P. Lynch, J. Mater. Sci. 21 (2) (1986) 692–704.
[5] C.J. McMahon, Eng. Fract. Mech. 68 (6) (2001) 773–788.
[6] M.L. Martin, B.P. Somerday, R.O. Ritchie, P. Sofronis, I.M. Robertson, Acta Mater. 60 (6–7) (2012) 2739–2745.
[7] S. Wang, M.L. Martin, P. Sofronis, S. Ohnuki, N. Hashimoto, I.M. Robertson, Acta Mater. 69 (2014) 275–282.
[8] A. Oudriss, J. Creus, J. Bouhattate, E. Conforto, C. Berziou, C. Savall, X. Feaugas, Acta Mater. 60 (19) (2012) 6814–6828.
[9] J. Chen, A.M. Dongare, J. Mater. Sci. 52 (1) (2017) 30–45.
[10] X. Zhou, D. Marchand, D.L. McDowell, T. Zhu, J. Song, Phys. Rev. Lett. 116 (7) (2016) 075–502.
[11] L. Wan, W.T. Geng, A. Ishii, J.P. Du, Q.S. Mei, N. Ishikawa, H. Kimizuka, S. Ogata, Int. J. Plast. 112 (2019) 206–219.
[12] J.Q. Li, C. Lu, L.Q. Pei, C. Zhang, R. Wang, K. Tieu, Comput. Mater. Sci. 165 (2019) 40–50.
[13] K. Zhao, J.Y. He, Z.L. Zhang, J. Appl. Phys. 127 (1) (2020) 015–101.
[14] H.Y. Yu, J.S. Olsen, V. Olden, A. Alvaro, J.Y. He, Z.L. Zhang, Eng. Fail. Anal. 81 (2017) 79–93.
[15] P. Sestak, M. Cerny, Z.L. Zhang, J. Pokluda, Crystals 10 (7) (2020) 590.
[16] S. Bechtle, M. Kumar, B.P. Somerday, M.E. Launey, R.O. Ritchie, Acta Mater. 57 (14) (2009) 4148–4157.
[17] P. Gong, J. Nutter, P.E.J. Rivera-Diaz-Del-Castillo, W.M. Rainforth, Sci. Adv. 6 (46) (2020) eabb6152.
[18] C.D. Beachem, Metall. Trans. 3 (2) (1972) 437–+.
[19] H.K. Birnbaum, P. Sofronis, Mater. Sci. Eng. A 176 (1–2) (1994) 191–202.
[20] M.L. Martin, J.A. Fenske, G.S. Liu, P. Sofronis, I.M. Robertson, Acta Mater. 59 (4) (2011) 1601–1606.
[21] T. Neeraj, R. Srinivasan, J. Li, Acta Mater. 60 (13–14) (2012) 5160–5171.
[22] A. Nagao, C.D. Smith, M. Dadfarnia, P. Sofronis, I.M. Robertson, Acta Mater. 60 (13–14) (2012) 5182–5189.
[23] A.R. Troiano, Metallogr. Microstruct. 5(6) (2016) 557–569.
[24] J.R. Rice, J.S. Wang, Mater. Sci. Eng. A Struct. 107 (1989) 23–40.
[25] S. Serebrinsky, E.A. Carter, M. Ortiz, J. Mech. Phys. Solids 52 (10) (2004) 2403–2430.
[26] J. Song, W.A. Curtin, Nat. Mater. 12 (2) (2013) 145–151.
[27] A. Tehranchi, W.A. Curtin, Model. Simul. Mater. Sci. 25 (7) (2017).
[28] M. Nagumo, M. Nakamura, K. Takai, Metallurgical and Materials Transactions A 32 (2) (2001) 339–347.
[29] K. Takai, H. Shoda, H. Suzuki, M. Nagumo, Acta Mater. 56 (18) (2008) 5158–5167.
[30] W.A. Counts, C. Wolverton, R. Gibala, Acta Mater. 58 (14) (2010) 4730–4741.
[31] S.Z. Li, Y.G. Li, Y.C. Lo, T. Neeraj, R. Srinivasan, X.D. Ding, J. Sun, L. Qi, P. Gumbsch, J. Li, Int. J. Plast. 74 (2015) 175–191.
[32] Y.X. Zhu, Z.H. Li, M.S. Huang, H.D. Fan, Int. J. Plast. 92 (2017) 31–44.
[33] Y.S. Chen, H.Z. Lu, J.T. Liang, A. Rosenthal, H.W. Liu, G. Sneddon, I. McCarroll, Z.Z. Zhao, W. Li, A.M. Guo, J.M. Cairney, Science 367 (6474) (2020) 171–+.
[34] S. Jothi, T.N. Croft, S.G.R. Brown, Int. J. Hydrog. Energy 39 (35) (2014) 20671–20688.
[35] A. Tehranchi, W.A. Curtin, Eng. Fract. Mech. (216) (2019) 106–502.
[36] C.J. O'Brien, S.M. Foiles, Philos. Mag. 96 (14) (2016) 1463–1484.
[37] C.J. O'Brien, S.M. Foiles, Philos. Mag. 96 (26) (2016) 2808–2828.
[38] A. Tehranchi, W.A. Curtin, J. Mech. Phys. Solids 101 (2017) 150–165.
[39] Z.D. Harris, S.K. Lawrence, D.L. Medlin, G. Guetard, J.T. Burns, B.P. Somerday, Acta Mater. 158 (2018) 180–192.
[40] K. Wada, J. Yamabe, Y. Ogawa, O. Takakuwa, T. Iijima, H. Matsunaga, Mater. Sci. Eng. A Struct. A 766 (2019) 138–349.
[41] S.K. Lawrence, Y. Yagodzinskyy, H. Hanninen, E. Korhonen, F. Tuomisto, Z.D. Harris, B.P. Somerday, Acta Mater. 128 (2017) 218–226.
[42] A.P. Thompson, S.J. Plimpton, W. Mattson, J. Chem. Phys. 131 (15) (2009) 154–107.
[43] C.L. Kelchner, S.J. Plimpton, J.C. Hamilton, Phys. Rev. B 58 (17) (1998) 11085–11088.
[44] J. Schiotz, F.D. Di Tolla, K.W. Jacobsen, Nature 391 (6667) (1998) 561–563.
[45] A. Stukowski, Model. Simul. Mater. Sci. 18 (1) (2010) 015012.
[46] D. Di Stefano, M. Mrovec, C. Elsasser, Acta Mater. 98 (2015) 306–312.
[47] J.Q. Li, C. Lu, L.Q. Pei, C. Zhang, K. Tieu, Scr. Mater. 173 (2019) 115–119.

[48] K.M. Bertsch, S. Wang, A. Nagao, I.M. Robertson, Mater. Sci. Eng. A Struct. 760 (2019) 58–67.
[49] Y. Ogawa, O. Takakuwa, S. Okazaki, K. Okita, Y. Funakoshi, H. Matsunaga, S. Matsuoka, Corros. Sci. 161 (2019) 108–186.
[50] Z.D. Harris, A.W. Thompson, J.T. Burns, Jom-Us 72 (5) (2020) 1993–2002.
[51] X. Wu, Y.T. Zhu, M.W. Chen, E. Ma, Scr. Mater. 54(9) (2006) 1685–1690.
[52] X.L. Wu, E. Ma, Appl. Phys. Lett. 88 (6) (2006).
[53] X. Guo, S. Zaefferer, F. Archie, W. Bleck, Int. J. Miner. Metall. Mater. 28 (5) (2021) 835–846.
[54] C. Zhang, H.H. Zhi, S. Antonov, L. Chen, Y.J. Su, Scr. Mater. 190 (2021) 108–112.

A.2 Paper 2

Hydrogen-enhanced grain boundary vacancy stockpiling causes transgranular to intergranular fracture transition

Authors: Yu Ding, Haiyang Yu, Meichao Lin, Kai Zhao, Senbo Xiao, Alexey Vinogradov, Lijie Qiao, Michael Ortiz, Jianying He, Zhiliang Zhang

Acta Materialia 239 (2022): 118279.

Paper 2

Acta Materialia 239 (2022) 118279

Contents lists available at ScienceDirect

Acta Materialia

journal homepage: www.elsevier.com/locate/actamat

Hydrogen-enhanced grain boundary vacancy stockpiling causes transgranular to intergranular fracture transition

Yu Ding[a], Haiyang Yu[b,*], Meichao Lin[a], Kai Zhao[c], Senbo Xiao[a], Alexey Vinogradov[d], Lijie Qiao[e], Michael Ortiz[f], Jianying He[a,*], Zhiliang Zhang[a,*]

[a] Department of Structural Engineering, Norwegian University of Science and Technology (NTNU), Trondheim 7491, Norway
[b] Division of Applied Mechanics, Department of Materials Science and Engineering, Uppsala University, Uppsala 75121, Sweden
[c] Jiangsu Key Laboratory of Advanced Food Manufacturing Equipment and Technology, Jiangnan University, Wuxi 214122, China
[d] Department of Mechanical and Industrial Engineering, Norwegian University of Science and Technology (NTNU), Trondheim 7491, Norway
[e] Beijing Advanced Innovation Center for Materials Genome Engineering, University of Science and Technology Beijing, Beijing 100083, China
[f] Graduate Aerospace Laboratories, California Institute of Technology, 1200 E. California Blvd., Pasadena, CA 91125, USA

ARTICLE INFO

Article history:
Received 24 April 2022
Revised 8 August 2022
Accepted 15 August 2022
Available online 17 August 2022

Keywords:
Hydrogen embrittlement
Intergranular failure
Vacancies
Grain boundaries
Molecular dynamics (MD)

ABSTRACT

The attention to hydrogen embrittlement (HE) has been intensified recently in the light of hydrogen as a carbon-free energy carrier. Despite worldwide research, the multifaceted HE mechanism remains a matter of debate. Here we report an atomistic study of the coupled effect of hydrogen and deformation temperature on the pathway to intergranular fracture of nickel. Uniaxial straining is applied to nickel $\Sigma5(210)[001]$ and $\Sigma9(1\text{-}10)[22\text{-}1]$ grain boundaries with or without pre-charged hydrogen at various temperatures. Without hydrogen, vacancy generation at grain boundary is limited and transgranular fracture mode dominates. When charged, hydrogen as a booster can enhance strain-induced vacancy generation by up to ten times. This leads to the superabundant vacancy stockpiling at the grain boundary, which agglomerates and nucleates intergranular nanovoids eventually causing intergranular fracture. While hydrogen tends to persistently enhance vacancy concentration, temperature plays an intriguing dual role as either an enhancer or an inhibitor for vacancy stockpiling. These results show good agreement with recent positron annihilation spectroscopy experiments. An *S*-shaped quantitative correlation between the proportion of intergranular fracture and vacancy concentration was for the first time derived, highlighting the existence of a critical vacancy concentration, beyond which fracture mode will be completely intergranular.

1. Introduction

The phenomenon of hydrogen in metals causing catastrophic degradation of mechanical properties, including strength, ductility, and fracture toughness, is known as hydrogen embrittlement (HE). Substantial efforts have been devoted to deciphering the genesis of this phenomenon at different scales since it was first observed in 1875 [1,2]. However, the fundamental mechanism of HE remains a matter of debate because of its multifaceted nature. The primary controversy is over the role of plasticity in hydrogen-induced degradation. Many theories have been proposed in this respect [3–6], and to name only a few, hydrogen-enhanced decohesion (HEDE) and hydrogen-enhanced localized plasticity (HELP). The HEDE mechanism postulates that dissolved hydrogen at a grain boundary (GB) or crack tip weakens interatomic bonds, thus reducing the fracture energy [7]. It reflects the nature of embrittlement and has been widely employed to rationalize the hydrogen-induced ductile to brittle transition [8–11]. However, HEDE does not explicitly address the intensive plasticity seemingly promoted by hydrogen, as revealed in many experiments [12,13]. In contrast, the HELP [14] mechanism regards hydrogen as an enhancer for dislocation mobility, as evidenced by a number of transmission electron microscopy (TEM) observations [15]. However, recent atomistic modeling [16] and *in-situ* experimental observation [17] showed that dislocation motion could be hindered by the Cottrell atmosphere built up by hydrogen. These contradictory results reflect the complexity of the interactions between plasticity and hydrogen when examined at different spatial and temporal scales.

Dislocation is not the sole carrier of plasticity, other types of defects such as GB and vacancy also exert an influence through

* Corresponding authors.
E-mail addresses: haiyang.yu@angstrom.uu.se (H. Yu), jianying.he@ntnu.no (J. He), zhiliang.zhang@ntnu.no (Z. Zhang).

https://doi.org/10.1016/j.actamat.2022.118279

their interaction with hydrogen. In polycrystalline materials, the embrittlement is usually accompanied by a transition from transgranular to intergranular fracture [18,19]. This transition has been attributed to decohesion caused by hydrogen segregation at GBs [20,21]. By observing extensive dislocation substructures beneath the intergranular fracture surface, Robertson et al. [5,22] claimed that hydrogen-enhanced dislocation activity was the necessary precursor for intergranular fracture. It should be noted that this conclusion is a posteriori interpretation of microstructural features observed after failure, whereas a time-resolved nanoscale mechanism is still lacking.

Superabundant vacancies have been shown to form in many hydrogen-metal systems [23]. With aid of positron annihilation spectroscopy (PAS), Nagumo et al. [24,25] pointed out the predominant role of vacancies in premature fracture, which is referred to as hydrogen-enhanced strain-induced vacancies (HESIV) mechanism. Hydrogen stabilizes vacancies by forming hydrogen-vacancy complex (Va-H) and participates in subsequent plastic deformation [17,26,27]. However, the direct connection between superabundant vacancies and the final intergranular fracture remains a mystery. Recent PAS experiments by Lawrence et al. [28] showed that the hydrogen-enhanced vacancy generation becomes more pronounced in fine-grained nickel alloys as temperature decreases, and the propensity for intergranular failure is also amplified [29,30]. These observations call for an in-depth investigation of the nanoscale interactions among hydrogen, vacancy, and GB.

It is still very challenging today to track hydrogen atoms precisely by experiment [31,32]. As a result, knowledge about hydrogen-microstructure interactions is limited. Atomistic modeling has proven as a powerful alternative tool for probing the nanoscale mechanisms of HE [9,10,15,17,33–35]. The atomistic studies of HE have been divided into several sub-processes, i.e., vacancy formation [36–38], dislocation dynamics [39–41], intergranular decohesion [42–44], and crack propagation [45–47]. In these studies, the respective contributions of hydrogen-influenced dislocation and vacancy to the intergranular fracture transition have been treated ambiguously. In order to explore a nanoscale mechanism that can directly link to the intergranular fracture transition, we employ atomistic modeling to study HE in bi-crystal nickel. Uniaxial straining tests with two representative GBs are carried out at varying hydrogen concentrations and temperatures, focusing on the time-resolved evolution of dislocations and vacancies as well as their contribution to the final separation of GBs. A large number of repeated simulations are performed for each condition to obtain a statistical representation of the results. The study enables quantification of the individual roles played by hydrogen, temperature, dislocations and vacancies in the transition to intergranular fracture. A quantitative relationship between vacancy concentration and intergranular fracture is for the first time derived to highlight the threshold vacancy concentration for fully intergranular fracture. The present findings unveil a nanoscale mechanism for intergranular fracture transition, more importantly, allow for the establishment of a quantitative mechanism-based prediction of HE.

2. Methodology

We utilized large-scale atomistic simulations to investigate the deformation behavior of the nickel-hydrogen system, focusing on the microstructure evolution during the hydrogen-induced intergranular fracture transition process. The atomic interactions were described by the embedded atom method potential developed by Angelo [48], which is widely adopted to study the deformation behavior of nickel [49–51]. The molecular dynamic (MD) simulations were performed using the LAMMPS code [52].

Two nickel bicrystal models were established with Σ5(210)[001] symmetric tilt GB and Σ9(1-10)[22-1] pure twist GB. Σ is the reciprocal density of coincident sites; (210) and (1-10) represent the GB planes, and [001] and [22-1] are the tilt or twist axes. The Σ5 and Σ9 GBs represent typical low-Σ and general GBs, respectively. The models were assumed to be in the vicinity of a crack tip, subjected to high stress triaxiality. An illustration was given in Fig. 1. The GBs were created by constructing two separate crystals with desired crystallographic orientations in a rectangular simulation box and then aligning the crystals along a plane normal to the Y-direction. Periodic boundary conditions were applied along the X and Z directions, while free boundary condition was employed along the Y direction. The initial configuration was then modified by shifting the upper grain in the X-Z plane, deleting overlapping atoms, and applying the conjugate gradient method to equilibrate the system. The resulting simulation box dimensions (L_x, L_y, L_z) were (11.9 nm, 23.8 nm, 10.6 nm) and (10.6 nm, 20.1 nm, 9.1 nm) for Σ5 and Σ9, respectively. All the simulation boxes were divided into three regions: the area 1 nm above and below the GB was referred to as the GB region, the 1 nm thick regions at the top and bottom of the simulation box were fixed as rigid blocks for the application of displacement, and the remaining was regarded as grain interior.

After relaxation in the isothermal–isobaric (NPT) ensemble at 300 K for 100 ps, the hybrid grand canonical Monte Carlo (GCMC)/molecular dynamic method [19] was utilized to obtain hydrogen distribution in the samples. The procedure consists of loops of hydrogen charging GCMC steps and subsequent MD steps and provides a hydrogen segregation map without considering the kinetic process, which would otherwise take a formidable long time in a pure MD simulation. At each GCMC step [53], hydrogen atoms were randomly inserted/deleted in the boxes in order to achieve a target chemical potential μ within a constant volume V and temperature T. In the end, the equilibrium hydrogen distribution in GB and grain interior will be under the same chemical potential μ. There exists a relationship between the chemical potential μ and the locally equilibrated hydrogen concentration c:

$$\mu = kTlnc + \triangle E, \tag{1}$$

where $\triangle E$ is the local segregation energy of one hydrogen atom and k is the Boltzmann constant. For all the cases, $\mu = -2.31\ eV$ was chosen as the charging potential which corresponds to the bulk hydrogen concentration in grains $c_0 = 0.001$ (H/Ni atomic ratio). This hydrogen concentration is in agreement with previous experiments [28,29]. In the subsequent MD steps, a canonical (NVT) ensemble was applied to equilibrate the system at $T = 300\ K$ after every hydrogen charging step. Each GCMC step was followed by 50 MD steps until the hydrogen concentration in the box fluctuated in a narrow range (±1% atomic ratio). The equilibrium hydrogenated GB after charging was regarded as a 100% saturation case, and the 0%, 13%, 25%, 40%, 60% saturation cases were simulated for comparison. All samples in these cases were further equilibrated at 77 K, 300 K, and 600 K in the NPT ensemble for 100 ps. Then uniaxial straining was applied in the NVT ensemble at the three temperatures by moving the upper boundary layer at a constant velocity along the Y direction while the lower layer was kept stationary. This loading method provides a high stress triaxiality and mimics the mechanical behavior close to the crack tip. In total, we had 2 GB types × 6 hydrogen concentrations × 3 temperatures = 36 different conditions. For each condition, we performed 20 independent mechanical tests with random temperature seeds. This guarantees statistical significance in capturing the thermal effect during mechanical deformation and produces the basis for calculating the intergranular fracture fraction.

The atomic stress during deformation was analyzed by Viral theory [54]. The local atomistic structures in the system were characterized by the centro-symmetry parameter (CSP) [55] and common neighbor analysis (CNA) [56]. Vacancy surface atoms were

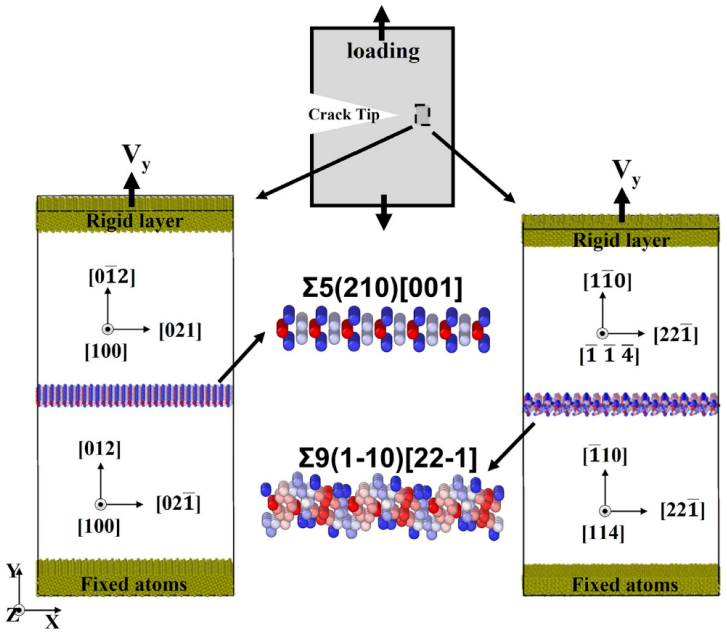

Fig. 1. Schematic of the atomistic models of nickel Σ5(210)[001] symmetric tilt and Σ9(1-10)[22-1] twist grain boundaries. Only atoms belonging to the GB are shown. The top and bottom are the rigid layers serving to apply deformation.

counted by calculating the coordination number of atoms in each snapshot after fast quenching and dislocations were identified with Ovito program [57].

3. Results and discussion

3.1. Hydrogen-induced transgranular to intergranular fracture transition

The dynamic GCMC/MD charging process with $\mu = -2.31$ *eV* is illustrated in Fig. 2c, d for the Σ5 and Σ9 GBs, respectively. The hydrogen concentration in the grains reached $c_0 = 0.001$ during the first 100,000 MC steps and stabilized gradually during the subsequent simulation steps. Meanwhile, hydrogen atoms keep pumping into the GB region due to the high excess volume and binding energy. After around 10,000,000 MC steps, hydrogen concentration at the Σ5 and Σ9 GBs also reached equilibrium (100% saturation) with $c = 0.240$ and $c = 0.215$, respectively. These two equilibrium GB configurations with saturated hydrogen in Fig. 2a are regarded as 100% (fully) charged cases at the chemical potential $\mu = -2.31$ *eV*. Apparently, a local hydrogen atmosphere has been formed around the Σ5 and Σ9 GB core, while the grain interior hydrogen concentration was slightly decreased to $c_0 = 0.0008$. The relationship between local equilibrium hydrogen concentration and applied chemical potential was further shown in Fig. 2b, agreeing with Eq. (1). These hydrogen distribution maps show good agreement with previous studies [31,58], where GBs are preferable accommodation sites for hydrogen.

After charging, uniaxial straining in the Y direction is applied on the bicrystal specimens at 300 K. This loading strategy provides a high stress triaxiality which mimics the stress state in the vicinity of a crack tip. During tension, plasticity occurs firstly with nucleation of 1/6<112> Shockley dislocations at the GBs (Fig. 3a_1, a_3, b_1, b_3). These dislocations enter the grains rapidly and interact with the top or bottom boundary, leaving stacking fault bands along the propagation pathway. As more dislocations nucleate and spread across the specimen, nanovoids start to nucleate, eventually leading to fracture. Compared to non-charged ones, hydrogen-charged samples are distinct both in mechanical response and in fracture mode. As shown in Fig. 3a and b, the first drop of the stress-strain curves corresponds to the first dislocation nucleation event as a sign of the onset of plasticity. Hydrogen facilitates the dislocation nucleation at Σ5 GB (first dislocation nucleates at strain $\varepsilon = 0.079$ and stress $\sigma_y = 11.06$ GPa in the hydrogen-free sample against $\varepsilon = 0.061$, $\sigma_y = 9.51$ GPa in the hydrogen charged specimen), while its influence on Σ9 GB seems negligible ($\varepsilon = 0.045$ and $\sigma_y = 8.48$ GPa without hydrogen versus $\varepsilon = 0.044$, $\sigma_y = 8.34$ GPa with hydrogen). In Fig.3 b_3, the dislocation nucleation at the lower half-grain will occur slightly later (0.001 strain) than in the upper grain. When the samples fracture by nanovoiding, the stress drops to zero. Hydrogen can significantly reduce the fracture stress and strain, and, more importantly, it switches the nanovoid nucleation site from the grain interior to GB (Fig. 3a_2, a_4, b_2, b_4). A distinctive companion of this process is the distortion of the crystal lattice in the vicinity of GB due to the accumulation of lattice defects. This distortion can be so significant that the translation symmetry breaks in some local regions leading to partial amorphization of the material as has been experimentally observed in hydrogen-charged steels [59,60] and nickel alloys [61,62]. In Fig. 3a_1, a_3, the local lattice distortion is noticed at the early stages of straining and is associated with the formation of Shockley dislocations and local HCP atomic packing. In Fig. 3a_4, b_4, the nanovoid at GB is formed

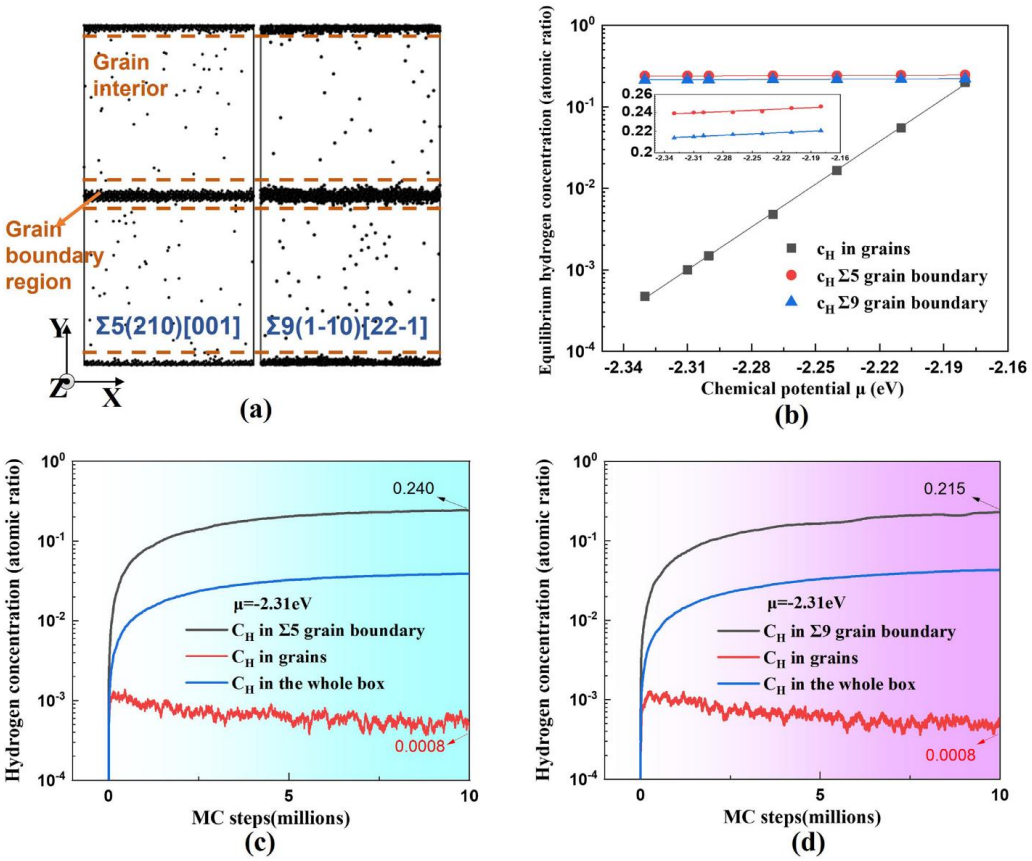

Fig. 2. (a) Equilibrium hydrogen distribution map around Σ5 and Σ9 GBs. Only hydrogen atoms are colored black. (b) The relationship between local equilibrium hydrogen concentration (H/Ni atomic ratio) and chemical potential. The relationship between equilibrium hydrogen concentration and chemical potential around Σ5 and Σ9 is highlighted in the inset. (c, d) Hydrogen concentration evolution around Σ5 and Σ9 GBs during GCMC/MD charging process.

by the expanding of those heavily distorted layers. The pivotal significance of the free volume associated with the excess vacancies and nanovoids in the local deformation and partial amorphization of the GB area will be further unfolded and clarified in Section 3.3. We repeat the simulation process 20 times with different random seeds for temperature. In the absence of hydrogen, transgranular fracture prevails over intergranular fracture: 19 out of 20 Σ5 samples, i.e., 95% of the samples, fail with nanovoid nucleation sites located inside the grains. The picture changes drastically in the presence of hydrogen: all 20 Σ5 samples fail with nanovoiding at GB. Thus, hydrogen enhances the intergranular fracture fraction from 5% to 100% for Σ5 GB at 300 K. This process is identified as the hydrogen-induced transgranular to intergranular fracture transition (see Supplementary movies 1 and 2). We should underline for clarity that the term "intergranular fracture" used in this study refers to the "intergranular nanovoiding" or "GB opening by nanovoiding" process, because the intergranular fracture occurs almost concurrently with the nanovoiding. This means the intergranular fracture here and below focuses only on the nanovoid nucleation behavior, which differs from the macroscopic intergranular fracture progressing through the void nucleation, coalescence, and crack propagation [3,63]. However, since the nanovoid nucleation is the prerequisite for void coalescence and crack propagation and since the nucleation site has been assigned to GB, the propensity for macroscopic intergranular fracture should also be enhanced.

3.2. Coupling effect of hydrogen and temperature

Both hydrogen and low temperature can cause embrittlement and intergranular fracture transition and their roles may be intertwined. We carried out simulations at various hydrogen concentrations and temperatures (77 K, 300 K, 600 K) to explore their coupling effect. Normalized hydrogen concentration at GB is defined as the relative ratio compared to the full saturation cases with Σ5 or Σ9 GBs. For instance, the 100% saturation at the Σ5 GB corresponds to a hydrogen concentration of $c = 0.240$. Hence, a normalized hydrogen concentration of 60% is equivalent to a concentration of $c = 0.144$. For each condition, 20 independent sim-

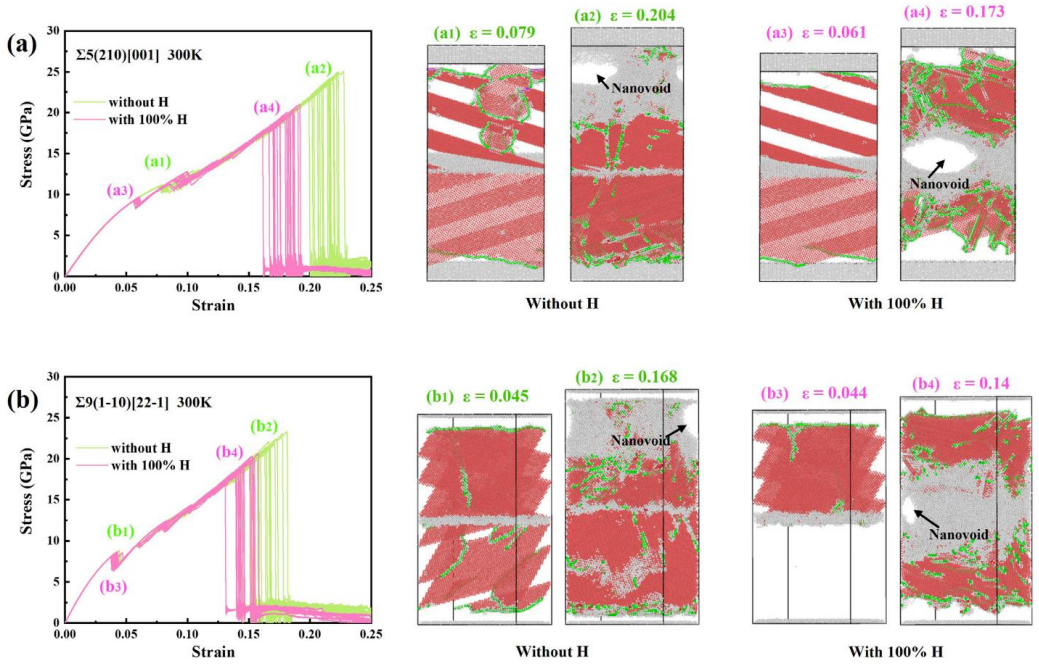

Fig. 3. Hydrogen-induced transgranular to intergranular facture transition: nanovoid nucleation site switching from grain interior to GB. (a, b) The stress-strain curves during uniaxial straining at 300 K for Σ5 and Σ9 GBs with and without hydrogen. Every line represents a MD simulation result with varying random seeds for temperature, which means all the atoms are given a different set of velocities according to the changed random seeds while the systems are kept at the same temperature of 300 K. (a_1, a_3, b_1, b_3) Snapshots show the events of first dislocation nucleation, corresponding to the first drop of stress in (a, b). (a_2, a_4, b_2, b_4) Snapshots show the events of nanovoid nucleation, corresponding to the maximum stress in (a, b). Atoms are colored by the common neighbor analysis parameters. FCC atoms are deleted, red HCP atoms indicate the glide paths of 1/6<112> Shockley dislocations (green pipelines), and grey atoms are in an amorphous structure.

ulations are performed to extract statistically reliable data. The coupling effect of hydrogen and temperature on dislocation nucleation varies depending on the GB type (Fig. 4a, d). Hydrogen could facilitate dislocation nucleation at the Σ5 GB with a more pronounced effect at 600 K, while Σ9 GB remains immune to hydrogen attack within the temperature range tested. In contrast, the coupling effect on nanovoid formation and final fracture manifests itself in a different manner (Fig. 4b, c, e, f). When sufficient hydrogen is charged, earlier fracture and increased proportions of intergranular fracture were observed. To avoid confusion with the customary notions where intergranular fracture usually addresses fractographic features indicative of the brittle nature of HE, the intergranular fracture in this study describes the GB opening process by nanovoiding accompanied by intense plasticity. Notably, the effect of hydrogen is always most pronounced at 77 K. This observation is consistent with the experimental results [29] that the hydrogen-promoted intergranular fracture was more frequently observed at low temperatures. However, the fact that hydrogen-enhanced dislocation nucleation and hydrogen-promoted earlier fracture have opposite temperature dependence suggests that hydrogen-dislocation interaction may not directly contribute to the final intergranular fracture. The change in the fracture mode should be attributed to other types of microstructural defects such as vacancies. This is elaborated in the subsequent sections.

3.3. *Vacancy stockpiling at GB and its temperature dependence*

A number of experimental observations [17,24,28] highlighted the importance of vacancy formation at GB. Here we explore the hydrogenated vacancies in the vicinity of GB and treat them as potential embryos for nanovoids. To quantify the evolution of vacancies at a deformed GB, the distorted atoms with coordination numbers less than 9 (featuring bond-breaking states) in the GB region are treated as vacancy surface atoms [33], and the fraction of these atoms is taken as the vacancy concentration. This definition differs from the conventional one for the vacancy-type of point defects, but it could well capture the amount of lattice distortions at GB, and give a comprehensive description of the enhanced excess free volume during GB amorphization [28,59,60]. Fig. 5b, g shows the distribution of vacancy surface atoms at GBs at a constant strain, as examples from the concentration plots in Fig. 5a, f. A dramatic increase in the number of vacancies is observed in all hydrogen-charged cases, with the maximum enhancement of over 10 times, as observed in the 100% saturated cases at 77 K for both Σ5 and Σ9 GBs. It should be noted that, to eliminate thermal noise, every snapshot is fast quenched to 10 K before calculating vacancy concentration. By repeating the quenching-and-calculating process for multiple times at different strains, we obtain the evolution of vacancy concentration as a function of strains in Fig. 5c–e, h–j. To avoid counting atoms on the nanovoid surface, we show only the

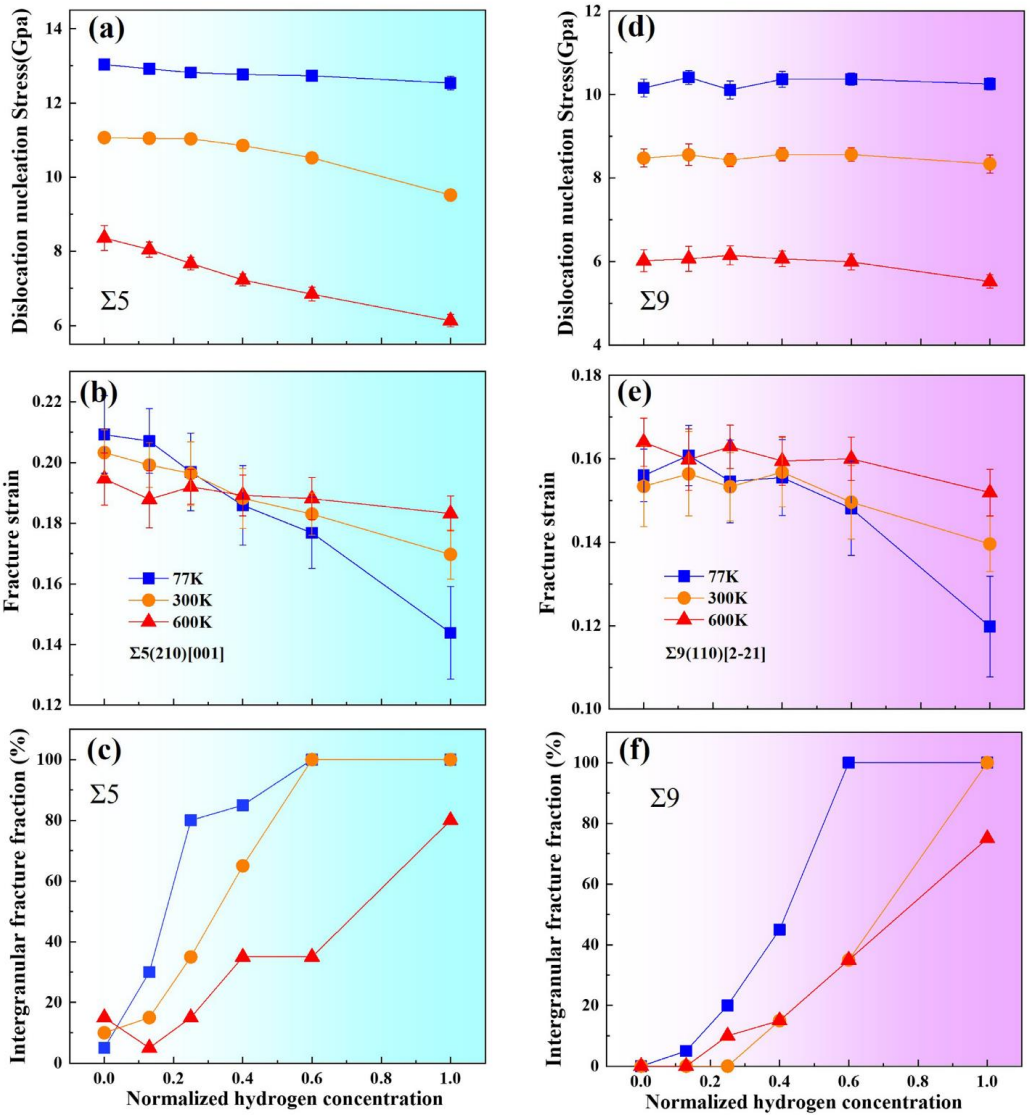

Fig. 4. The coupling effect of hydrogen and temperature on mechanical responses. (a, d) Dislocation nucleation stress is the critical stress for the first dislocation nucleation corresponding to the snapshots in Fig. 3(a_1, a_3, b_1, b_3). (b, e) Fracture strain is the strain for the onset of fracture, or on the other hand, failure corresponding to the snapshots in Fig. 3(a_7, a_4, b_2, b_4). (c, f) Fraction of intergranular fracture is a statistical quantity for samples exhibiting intergranular nanovoiding behavior. Hydrogen concentrations are normalized by the full saturation concentration at Σ5 and Σ9 GBs, respectively. The error bar on each data point in (a, b, d, e) indicates the standard deviation obtained from 20 independent simulations under the same conditions. All the samples are of the same size and a total amount of strain of 0.25 is applied to make sure that the nanovoid formation is observed in the course of deformation. The fraction of intergranular fracture is calculated as the proportion of samples with intergranular nanovoiding among the 20 independent simulations.

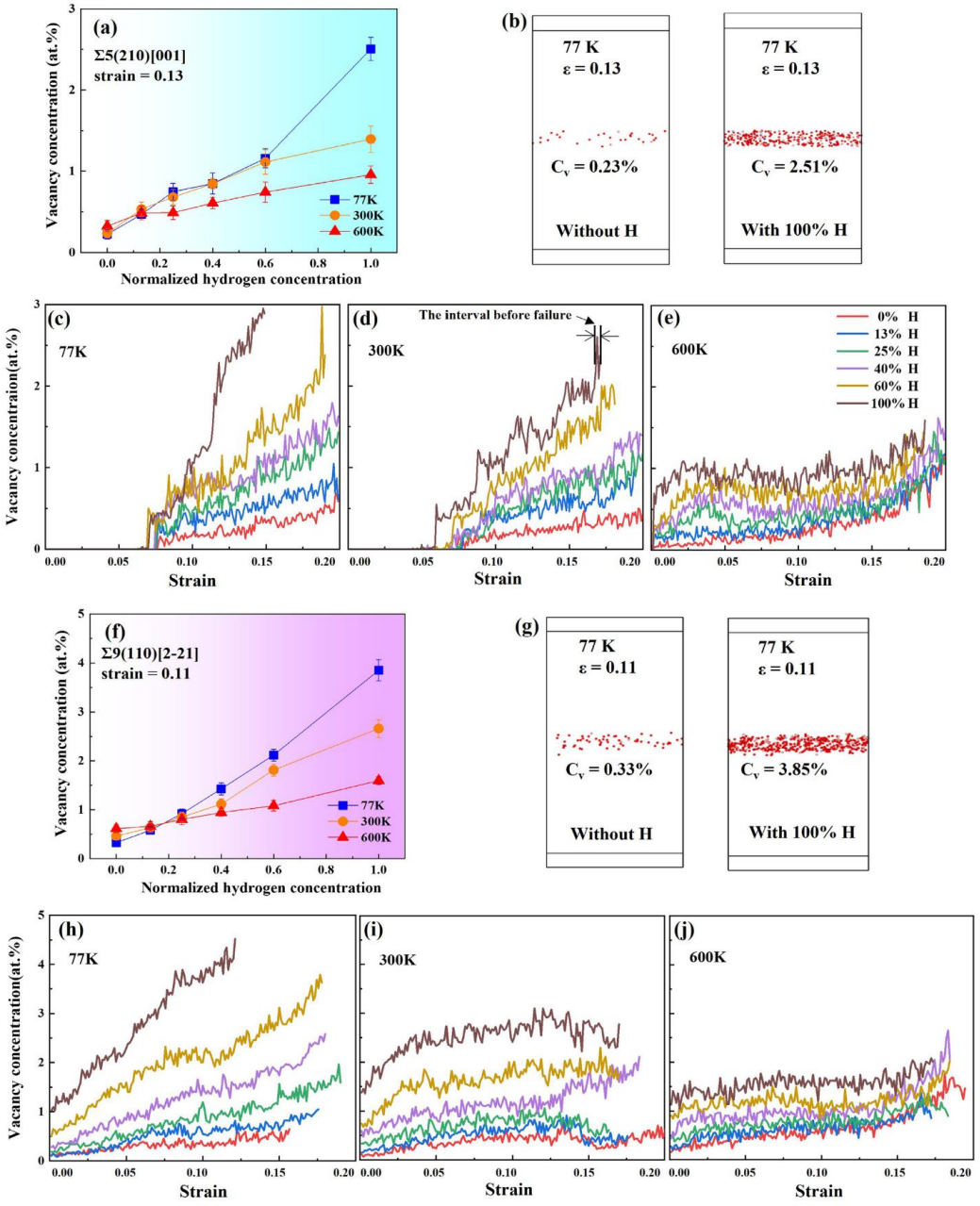

Fig. 5. Hydrogen-boosted vacancy stockpiling at GBs. (a,f) Vacancy concentration versus hydrogen concentration at different temperatures at the late plastic deformation stage. (b,g) Quenched snapshots illustrating the vacancy surface atoms for Σ5, 77 K, strain $\varepsilon = 0.13$ and Σ9, 77 K, strain $\varepsilon = 0.11$, respectively. Only highly distorted atoms with coordination numbers less than 9 in the GB region are colored. (c–e, h–j) Vacancy concentration evolves with strain under different conditions. Each data point in the figures is extracted from the fast quenched snapshots at the same strain.

strain range before failure. For the Σ5 GB at relatively low temperatures, 77 K and 300 K, vacancy is not observed at a small strain ($\varepsilon < 0.05$); the concentration starts to increase only after the onset of plasticity (Fig. 5c, d), and hydrogen acts as a powerful booster for the subsequent vacancy generation process. At 600 K, vacancies could be generated solely by hydrogen charging without external loading, and the vacancy concentration increases continuously at a very early stage (Fig. 5e). For the Σ9 GB, the insertion of hydrogen triggers vacancy generation at all three temperatures, while this only happens at 600 K for Σ5. This difference is caused by the less uniform structure of the Σ9 twist GB compared to the Σ5 symmetric tilt GB. Local plasticity could be activated during the elastic stage through self-amorphization before dislocation nucleation [64,65] at Σ9 GB. However, for the Σ5 boundary with a regular atomic structure, this deformation mechanism works only at high temperatures, where the conditions for sufficient thermal activation are fulfilled.

While hydrogen tends to persistently enhance the vacancy concentration, the temperature plays an intriguing dual role as either an enhancer or an inhibitor. In the absence of hydrogen, temperature increases lattice vibrations, and thus the probability of the thermally activated nucleation of lattice defects. The increased vacancy concentration can be expected at higher temperatures, where the highest vacancy concentration is observed at 600 K. When the specimen is pre-charged, the trapped hydrogen atoms reduce the vacancy formation energy by forming Va-H complexes, accelerating vacancy generation. Nevertheless, according to the previous thermodynamics work [66–68], those Va-H complexes become unstable at high temperatures and can dissociate into vacancy and interstitial hydrogen, which suppresses the role of hydrogen as a booster for vacancy generation. The enhanced diffusion at high temperature also accelerates the transport of hydrogen atoms from the GB region to the grain interior, driven by a decreased excess free volume ratio of GB [69,70]. This further restrains the influence of hydrogen at GB. All the above factors lead to the competition between thermal-activated vacancy generation and hydrogen detrapping mediated vacancy annihilation at elevated temperature, depending on the hydrogen concentration. As the concentration is low or zero, high temperature is favorable for strain-induced vacancy generation by thermal activation. When the concentration is high, however, low temperature becomes favorable, where detrapping of hydrogen is suppressed and the Va-H complex stays stable. These observations agree very well with the positron annihilation spectroscopy measurement [28] where grain refinement and cryogenic temperature amplify the hydrogen-enhanced vacancy effect and can be further rationalized with the equation for equilibrium vacancy concentration c_v:

$$c_v = g\exp\left(-\frac{E_v(c_H, \epsilon, T)}{k_b T}\right), \tag{2}$$

where g is the geometry factor depending on the arrangement of vacancies, E_v is a positive value of vacancy formation energy as a function of trapped hydrogen concentration c_H, local strain ϵ, and absolute temperature T. k_B is Boltzmann's constant. The magnitude of E_v reduces with increasing hydrogen concentration, favoring the formation of Va-H complex and an increasing c_v. Meanwhile, E_v increases with temperature, promoting the decomposition of Va-H complexes and decreasing c_v. In a heuristic way, one can assume that c_v is controlled primarily by temperature at low hydrogen concentration; at high concentration, the influence of hydrogen on vacancy formation prevails over the effect of temperature. This explains the trend observed earlier.

3.4. Critical vacancy concentration for intergranular fracture

To shed light on the relationship between vacancy stockpiling at GB and fracture mode, we extracted the vacancy concentration within the narrow strain interval before failure in Fig. 6a, c. The interval has a width of 0.01, as indicated in Fig. 5d, and the vacancy concentration is averaged within this strain interval prior to nanovoid nucleation. The vacancy concentrations show a similar dependence on hydrogen and temperature as in Fig. 5. Interestingly is that a fully intergranular fracture (with 100% frequency of observations) is observed when a sufficient number of vacancies is accumulated at GB. All these vacancy concentrations are measured and plotted against the intergranular fracture fraction in Fig. 6b, d. Surprisingly, both Σ5 and Σ9 GBs reveal an S-shape correlation between the intergranular fracture fraction and the vacancy concentration. At the low vacancy concentration (below 1.0% for Σ5 and 1.5% for Σ9), which usually means a low hydrogen concentration, the transgranular fracture mode prevails. Vacancies mainly nucleate and coagulate to form nanovoids in the grain interior; while the number of vacancies at GB is small. As the vacancy concentration increases (to 1.0% ∼ 1.7% for the Σ5 and 1.5% ∼ 2.8% for Σ9), the intergranular fracture fraction increases rapidly. At this stage, the concentrations of both hydrogen and vacancies reach high values, and hydrogen further promotes vacancy agglomeration at GB. Nanovoid nucleation at GB eventually wins the competition over that in grain interior. As the vacancy concentration exceeds a certain critical value (of 1.7% for Σ5 and 2.8% for Σ9, respectively), the fully intergranular fracture is observed. In this regime, all the samples fail intergranularly. We should note that all vacancy concentrations used in the above considerations are still defined in the local region close to the GB (± 1 nm). The existence of this critical value reveals the pivotal role played by vacancies in the hydrogen-induced transgranular to intergranular facture transition. Understanding of this fact can be further utilized to predict the nanovoid nucleation site. That is, if we can estimate the vacancy concentration based on its relationship with hydrogen concentration and temperature, c.f., Fig. 6a, c, or through direct measurements, then it is possible to compare the estimated or measured value of the vacancy concentration with the simulated critical value to unveil the proportion of the intergranular fracture in all samples. Take the Σ9 GB for example, the critical vacancy concentration is about 2.8 at.%. The normalized hydrogen concentration for achieving this vacancy concentration is about 0.6 for T =77K and 1 for T =300K, respectively. Considering that the real hydrogen concentration is 0.215 corresponding to a normalized hydrogen concentration of 1 for Σ9, we obtain the critical hydrogen concentration for the intergranular fracture in the Σ9 GB, which is 0.129 for T =77K and 0.215 for T =300K, respectively. Those critical hydrogen concentrations can be utilized as the threshold for intergranular fracture transition. Another interesting observation is that at high temperature, e.g. T =600K, the critical hydrogen concentration does not exist; in other words, it is impossible to have fully intergranular fracture. These findings also explain the recent observations made in low-temperature HE experiments [28,29] where the hydrogen-dislocation interaction was highly suppressed whereas the intergranular fracture was still observed. The rationale standing behind this observation is that it is the enhanced vacancy generation due to hydrogen that made a major contribution to the increased propensity towards intergranular failure.

3.5. Role of dislocations in vacancy stockpiling

Further analysis is carried out to elucidate the relationship between dislocation activity in grains and vacancy evolution at GB. Fig. 7a, b show the atomic structures and the vacancy distribution in the Σ5 GB case at 300 K. Before dislocation nucleation, there

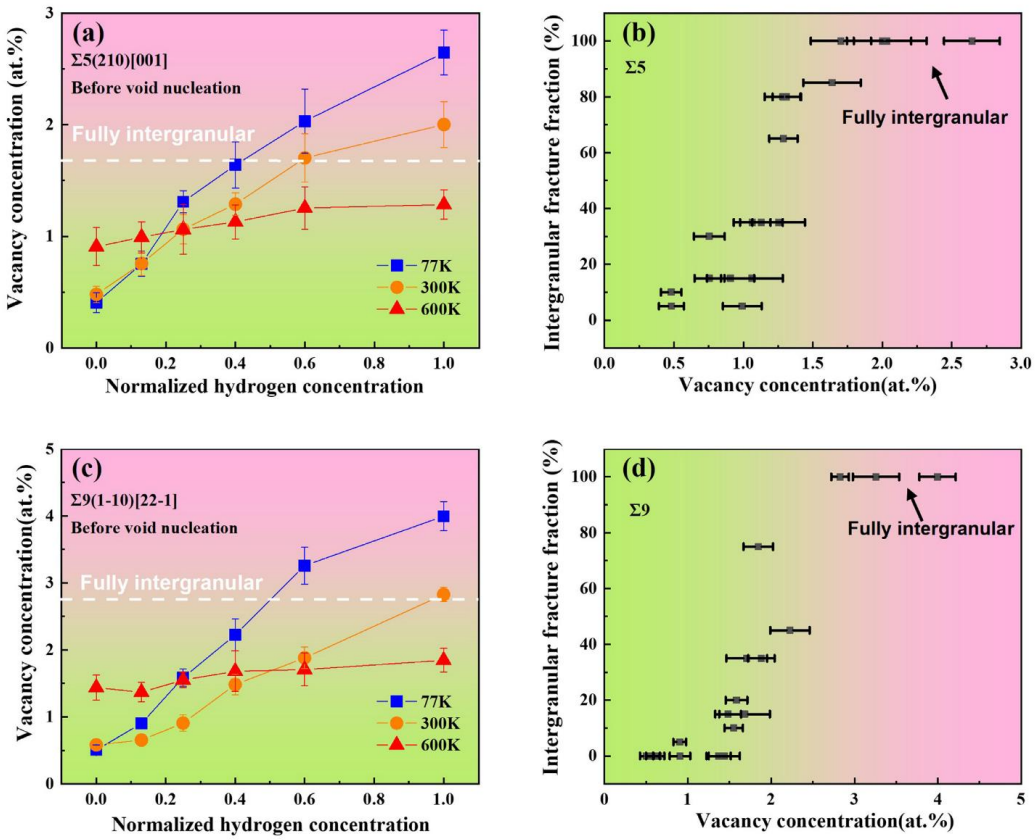

Fig. 6. GB vacancy stockpiling is responsible for intergranular fracture. (a, c) GB vacancy concentration before nanovoid nucleation versus varying hydrogen concentrations and temperatures. Each data point is collected at a point right before fracture. (b, d) Relationship between intergranular fracture fraction and vacancy concentration at GB. Intergranular fracture fraction becomes 100% as critical vacancy concentration (1.7% for Σ5 and 2.8% for Σ9) is reached, i.e. all the samples are expected to fail by intergranular fracture. Error bars correspond to the standard deviation of 20 individual simulations under the same conditions.

are few vacancies at the GB, with or without hydrogen. Once plasticity emerges in the grains, the vacancy concentration increases rapidly, with line-shaped vacancy clusters occurring at sites where dislocations nucleated. In the presence of hydrogen, the vacancy clusters become more distinguished, indicating enhanced vacancy multiplication. The enhancement is often thought to be mediated by hydrogen enhanced dislocation activity, in line with the HESIV theory. This assumption is also examined. We take the fraction of HCP atoms along the dislocation path as an indicator of dislocation glide volume, i.e., the amount of dislocation activity. Every sudden increase or drop of this indicator signifies the interaction between dislocations and GB. Fig. 7c–h show the evolution of vacancy concentration and dislocation glide volume. Surprisingly, the enhancement due to hydrogen on the amount of dislocation activity in all the cases is limited, while the enhancement due to hydrogen on vacancy generation is far more pronounced. It is particularly the case for the Σ9 GB and for the Σ5 GB at 600K. As mentioned earlier, the generation of vacancies is thermally activated in these cases, which can be triggered by hydrogen charging [71]. Hydrogen increases the vacancy concentration by multiple times, even before plasticity occurs. It appears that hydrogen-enhanced vacancy generation in these cases is not related to dislocation nucleation or in other words, plasticity in the grains. It is more likely that hydrogen directly participates in the thermodynamics of vacancy formation and interacts with existing vacancies, whether there is plasticity or not. In other words, plasticity does not seem to be a premise for this to happen. Deviation appears in the case of Σ5 GB at 77K and 300K. There is no vacancy formation before the onset of plasticity with or without hydrogen. Then the vacancy concentration suddenly increases accompanied by a rise in dislocation glide volume in Fig. 7c, d, approximately at a strain of 0.07. This applies also to hydrogen-free cases. The development of vacancies aligns very well with plasticity in the grains. This alignment shows the important role of GB-dislocation interaction in producing vacancies but is still insufficient to explain the large enhancement in vacancy generation, considering that the enhancement in dislocation activity is still limited. Those observations show good agreement with recent experimental measurements [72]. All these cases convey the same important message that hydrogen enhanced vacancy generation in Σ5 and Σ9 GBs primarily has to do with the direct interaction be-

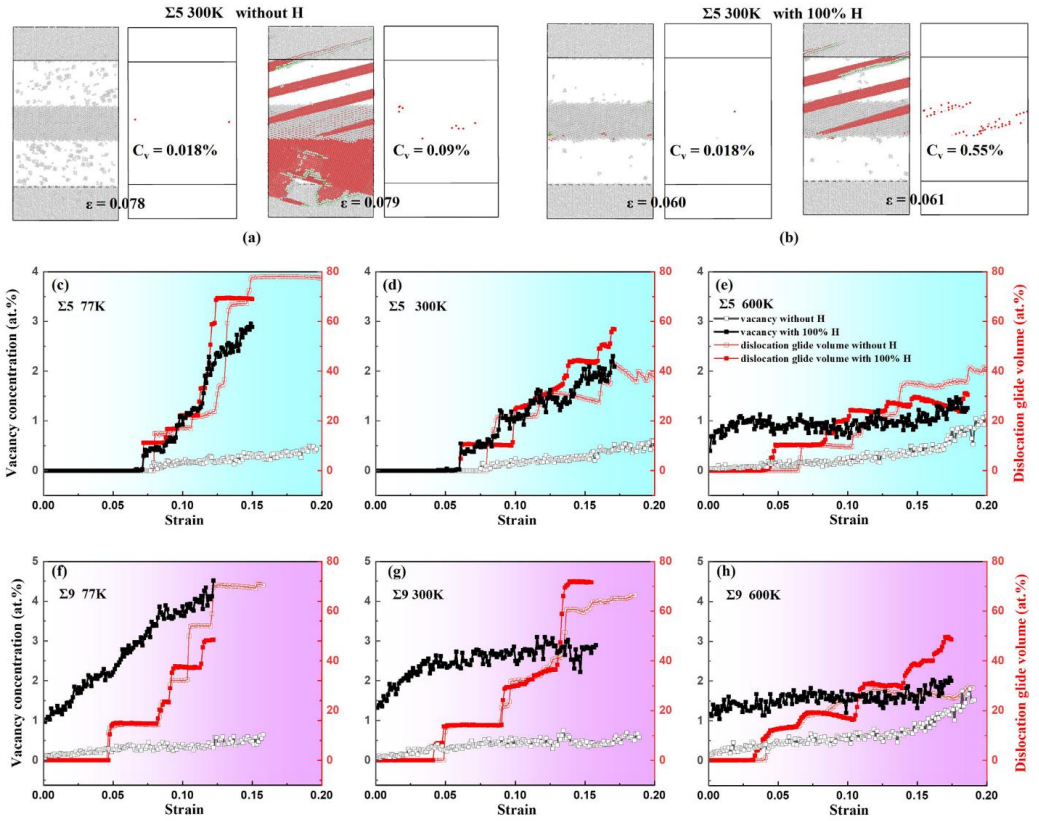

Fig. 7. Effects of hydrogen on vacancy generation and dislocation activity. (a,b) Snapshots of atomic structures and vacancy distributions for the Σ5 GB at 300 K. (c-h) Vacancy concentration and dislocation glide volume evolutions in the absence and presence of hydrogen for different conditions. Dislocation glide volumes are obtained by calculating the fraction of atoms through which dislocations have traveled.

tween hydrogen and existing vacancies, while the interaction with dislocations does not seem to be a prerequisite.

4. Conclusion

Through atomistic simulations on the interaction between hydrogen and two types of representative GBs, we were able to probe the nanoscale mechanism of hydrogen-induced transgranular to intergranular fracture transition. Hydrogen-boosted vacancy stockpiling at GB is revealed to be responsible for the increased propensity towards intergranular failure. This process can be termed hydrogen-enhanced vacancy stockpiling-induced nanovoiding mechanism, which is in harmony with the recent experimental studies [73–75]. During straining, vacancies are generated in the vicinity of GBs as a result of dislocation-GB interaction giving rise to local GB amorphization. Hydrogen works as a promoting agent for vacancy generation and can enhance vacancy concentration at GB by up to 10 times. The subsequent vacancy agglomeration causes earlier nanovoid formation at GB, which otherwise should nucleate in a much later stage inside the grains. This proposed mechanism covers the interactions among hydrogen, dislocations, vacancies, and GB, which is essential for interpreting experimental observations. It should be noted that this mechanism is not in conflict with the existing theories, rather, it should be regarded as a synergistic action of HELP, HESIV, and HEDE mechanisms, although there may be certain discrepancies when compared to a single mechanism. For example, the HELP mechanism emphasizes the role of hydrogen-enhanced plasticity in establishing the condition for final failure. In this study, we did observe intense dislocation activities beneath the fracture surface. However, the hydrogen effect on dislocation gliding is limited. The main effect of hydrogen-dislocation interaction is exerted at the GB, which increases the vacancy concentration and furnishes the condition for final decohesion. Compared to hydrogen which persistently boosts the vacancy generation, temperature plays a dual role depending on the charged hydrogen level. When hydrogen concentration is low, temperature facilitates vacancy generation by thermal activation. While at a high hydrogen level, temperature inhabits vacancy formation by destabilizing the Va-H complex. This temperature dependence revealed in our simulations is in good agreement with the recent PAS experiments [28]. Furthermore, a GB-specific quantitative relation between the probability of intergranular fracture and vacancy concentration under different conditions was further drawn. It highlights the existence of critical va-

cancy concentration acting as a threshold for the complete intergranular fracture and enables the quantitative prediction of HE in polycrystalline materials. A case in point is, given the microstructure (GB type and fraction), temperature and loading, it is possible to utilize the critical vacancy concentration to calculate the threshold hydrogen concentration for intergranular fracture. In summary, by quantitative analysis of the time-resolved microstructure evolution, we pinpoint the key role of vacancy stockpiling in HE and provide a vacancy-based criterion for hydrogen-induced intergranular fracture.

Data availability

The data that support the findings of this study are available from the corresponding authors upon request.

Declaration of Competing Interest

The authors declare that they have no known competing financial interests or personal relationships that could have appeared to influence the work reported in this paper.

CRediT authorship contribution statement

Yu Ding: Visualization, Formal analysis, Writing – original draft. **Haiyang Yu:** Supervision, Project administration, Writing – original draft. **Meichao Lin:** Writing – original draft. **Kai Zhao:** Writing – original draft. **Senbo Xiao:** Writing – original draft. **Alexey Vinogradov:** Writing – original draft. **Lijie Qiao:** Writing – original draft. **Michael Ortiz:** Writing – original draft. **Jianying He:** Supervision, Project administration, Writing – original draft. **Zhiliang Zhang:** Supervision, Project administration, Writing – original draft.

Acknowledgments

Y.D. acknowledge the financial support provided by the Research Council of Norway under the M-HEAT project (Grant No. 294689) and the HyLINE project (Grant No. 294739). All simulations are carried out on the Fram (Grant No. NN9110K, NN9391K) high-performance computer clusters at NTNU, Trondheim.

Supplementary materials

Supplementary material associated with this article can be found, in the online version, at doi:10.1016/j.actamat.2022.118279.

References

[1] W.H. Johnson, On some remarkable changes produced in iron and steel by the action of hydrogen and acids, Proc. R. Soc. Lond. 23 (156-163) (1875) 168–179.
[2] R.P. Gangloff, B.P. Somerday, Gaseous Hydrogen Embrittlement of Materials in Energy Technologies: Mechanisms, Modelling and Future Developments, Elsevier, 2012.
[3] S. Lynch, Hydrogen embrittlement phenomena and mechanisms, Corros. Rev. 30 (3-4) (2012) 105–123.
[4] R. Kirchheim, Reducing grain boundary, dislocation line and vacancy formation energies by solute segregation. I. Theoretical background, Acta Mater. 55 (15) (2007) 5129–5138.
[5] I.M. Robertson, P. Sofronis, A. Nagao, M.L. Martin, S. Wang, D.W. Gross, K.E. Nygren, Hydrogen embrittlement understood, Metall. Mater. Trans. B-Process Metall. Mater. Process. Sci. 46 (3) (2015) 1085–1103.
[6] M.B. Djukic, G.M. Bakic, V.S. Zeravcic, A. Sedmak, B. Rajicic, The synergistic action and interplay of hydrogen embrittlement mechanisms in steels and iron: localized plasticity and decohesion, Eng. Fract. Mech. 216 (2019).
[7] R. Oriani, A mechanistic theory of hydrogen embrittlement of steels, Ber. Bunsenges. Phys. Chem. 76 (8) (1972) 848–857.
[8] S. Serebrinsky, E.A. Carter, M. Ortiz, A quantum-mechanically informed continuum model of hydrogen embrittlement, J. Mech. Phys. Solids 52 (10) (2004) 2403–2430.
[9] J. Song, W.A. Curtin, Atomic mechanism and prediction of hydrogen embrittlement in iron, Nat. Mater. 12 (2) (2013) 145–151.
[10] A. Tehranchi, X. Zhou, W.A. Curtin, A decohesion pathway for hydrogen embrittlement in nickel: mechanism and quantitative prediction, Acta Mater. 185 (2020) 98–109.
[11] M. Lin, H. Yu, Y. Ding, G. Wang, V. Olden, A. Alvaro, J. He, Z. Zhang, A predictive model unifying hydrogen enhanced plasticity and decohesion, Scr. Mater. 215 (2022) 114707.
[12] D. Wan, Y. Deng, J.I.H. Meling, A. Alvaro, A. Barnoush, Hydrogen-enhanced fatigue crack growth in a single-edge notched tensile specimen under *in-situ* hydrogen charging inside an environmental scanning electron microscope, Acta Mater. 170 (2019) 87–99.
[13] Z. Zhang, Z. Yang, S. Lu, A. Harte, R. Morana, M. Preuss, Strain localisation and failure at twin-boundary complexions in nickel-based superalloys, Nat. Commun. 11 (1) (2020) 1–11.
[14] H.K. Birnbaum, P. Sofronis, Hydrogen-enhanced localized plasticity - a mechanism for hydrogen-related fracture, Mat. Sci. Eng. A Struct. 176 (1-2) (1994) 191–202.
[15] M.L. Martin, M. Dadfarnia, A. Nagao, S. Wang, P. Sofronis, Enumeration of the hydrogen-enhanced localized plasticity mechanism for hydrogen embrittlement in structural materials, Acta Mater. 165 (2019) 734–750.
[16] J. Song, W.A. Curtin, Mechanisms of hydrogen-enhanced localized plasticity: an atomistic study using alpha-Fe as a model system, Acta Mater. 68 (2014) 61–69.
[17] D. Xie, S. Li, M. Li, Z. Wang, P. Gumbsch, J. Sun, E. Ma, J. Li, Z. Shan, Hydrogenated vacancies lock dislocations in aluminium, Nat. Commun. 7 (1) (2016) 13341.
[18] X. Lu, D. Wang, D. Wan, Z.B. Zhang, N. Kheradmand, A. Barnoush, Effect of electrochemical charging on the hydrogen embrittlement susceptibility of alloy 718, Acta Mater. 179 (2019) 36–48.
[19] Y. Ding, H. Yu, K. Zhao, M. Lin, S. Xiao, M. Ortiz, J. He, Z. Zhang, Hydrogen-induced transgranular to intergranular fracture transition in bi-crystalline nickel, Scr. Mater. 204 (2021) 114122.
[20] S. Wang, M.L. Martin, I.M. Robertson, P. Sofronis, Effect of hydrogen environment on the separation of Fe grain boundaries, Acta Mater. 107 (2016) 279–288.
[21] A. Tehranchi, W. Curtin, Atomistic study of hydrogen embrittlement of grain boundaries in nickel: I. Fracture, J. Mech. Phys. Solids 101 (2017) 150–165.
[22] M.L. Martin, B.P. Somerday, R.O. Ritchie, P. Sofronis, I.M. Robertson, Hydrogen-induced intergranular failure in nickel revisited, Acta Mater. 60 (6-7) (2012) 2739–2745.
[23] Y. Fukai, Formation of superabundant vacancies in M–H alloys and some of its consequences: a review, J. Alloys Compd. 356 (2003) 263–269.
[24] M. Nagumo, Hydrogen related failure of steels - a new aspect, Mater. Sci. Technol. Lond. 20 (8) (2004) 940–950.
[25] M. Nagumo, K. Takai, The predominant role of strain-induced vacancies in hydrogen embrittlement of steels: overview, Acta Mater. 165 (2019) 722–733.
[26] S.Z. Li, Y.G. Li, Y.C. Lo, T. Neeraj, R. Srinivasan, X.D. Ding, J. Sun, L. Qi, P. Gumbsch, J. Li, The interaction of dislocations and hydrogen-vacancy complexes and its importance for deformation-induced proto nano-voids formation in alpha-Fe, Int. J. Plast. 74 (2015) 175–191.
[27] Y.X. Zhu, Z.H. Li, M.S. Huang, H.D. Fan, Study on interactions of an edge dislocation with vacancy-H complex by atomistic modelling, Int. J. Plast. 92 (2017) 31–44.
[28] S.K. Lawrence, Y. Yagodzinskyy, H. Hanninen, E. Korhonen, F. Tuomisto, Z.D. Harris, B.P. Somerday, Effects of grain size and deformation temperature on hydrogen-enhanced vacancy formation in Ni alloys, Acta Mater. 128 (2017) 218–226.
[29] Z.D. Harris, S.K. Lawrence, D.L. Medlin, G. Guetard, J.T. Burns, B.P. Somerday, Elucidating the contribution of mobile hydrogen-deformation interactions to hydrogen-induced intergranular cracking in polycrystalline nickel, Acta Mater. 158 (2018) 180–192.
[30] Y. Ogawa, K. Noguchi, O. Takakuwa, Criteria for hydrogen-assisted crack initiation in Ni-based superalloy 718, Acta Mater. (2022) 117789.
[31] Y.S. Chen, H. Lu, J. Liang, A. Rosenthal, H. Liu, G. Sneddon, I. McCarroll, Z. Zhao, W. Li, A. Guo, Observation of hydrogen trapping at dislocations, grain boundaries, and precipitates, Science 367 (6474) (2020) 171–175.
[32] H. Zhao, P. Chakraborty, D. Ponge, T. Hickel, B. Sun, C.H. Wu, B. Gault, D. Raabe, Hydrogen trapping and embrittlement in high-strength Al alloys, Nature 602 (7897) (2022) 437–441.
[33] L. Wan, W.T. Geng, A. Ishii, J.P. Du, Q.S. Mei, N. Ishikawa, H. Kimizuka, S. Ogata, Hydrogen embrittlement controlled by reaction of dislocation with grain boundary in alpha-iron, Int. J. Plast. 112 (2019) 206–219.
[34] A. Tehranchi, W.A. Curtin, The role of atomistic simulations in probing hydrogen effects on plasticity and embrittlement in metals, Eng. Fract. Mech. 216 (2019) 106502.
[35] S. Yin, G.M. Cheng, T.H. Chang, G. Richter, Y. Zhu, H.J. Gao, Hydrogen embrittlement in metallic nanowires, Nat. Commun. 10 (2019).
[36] X.S. Kong, S. Wang, X. Wu, Y.W. You, C. Liu, Q. Fang, J.L. Chen, G.N. Luo, First-principles calculations of hydrogen solution and diffusion in tungsten: temperature and defect-trapping effects, Acta Mater. 84 (2015) 426–435.
[37] W. Geng, L. Wan, J.P. Du, A. Ishii, N. Ishikawa, H. Kimizuka, S. Ogata, Hydrogen bubble nucleation in α-iron, Scr. Mater. 134 (2017) 105–109.
[38] J. Hou, X.S. Kong, X.B. Wu, J. Song, C.S. Liu, Predictive model of hydrogen trapping and bubbling in nanovoids in bcc metals, Nat. Mater. 18 (8) (2019) 833–839.

[39] S. Taketomi, R. Matsumoto, N. Miyazaki, Atomistic study of hydrogen distribution and diffusion around a {1 1 2}< 1 1 1>edge dislocation in alpha iron, Acta Mater. 56 (15) (2008) 3761–3769.
[40] J. Von Pezold, L. Lymperakis, J. Neugebeauer, Hydrogen-enhanced local plasticity at dilute bulk H concentrations: the role of H–H interactions and the formation of local hydrides, Acta Mater. 59 (8) (2011) 2969–2980.
[41] P. Yu, Y.G. Cui, G.Z. Zhu, Y. Shen, M. Wen, The key role played by dislocation core radius and energy in hydrogen interaction with dislocations, Acta Mater. 185 (2020) 518–527.
[42] B. Kuhr, D. Farkas, I.M. Robertson, Atomistic studies of hydrogen effects on grain boundary structure and deformation response in FCC Ni, Comput. Mater. Sci. 122 (2016) 92–101.
[43] K.N. Solanki, M.A. Tschopp, M.A. Bhatia, N.R. Rhodes, Atomistic investigation of the role of grain boundary structure on hydrogen segregation and embrittlement in alpha-Fe, Metall. Mater. Trans. A 44a (3) (2013) 1365–1375.
[44] J. Li, C. Lu, L. Pei, C. Zhang, R. Wang, Atomistic investigation of hydrogen induced decohesion of Ni grain boundaries, Mech. Mater. 150 (2020) 103586.
[45] R. Matsumoto, S. Taketomi, S. Matsumoto, N. Miyazaki, Atomistic simulations of hydrogen embrittlement, Int. J. Hydrog. Energy 34 (23) (2009) 9576–9584.
[46] J. Song, W. Curtin, Mechanisms of hydrogen-enhanced localized plasticity: an atomistic study using α-Fe as a model system, Acta Mater. 68 (2014) 61–69.
[47] A. Tehranchi, W. Curtin, Atomistic study of hydrogen embrittlement of grain boundaries in nickel: II. Decohesion, modelling and simulation in, Mater. Sci. Eng. 25 (7) (2017) 075013.
[48] J.E. Angelo, N.R. Moody, M.I. Baskes, Trapping of hydrogen to lattice-defects in nickel, Model. Simul. Mater. Sci. 3 (3) (1995) 289–307.
[49] W. Shinoda, M. Shiga, M. Mikami, Rapid estimation of elastic constants by molecular dynamics simulation under constant stress, Phys. Rev. B 69 (13) (2004) 134103.
[50] M.Q. Chandler, M.F. Horstemeyer, M.I. Baskes, P.M. Gullett, G.J. Wagner, B. Jelinek, Hydrogen effects on nanovoid nucleation in face-centered cubic single-crystals, Acta Mater. 56 (1) (2008) 95–104.
[51] M. Koyama, S.M. Taheri-Mousavi, H. Yan, J. Kim, B.C. Cameron, S.S. Moeini-Ardakani, J. Li, C.C. Tasan, Origin of micrometer-scale dislocation motion during hydrogen desorption, Sci. Adv. 6 (23) (2020) eaaz1187.
[52] S. Plimpton, Fast parallel algorithms for short-range molecular-dynamics, J. Comput. Phys. 117 (1) (1995) 1–19.
[53] D.J. Adams, Grand canonical ensemble monte-carlo for a lennard-jones fluid, Mol. Phys. 29 (1) (1975) 307–311.
[54] A.P. Thompson, S.J. Plimpton, W. Mattson, General formulation of pressure and stress tensor for arbitrary many-body interaction potentials under periodic boundary conditions, J. Chem. Phys. 131 (15) (2009) 154107.
[55] C.L. Kelchner, S.J. Plimpton, J.C. Hamilton, Dislocation nucleation and defect structure during surface indentation, Phys. Rev. B 58 (17) (1998) 11085–11088.
[56] J. Schiotz, F.D. Di Tolla, K.W. Jacobsen, Softening of nanocrystalline metals at very small grain sizes, Nature 391 (6667) (1998) 561–563.
[57] A. Stukowski, Visualization and analysis of atomistic simulation data with OVITO–the open visualization tool, Modell. Simul. Mater. Sci. Eng. 18 (1) (2009) 015012.
[58] D. Di Stefano, M. Mrovec, C. Elsasser, First-principles investigation of hydrogen trapping and diffusion at grain boundaries in nickel, Acta Mater. 98 (2015) 306–312.
[59] M. Nagumo, T. Ishikawa, T. Endoh, Y. Inoue, Amorphization associated with crack propagation in hydrogen-charged steel, Scr. Mater. 49 (9) (2003) 837–842.
[60] A. Harada, K. Kusunoki, K. Moritani, K. Matsumoto, M. Hatano, Y. Horibe, Amorphization under fracture surface in hydrogen-charged and low-temperature tensile-tested austenitic stainless steel, Philos. Mag. Lett. 101 (1) (2021) 40–50.
[61] K. Young, T. Ouchi, H. Shen, L. Bendersky, Hydrogen induced amorphization of LaMgNi4 phase in metal hydride alloys, Int. J. Hydrog. Energy 40 (29) (2015) 8941–8947.
[62] Y. Li, H. Ren, Y. Zhang, Z. Liu, H. Zhang, Hydrogen induced amorphization behaviors of multiphase La0. 8Mg0. 2Ni3. 5 alloy, Int. J. Hydrog. Energy 40 (22) (2015) 7093–7102.
[63] T. Neeraj, R. Srinivasan, J. Li, Hydrogen embrittlement of ferritic steels: Observations on deformation microstructure, nanoscale dimples and failure by nanovoiding, Acta Mater. 60 (13-14) (2012) 5160–5171.
[64] R. Benedictus, A. Böttger, E. Mittemeijer, Thermodynamic model for solid-state amorphization in binary systems at interfaces and grain boundaries, Phys. Rev. B 54 (13) (1996) 9109.
[65] M.Y. Gutkin, I. Ovid'Ko, Disclinations, amorphization and microcrack generation at grain boundary junctions in polycrystalline solids, Philos. Mag. A 70 (4) (1994) 561–575.
[66] J.M. Polfus, O.M. Løvvik, R. Bredesen, T. Peters, Hydrogen induced vacancy clustering and void formation mechanisms at grain boundaries in palladium, Acta Mater. 195 (2020) 708–719.
[67] D. Tanguy, Y. Wang, D. Connetable, Stability of vacancy-hydrogen clusters in nickel from first-principles calculations, Acta Mater. 78 (2014) 135–143.
[68] N. Fernandez, Y. Ferro, D. Kato, Hydrogen diffusion and vacancies formation in tungsten: density functional theory calculations and statistical models, Acta Mater. 94 (2015) 307–318.
[69] A. Oudriss, J. Creus, J. Bouhattate, E. Conforto, C. Berziou, C. Savall, X. Feaugas, Grain size and grain-boundary effects on diffusion and trapping of hydrogen in pure nickel, Acta Mater. 60 (19) (2012) 6814–6828.
[70] H. Sun, C.V. Singh, Temperature dependence of grain boundary excess free volume, Scr. Mater. 178 (2020) 71–76.
[71] L. Chiari, K. Kojima, Y. Endo, H. Teshigahara, M. Butterling, M.O. Liedke, E. Hirschmann, A.G. Attallah, A. Wagner, M. Fujinami, Formation and time dynamics of hydrogen-induced vacancies in nickel, Acta Mater. (2021) 117264.
[72] Y. Sugiyama, K. Takai, Quantities and distribution of strain-induced vacancies and dislocations enhanced by hydrogen in iron, Acta Mater. 208 (2021) 116663.
[73] S. Jothi, S. Merzlikin, T. Croft, J. Andersson, S. Brown, An investigation of micro-mechanisms in hydrogen induced cracking in nickel-based superalloy 718, J. Alloys Compd. 664 (2016) 664–681.
[74] D.M. Symons, A.W. Thompson, The effect of hydrogen on the fracture of alloy X-750, Metall. Mater. Trans. A 27 (1) (1996) 101–110.
[75] T. Homma, T. Chiba, K. Takai, E. Akiyama, W. Oshikawa, M. Nagumo, Cracking process in delayed fracture of high-strength steel after long atmospheric exposure, ISIJ Int. (2022) ISIJINT-2021-238.

A.3 Paper 3

The dual role of hydrogen in grain boundary mobility

Authors: Yu Ding, Kai Zhao, Meichao Lin, Haiyang Yu, Senbo Xiao, Jianying He, Zhiliang Zhang

Journal of Applied Physics 133.4 (2023): 045103.

Paper 3

The dual role of hydrogen in grain boundary mobility

Cite as: J. Appl. Phys. **133**, 045103 (2023); https://doi.org/10.1063/5.0132488
Submitted: 28 October 2022 • Accepted: 31 December 2022 • Published Online: 26 January 2023

Yu Ding, Kai Zhao, Meichao Lin, et al.

Journal of Applied Physics ARTICLE scitation.org/journal/jap

The dual role of hydrogen in grain boundary mobility

Cite as: J. Appl. Phys. 133, 045103 (2023); doi: 10.1063/5.0132488
Submitted: 28 October 2022 · Accepted: 31 December 2022 ·
Published Online: 26 January 2023

Yu Ding,[1] Kai Zhao,[2] Meichao Lin,[1] Haiyang Yu,[3,a)] Senbo Xiao,[1] Jianying He,[1,a)] and Zhiliang Zhang[1,a)]

AFFILIATIONS

[1]Department of Structural Engineering, Norwegian University of Science and Technology (NTNU), Trondheim 7491, Norway
[2]Jiangsu Key Laboratory of Advanced Food Manufacturing Equipment and Technology, Jiangnan University, Wuxi 214122, China
[3]Division of Applied Mechanics, Department of Materials Science and Engineering, Uppsala University, SE-75121 Uppsala, Sweden

[a)]**Authors to whom correspondence should be addressed:** haiyang.yu@angstrom.uu.se; jianying.he@ntnu.no; and zhiliang.zhang@ntnu.no

ABSTRACT

The effect of solute hydrogen on shear-coupled grain boundary (GB) migration is investigated with the dislocation-array type Σ25(430)[001] GB and a dual role of hydrogen on GB mobility is unraveled. In the low temperature and high loading rate regime, where hydrogen diffusion is substantially slower than GB motion, GB breaks away from the hydrogen atmosphere and transforms into a new stable phase with highly enhanced mobility. In the reverse regime, hydrogen atoms move along with GB, exerting a drag force on GB and decreasing its mobility. These findings provide rationale for the coexistence of hydrogen hardening and softening observed experimentally in polycrystalline materials.

I. INTRODUCTION

Hydrogen as a clean energy carrier is attracting enormous attention nowadays and is envisioned as the fuel of future. However, the safety of engineering components for hydrogen storage and transport is often undermined due to a phenomenon called hydrogen embrittlement (HE), where dissolved hydrogen in metals can cause dramatic degradation of mechanical properties leading to sudden and catastrophic failure. Despite studies over one century, the fundamental mechanisms of HE remain controversial.[1–5] The core debate is over the effects of hydrogen on dislocation motion. The hydrogen-enhanced localized plasticity (HELP)[2] mechanism proposes that hydrogen exerts a shielding effect on the elastic field to enhance dislocation mobility. This is supported by a number of transmission electron microscopy observations[6–8] and has been correlated to a global softening effect. However, HELP cannot rationalize the hydrogen-induced hardening observed in some macroscopic experiments,[9–11] which is often attributed to the pinning effect of hydrogen on dislocations.[12–14] The hydrogen-enhanced decohesion (HEDE)[15] mechanism assumes a weakening of the interatomic bonds by hydrogen; it is always associated with locally high hydrogen concentrations where hardening is observed but cannot explain the softening behaviors. Recently, more researchers suggested synergistic action of mixed mechanisms where HEDE and HELP play their respective roles in hardening and softening with the dominance of a particular mechanism depending on numerous factors,[16] but the nanoscale detail about those mechanisms is still lacking. It should be noted that in addition to the intensively studied hydrogen–dislocation interaction, the grain boundary (GB), as a type of interface separating differently oriented crystallites, works as an important plasticity carrier in polycrystalline materials and can, therefore, also play a significant role in HE.[17–22] Among the topics, the study on hydrogen-influenced GB mobility has been rather limited.

II. METHODOLOGY

Traditional models treat GBs as immobile structures that pose an obstacle to dislocation motion. However, increasing evidence[23–26] showed that GBs can also move under shear stress. This phenomenon is referred to as coupling GB motion to shear deformation,[27] where the normal motion of GB is always coupled with a simultaneous relative translation of adjacent grains parallel to the GB plane.

The ideal coupling is described by a linear relationship,

$$v_{\parallel} = \beta v_n, \tag{1}$$

where β is a coupling factor between grain translation velocity $v_{\parallel}$ and GB normal velocity v_n. Both theoretical[27–32] and experimental studies[33–35] revealed that β is purely a geometric parameter when it comes to a perfect coupling. Continuous efforts have been devoted to quantifying GB mobility M_n,[29–32,36,37] which is an inherent property of GB defined as the normalized v_n by the normal driving force F_n (in stress unit),

$$M_n = v_n/F_n. \tag{2}$$

Considering that the rate of energy dissipation by normal GB motion is equal to the work done by the shear stress τ per GB unit area, $F_n v_n = \tau v_{\parallel}$, and the Eq. (1), we get

$$M_n = \frac{v_n}{\beta \tau}. \tag{3}$$

GB mobility depends on several factors, e.g., temperature, loading rate, and solute concentration. The force produced by the segregation of a solute atmosphere on the GB is known as solute drag which depends strongly on the velocity of the GB relative to the diffusivity of the solute.[38–40] At low velocity, the segregation atmosphere moves together with GB and causes an additional friction force (hereinafter referred to as the solute drag model). At high velocity, the GB breaks away from the atmosphere and the friction force decreases (referred to as the breakaway model). In both velocity regimes, hydrogen as a solute should exert a strong or weak hardening effect which is, however, contradictory to the HELP mechanism. To explore those mysteries, we perform atomistic modeling and reveal that hydrogen could induce GB phase transition and work either as an enhancer or inhibitor for GB mobility at varying temperature and loading rate regimes.

Molecular dynamics (MD) simulations are carried out in a nickel-hydrogen bicrystal system with an embedded atom method potential[41] using the LAMMPS code,[42] and atomic structures are visualized in Ovito.[43] As illustrated in Fig. 1(a), Σ25(430)[001] symmetric tilt GB is created by constructing two perfect FCC crystals with desired crystallographic orientations in a rectangular box and joining the crystals along a plane normal to the Y-direction. The GB interface shows a typical structure composed of an array of lattice dislocations and its migration behavior has been intensively studied before.[27] Periodic boundary conditions are applied along the X (10.6 nm) and Z (5.3 nm) directions while a free boundary condition is employed along the Y (12.7 + 25.4 nm) direction.

After equilibrium in the isothermal-isobaric (NPT) ensemble at 300 K for 100 ps, the system is put into hybrid grand canonical Monte Carlo (GCMC)/molecular dynamic simulation[20] to obtain the hydrogen distribution around GB. In the GCMC process, hydrogen atoms are randomly inserted or deleted to achieve a desired chemical potential (−2.31 eV) within a constant volume (grand canonical ensemble). This chemical potential corresponds to a bulk hydrogen concentration of 1000 appm at a similar level to previous experimental studies in polycrystalline nickel[44,45] (see the relationship between bulk hydrogen concentration for the perfect fcc nickel and hydrogen charging chemical potential in Fig. 1 in the supplementary material). In the MD part, each GCMC step is followed by ten steps in the canonical (NVT) ensemble at 300 K until the hydrogen concentration in the box fluctuates in a narrow range (±1% atomic ratio), and the final configuration is taken as the 100% hydrogenated GB. Figure 1(b) shows the hydrogen concentration c_H evolution at the GB region (the vicinity ±1 nm to the GB) and in the grains (the remaining part in the box). Hydrogen tends to form an atmosphere (0.194 atomic ratio) in the GB region, while the hydrogen concentration in the grains stays at a level (0.001 atomic ratio) often seen in experiments. After charging and further equilibrating in the NPT ensemble for 100 ps, the migration behavior of the 0%, 13%, and 100% hydrogenated GBs in response to an external shear deformation are investigated. Figure 1(c) shows the local GB structures, clearly, hydrogen atoms mainly accumulate in the vicinity of the GB. Displacement-controlled loading is applied by shearing the upper rigid slab at a constant velocity ($v_{\parallel}$ = 0.02, 0.2, and 2 m/s) while keeping the lower rigid slab stationary, and the NVT ensemble is carried out in the middle region at varying temperatures (T = 300, 400, 500, and 600 K). During the deformation stage, the external charging reservoir is not applied to keep the hydrogen concentration unchanged.

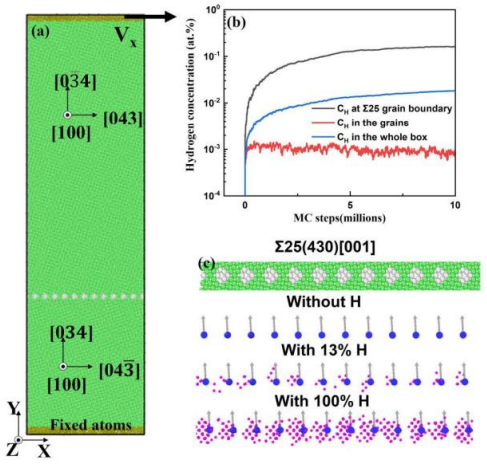

FIG. 1. (a) Schematic of the nickel Σ25(430)[001] symmetric tilt GB. Atoms representing ordinary FCC structures are marked green, those belonging to GB dislocation cores are marked white, and atoms in the lower stationary slab and in the upper rigid slab with a constant shearing velocity are marked brown. (b) Hydrogen concentration evolution around the Σ25 GB during the GCMC/MD charging process. (c) Local structure of hydrogenated GB with 0%, 13%, and 100% hydrogen. The blue circle represents the GB dislocation line perpendicular to the paper plane with its Burgers vector indicated by the gray arrow, and hydrogen atoms are colored pink.

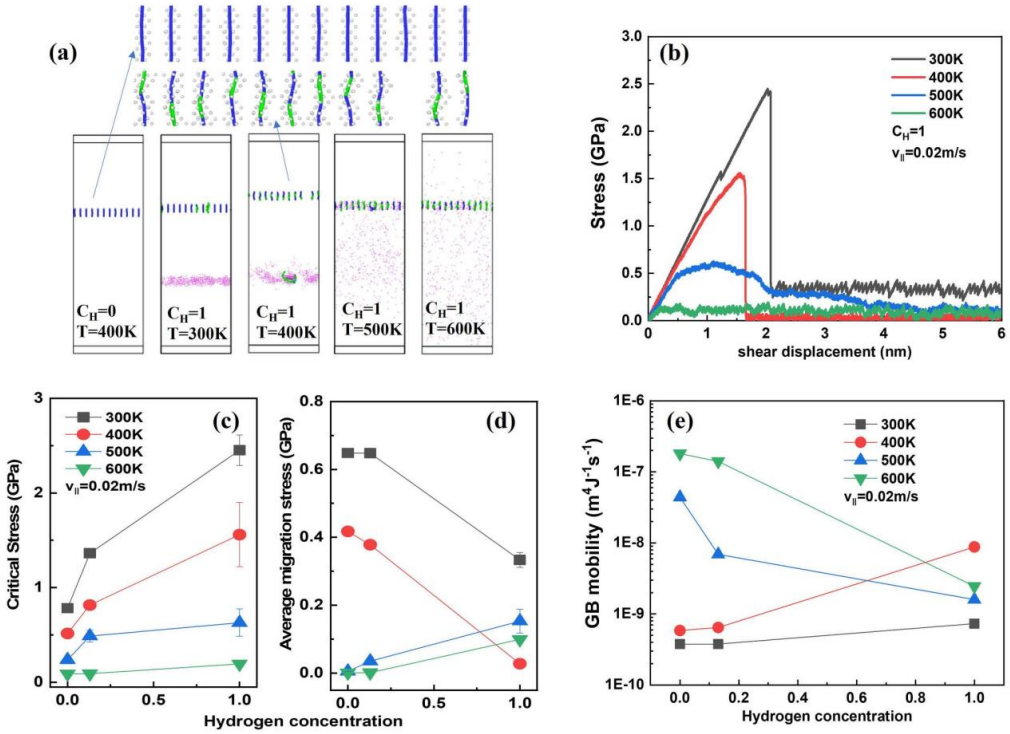

FIG. 3. (a) The position of GB and hydrogen atoms for varying temperatures with the shear displacement $\delta_{\parallel} = 4$ nm. $c_H = 0$, $T = 400$ K case is set as a control group for the cases with hydrogen (see supplementary movie 2 in the supplementary material). (b) Shear stress τ_{xz}–shear displacement $\delta_{\parallel}$ curves for varying temperatures. (c) and (d) Critical stress and average migration stress for varying hydrogen concentrations and temperatures. (e) GB mobility for varying hydrogen concentrations and temperatures.

atmosphere for all the cases at 300 K where hydrogen diffusion is slower than the GB velocity (0.0701 m/s). The relationship between shear stress τ_{xz} and shear displacement $\delta_{\parallel}$ is shown in Fig. 2(e). In the absence of hydrogen, τ_{xz} first increases linearly with $\delta_{\parallel}$ corresponding to an elastic regime where the system is uniformly deformed and the GB structure remains unchanged. This regime ends when τ_{xz} reaches a critical value ($\delta_{\parallel} = 0.65$ nm, $\tau_{critical} = 0.78$ GPa) and GB starts to move by the nucleation and propagation of disconnections.[28] When the shear stress enters a steady-state regime, it shows a stick-slip pattern and continues to fluctuate around a constant value, which is termed the average migration stress ($\tau_{average} = 0.65$ GPa). Under perfect coupling conditions, the average stress for this regime is proportional to the GB driving force $F_n = \beta\tau_{average}$ and directly reflects the reciprocal of GB mobility in Eq. (3). Hydrogen inhibits the normal motion of GB by suppressing the formation of disconnection steps. The elastic region is elongated, and it causes larger strain and stress in the system before migration. The shear stress continues to rise until a new critical stress for activating GB migration is reached ($\delta_{\parallel} = 1.05$ nm, $\tau_{critical} = 1.36$ GPa for $c_H = 0.13$, and $\delta_{\parallel} = 2.02$ nm, $\tau_{critical} = 2.45$ GPa for $c_H = 1$). Then, GB breaks away from the hydrogen atmosphere and jumps (by a distance of 2.2 nm for $c_H = 0.13$ and 6 nm for $c_H = 1$) to the same position as in the absence of hydrogen. The shear stress drops instantaneously and falls into the stick-slip regime. However, the average migration stress in this regime is highly decreased for $c_H = 1$ ($\tau_{average} = 0.64$ GPa for $c_H = 0.13$ and $\tau_{average} = 0.33$ GPa for $c_H = 1$). This indicates that the mobility of GB is enhanced due to

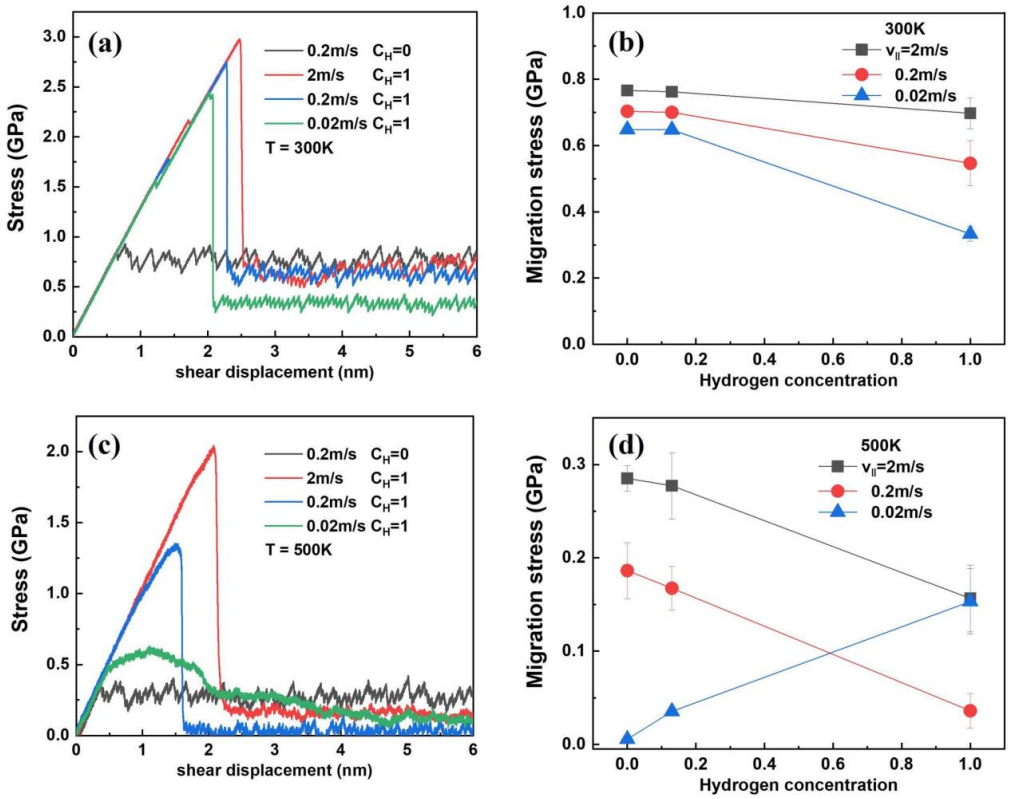

FIG. 4. (a) and (c) Shear stress τ_{xz}–shear displacement $\delta_{\|}$ curves for varying loading rates at 300 and 500 K, respectively. (b) and (d) Average migration stress for varying hydrogen concentrations and loading rates at 300 and 500 K, respectively.

the interaction with hydrogen, which could be attributed to the forming of a new stable GB phase. As shown in Fig. 2(d), for $c_H = 0$ and 0.13, GB remains an array of perfect dislocations during migration with almost the same average migration stress. For $c_H = 1$, the activation stress for GB migration is much higher, and local dislocation interaction could happen on the GB plane. For $\delta_{\|} = 2$ nm before migration, as a result of hydrogen and high local stress, the perfect GB dislocations decompose into Shockley dislocations and interact with other dislocations on the XZ plane. Upon reaching the critical stress, the GB breaks away but its configuration has been permanently changed, with vacancies and even dislocation loops (part of original GB dislocations) detected in the hydrogen atmosphere left behind. The newly formed GB structure is more compact than the original one. By fast quenching and calculating the excess free energy compared with the perfect FCC lattice per area, we find that GB energy E_{GB} after breaking away for $c_H = 0$, 0.13, and 1 are 1.057, 1.055, and 0.974 J/m^2, respectively. This new GB phase has lower energy and higher mobility. In the case at 300 K, hydrogen exerts a dual effect on GB motion. On one hand, it increases the energy barrier and, thus, the critical stress for the activation of GB migration; on the other hand, it induces the GB phase transition which alters the structure and energetics of the GB and enhances the mobility.

To further investigate the coupling effect of solute concentration and temperature on GB mobility, the same cases in Fig. 2 are studied at different temperatures. Figure 3(a) shows the hydrogen

distribution with $\delta_{\|} = 4$ nm, a clear transition from the breakaway model to the solute drag model could be observed by increasing the temperature. For $T = 300$ and 400 K, hydrogen moves slowly and is not able to follow the GB, which causes the GB to finally break away from the hydrogen atmosphere and transform into a new phase. As the temperature increases, the diffusivity of hydrogen is enhanced. At 500 K, hydrogen atoms can move along with GB dislocations and some of the atoms can be trapped along the path traveled by the GB. At 600 K, hydrogen atoms move even faster than the GB. These cases fall into the regime of the solute drag model where hydrogen exerts friction force on the moving GB. The shear stress–displacement curve is shown in Fig. 3(b), and the critical stress and average migration stress are presented in Figs. 3(c) and 3(d), respectively. Each case was repeated 10 times with different temperature seeds to extract statistically reliable data. As shown in Fig. 3(c), hydrogen increases the barrier for the activation of GB migration at all the temperatures investigated, as evidenced by the elevated critical stress with increasing hydrogen concentration. In contrast, the average migration stress shows opposite trends at different temperature regimes. For the breakaway regime (below 500 K), migration stress decreases with increasing hydrogen concentration. It is caused by the formation of a new GB phase with higher mobility. For the solute drag regime (500 K and above), the hydrogen atoms transported by GB motion impose a drag force on the GB, which degrades the GB mobility. Using Eq. (3), the GB mobility is calculated and shown in Fig. 3(e), and the dual role of hydrogen in GB mobility under different temperature regimes is quantitatively presented.

By changing the shear velocity of the slabs (from 0.02 to 2 m/s), the migration behavior under different loading rates is also studied. Figure 4 shows the stress–displacement curves under varying loading rates and the corresponding averaging stresses. Under the breakaway model at 300 K, increased GB velocity tends to weaken the effect of hydrogen and reduce the migration stress, i.e., hydrogen has less potential to transform the GB into a low-energy and high-mobility phase. At 500 K, the enhanced GB velocity promotes the transition from solute drag model ($v_{\|} = 0.02$ m/s) to breakaway model ($v_{\|} = 0.2$ and 2 m/s) because hydrogen atoms are unable to keep pace with the accelerated GB. Thus, the role of hydrogen on GB mobility switches from an inhibitor to a booster when strain rate elevates.

IV. CONCLUSION

In summary, we studied the effect of hydrogen on the migration behavior of Σ25(430)[001] GB using Monte Carlo and molecular dynamics methods. A dual role of hydrogen in GB mobility was unraveled. In the low temperature and high loading rate regime, hydrogen atoms move slower than GB, so the hydrogen atmosphere exerts a pinning effect on the GB before the GB motion is activated; this results in increased critical stress for GB activation. Once the critical stress is reached, GB breaks away from the hydrogen atmosphere and transforms into a new stable phase with lower energy and higher mobility, so the migration stress is lower with hydrogen. In the high temperature and low loading rate regime, hydrogen atoms travel along with GB, pose a drag force on the GB, and decrease its mobility, in line with classical solute drag theory. Considering GB as a plasticity carrier, the dual role of hydrogen can lead either to plastic softening or hardening. This dual role can also be relevant to hydrogen–dislocation interaction since the Σ25 GB is composed of rows of edge dislocations, and hydrogen may facilitate the transformation of dislocation core structures. These findings can thus help rationalize the controversial observations of hydrogen hardening and hydrogen softening in polycrystalline materials under different experimental conditions. Local hydrogen accumulation hinders the mobility of GBs or dislocations and induces hardening, at the same time it can also enhance their mobility by reconstructing their core structure, with the transition between them depending on several factors such as hydrogen concentrations, temperatures, and loading rates.

SUPPLEMENTARY MATERIAL

See the supplementary material for the relationship between equilibrium bulk hydrogen concentration c_0 in perfect fcc nickel and chemical potential u used in the charging process (Fig. 1), energy/atom-MC steps plot during GCMC/MD charging process (Fig. 2), migration behaviors of Σ25(430)[001] GB at 300 K with varying hydrogen concentration $c_H = 0$, 0.13, and 1, respectively (Movie 1), and migration behaviors of Σ25(430)[001] GB in the presence of hydrogen with varying temperatures T = 300, 400, 500, and 600 K, respectively.

ACKNOWLEDGMENTS

Y.D. acknowledges the financial support provided by the Research Council of Norway under the M-HEAT project (Grant No. 294689) and the HyLINE project (Grant No. 294739). All simulations are carried out on the Betzy (Grant Nos. NN9110K and NN9391K) high-performance computer clusters at NTNU, Trondheim.

AUTHOR DECLARATIONS

Conflict of Interest

The authors have no conflicts to disclose.

Author Contributions

Yu Ding: Conceptualization (equal); Investigation (equal); Writing – original draft (equal). **Kai Zhao:** Writing – original draft (equal). **Meichao Lin:** Writing – original draft (equal). **Haiyang Yu:** Supervision (equal); Writing – original draft (equal). **Senbo Xiao:** Writing – original draft (equal). **Jianying He:** Supervision (equal); Writing – original draft (equal). **Zhiliang Zhang:** Supervision (equal); Writing – original draft (equal).

DATA AVAILABILITY

The data that support the findings of this study are available from the corresponding authors upon request.

REFERENCES

[1]W. H. Johnson, Philos. Trans. R. Soc. London A **23**, 168 (1875).
[2]H. K. Birnbaum and P. Sofronis, Mater. Sci. Eng. A **176**, 191 (1994).
[3]A. R. Troiano, Metallogr. Microstruct. Anal. **5**, 557 (2016).
[4]M. Nagumo, Mater. Sci. Technol. **20**, 940 (2004).

[5]M. Lin, H. Yu, Y. Ding, G. Wang, V. Olden, A. Alvaro, J. He, and Z. Zhang, Scr. Mater. **215**, 114707 (2022).
[6]P. J. Ferreira, I. M. Robertson, and H. K. Birnbaum, Acta Mater. **46**, 1749 (1998).
[7]P. J. Ferreira, I. M. Robertson, and H. K. Birnbaum, Acta Mater. **47**, 2991 (1999).
[8]I. Robertson, Eng. Fracture Mech. **64**, 649 (1999).
[9]J. P. Hirth, Metall. Trans. A **11**, 861 (1980).
[10]Y. Zhao, M.-Y. Seok, I.-C. Choi, Y.-H. Lee, S.-J. Park, U. Ramamurty, J.-Y. Suh, and J.-i. Jang, Scr. Mater. **107**, 46 (2015).
[11]A. Tehranchi, B. Yin, and W. Curtin, Philos. Mag. **97**, 400 (2017).
[12]J. Song and W. Curtin, Acta Mater. **68**, 61 (2014).
[13]D. Xie, S. Li, M. Li, Z. Wang, P. Gumbsch, J. Sun, E. Ma, J. Li, and Z. Shan, Nat. Commun. **7**, 13341 (2016).
[14]X. Lu and D. Wang, J. Mater. Sci. Technol. **67**, 243 (2021).
[15]R. A. Oriani, Ber. Bunsen-Ges. Phys. Chem. **76**, 848 (1972).
[16]M. B. Djukic, G. M. Bakic, V. S. Zeravcic, A. Sedmak, and B. Rajicic, Eng. Fracture Mech. **216**, 106528 (2019).
[17]S. Bechtle, M. Kumar, B. P. Somerday, M. E. Launey, and R. O. Ritchie, Acta Mater. **57**, 4148 (2009).
[18]X. Zhou, D. Marchand, D. L. McDowell, T. Zhu, and J. Song, Phys. Rev. Lett. **116**, 075502 (2016).
[19]Y. Ding, H. Yu, K. Zhao, M. Lin, S. Xiao, M. Ortiz, J. He, and Z. Zhang, Scr. Mater. **204**, 114122 (2021).
[20]Y. Ding *et al.*, Acta Mater. **239**, 118279 (2022).
[21]J. Q. Li, C. Lu, L. Q. Pei, C. Zhang, and R. Wang, Int. J. Hydrogen Energy **45**, 9174 (2020).
[22]J. Chen, S. Liang, Y. Zhu, L. Zhao, M. Huang, and Z. Li, Comput. Mater. Sci. **212**, 111569 (2022).
[23]C. H. Li, E. H. Edwards, J. Washburn, and E. R. Parker, Acta Metall. **1**, 223 (1953).
[24]M. Winning, G. Gottstein, and L. Shvindlerman, Acta Mater. **49**, 211 (2001).
[25]T. Rupert, D. Gianola, Y. Gan, and K. Hemker, Science **326**, 1686 (2009).
[26]J. A. Moriarty, J. F. Belak, R. E. Rudd, P. Soderlind, F. H. Streitz, and L. H. Yang, J. Phys.: Condens. Matter **14**, 2825 (2002).
[27]J. W. Cahn, Y. Mishin, and A. Suzuki, Acta Mater. **54**, 4953 (2006).
[28]J. Han, S. L. Thomas, and D. J. Srolovitz, Prog. Mater. Sci. **98**, 386 (2018).
[29]V. A. Ivanov and Y. Mishin, Phys. Rev. B **78**, 064106 (2008).
[30]A. Karma, Z. T. Trautt, and Y. Mishin, Phys. Rev. Lett. **109**, 095501 (2012).
[31]A. Rajabzadeh, F. Mompiou, M. Legros, and N. Combe, Phys. Rev. Lett. **110**, 265507 (2013).
[32]L. Zhang, J. Han, Y. Xiang, and D. J. Srolovitz, Phys. Rev. Lett. **119**, 246101 (2017).
[33]F. Mompiou, D. Caillard, and M. Legros, Acta Mater. **57**, 2198 (2009).
[34]T. Gorkaya, D. A. Molodov, and G. Gottstein, Acta Mater. **57**, 5396 (2009).
[35]A. Rajabzadeh, M. Legros, N. Combe, F. Mompiou, and D. Molodov, Philos. Mag. **93**, 1299 (2013).
[36]J. Powers and A. Glaeser, Interface Sci **6**, 23 (1998).
[37]K. Chen, J. Han, X. Pan, and D. J. Srolovitz, Proc. Natl. Acad. Sci. U.S.A. **117**, 4533 (2020).
[38]J. W. Cahn, Acta Metall. **10**, 789 (1962).
[39]K. Lücke and H. Stüwe, Acta Metall. **19**, 1087 (1971).
[40]R. K. Koju and Y. Mishin, Acta Mater. **198**, 111 (2020).
[41]J. E. Angelo, N. R. Moody, and M. I. Baskes, Modell. Simul. Mater. Sci. Eng. **3**, 289 (1995).
[42]S. Plimpton, J. Comput. Phys. **117**, 1 (1995).
[43]A. Stukowski, Modell. Simul. Mater. Sci. Eng. **18**, 015012 (2009).
[44]K. Wada, J. Yamabe, and H. Matsunaga, Materialia **8**, 100478 (2019).
[45]Z. D. Harris, S. K. Lawrence, D. L. Medlin, G. Guetard, J. T. Burns, and B. P. Somerday, Acta Mater. **158**, 180 (2018).

A.4 Paper 4

Hydrogen trapping and diffusion in polycrystalline nickel: the spectrum of grain boundary segregation

Authors: Yu Ding, Jianying He, Zhiliang Zhang

To be submitted 2023

This paper will be submitted for publishing and is therefore not included.

Paper 4

Appendix B Appended Papers

List of previous PhD theses at Department of Structural Engineering

Appendix B

DEPARTMENT OF STRUCTURAL ENGINEERING
NORWEGIAN UNIVERSITY OF SCIENCE AND TECHNOLOGY

N–7491 TRONDHEIM, NORWAY
Telephone: +47 73 59 47 00

"Reliability Analysis of Structural Systems using Nonlinear Finite Element Methods",
C. A. Holm, 1990:23, ISBN 82-7119-178-0.

"Uniform Stratified Flow Interaction with a Submerged Horizontal Cylinder",
Ø. Arntsen, 1990:32, ISBN 82-7119-188-8.

"Large Displacement Analysis of Flexible and Rigid Systems Considering Displacement-Dependent Loads and Nonlinear Constraints",
K. M. Mathisen, 1990:33, ISBN 82-7119-189-6.

"Solid Mechanics and Material Models including Large Deformations",
E. Levold, 1990:56, ISBN 82-7119-214-0, ISSN 0802-3271.

"Inelastic Deformation Capacity of Flexurally-Loaded Aluminium Alloy Structures",
T. Welo, 1990:62, ISBN 82-7119-220-5, ISSN 0802-3271.

"Visualization of Results from Mechanical Engineering Analysis",
K. Aamnes, 1990:63, ISBN 82-7119-221-3, ISSN 0802-3271.

"Object-Oriented Product Modeling for Structural Design",
S. I. Dale, 1991:6, ISBN 82-7119-258-2, ISSN 0802-3271.

"Parallel Techniques for Solving Finite Element Problems on Transputer Networks",
T. H. Hansen, 1991:19, ISBN 82-7119-273-6, ISSN 0802-3271.

"Statistical Description and Estimation of Ocean Drift Ice Environments",
R. Korsnes, 1991:24, ISBN 82-7119-278-7, ISSN 0802-3271.

“Properties of concrete related to fatigue damage: with emphasis on high strength concrete”,
G. Petkovic, 1991:35, ISBN 82-7119-290-6, ISSN 0802-3271.

"Turbidity Current Modelling",
B. Brørs, 1991:38, ISBN 82-7119-293-0, ISSN 0802-3271.

"Zero-Slump Concrete: Rheology, Degree of Compaction and Strength. Effects of Fillers as Part Cement-Replacement",
C. Sørensen, 1992:8, ISBN 82-7119-357-0, ISSN 0802-3271.

"Nonlinear Analysis of Reinforced Concrete Structures Exposed to Transient Loading",
K. V. Høiseth, 1992:15, ISBN 82-7119-364-3, ISSN 0802-3271.

"Finite Element Formulations and Solution Algorithms for Buckling and Collapse Analysis of Thin Shells",
R. O. Bjærum, 1992:30, ISBN 82-7119-380-5, ISSN 0802-3271.

"Response Statistics of Nonlinear Dynamic Systems",
J. M. Johnsen, 1992:42, ISBN 82-7119-393-7, ISSN 0802-3271.

"Digital Models in Engineering. A Study on why and how engineers build and operate digital models for decisison support",
J. Høyte, 1992:75, ISBN 82-7119-429-1, ISSN 0802-3271.

"Sparse Solution of Finite Element Equations",
A. C. Damhaug, 1992:76, ISBN 82-7119-430-5, ISSN 0802-3271.

"Some Aspects of Floating Ice Related to Sea Surface Operations in the Barents Sea",
S. Løset, 1992:95, ISBN 82-7119-452-6, ISSN 0802-3271.

"Modelling of Cyclic Plasticity with Application to Steel and Aluminium Structures",
O. S. Hopperstad, 1993:7, ISBN 82-7119-461-5, ISSN 0802-3271.

"The Free Formulation: Linear Theory and Extensions with Applications to Tetrahedral Elements
with Rotational Freedoms",
G. Skeie, 1993:17, ISBN 82-7119-472-0, ISSN 0802-3271.

"Høyfast betongs motstand mot piggdekkslitasje. Analyse av resultater fra prøving i Veisliter'n",
T. Tveter, 1993:62, ISBN 82-7119-522-0, ISSN 0802-3271.

"A Nonlinear Finite Element Based on Free Formulation Theory for Analysis of Sandwich Structures",
O. Aamlid, 1993:72, ISBN 82-7119-534-4, ISSN 0802-3271.

"The Effect of Curing Temperature and Silica Fume on Chloride Migration and Pore Structure of High Strength Concrete",
C. J. Hauck, 1993:90, ISBN 82-7119-553-0, ISSN 0802-3271.

"Failure of Concrete under Compressive Strain Gradients",
G. Markeset, 1993:110, ISBN 82-7119-575-1, ISSN 0802-3271.

"An experimental study of internal tidal amphidromes in Vestfjorden",
J. H. Nilsen, 1994:39, ISBN 82-7119-640-5, ISSN 0802-3271.

"Structural analysis of oil wells with emphasis on conductor design",
H. Larsen, 1994:46, ISBN 82-7119-648-0, ISSN 0802-3271.

"Adaptive methods for non-linear finite element analysis of shell structures",
K. M. Okstad, 1994:66, ISBN 82-7119-670-7, ISSN 0802-3271.

"On constitutive modelling in nonlinear analysis of concrete structures",
O. Fyrileiv, 1994:115, ISBN 82-7119-725-8, ISSN 0802-3271.

"Fluctuating wind load and response of a line-like engineering structure with emphasis on motion-induced wind forces",
J. Bogunovic Jakobsen, 1995:62, ISBN 82-7119-809-2, ISSN 0802-3271.

"An experimental study of beam-columns subjected to combined torsion, bending and axial actions",
A. Aalberg, 1995:66, ISBN 82-7119-813-0, ISSN 0802-3271.

"Scaling and cracking in unsealed freeze/thaw testing of Portland cement and silica fume concretes",
S. Jacobsen, 1995:101, ISBN 82-7119-851-3, ISSN 0802-3271.

"Damping of water waves by submerged vegetation. A case study of laminaria hyperborea",
A. M. Dubi, 1995:108, ISBN 82-7119-859-9, ISSN 0802-3271.

"The dynamics of a slope current in the Barents Sea",
Sheng Li, 1995:109, ISBN 82-7119-860-2, ISSN 0802-3271.

"Modellering av delmaterialenes betydning for betongens konsistens",
Ernst Mørtsell, 1996:12, ISBN 82-7119-894-7, ISSN 0802-3271.

"Bending of thin-walled aluminium extrusions",
Birgit Søvik Opheim, 1996:60, ISBN 82-7119-947-1, ISSN 0802-3271.

"Material modelling of aluminium for crashworthiness analysis",
Torodd Berstad, 1996:89, ISBN 82-7119-980-3, ISSN 0802-3271.

"Estimation of structural parameters from response measurements on submerged floating tunnels",
Rolf Magne Larssen, 1996:119, ISBN 82-471-0014-2, ISSN 0802-3271.

“Numerical modelling of plain and reinforced concrete by damage mechanics”,
Mario A. Polanco-Loria, 1997:20, ISBN 82-471-0049-5, ISSN 0802-3271.

“Nonlinear random vibrations - numerical analysis by path integration methods”,
Vibeke Moe, 1997:26, ISBN 82-471-0056-8, ISSN 0802-3271.
“Numerical prediction of vortex-induced vibration by the finite element method”,
Joar Martin Dalheim, 1997:63, ISBN 82-471-0096-7, ISSN 0802-3271.

“Time domain calculations of buffeting response for wind sensitive structures”,
Ketil Aas-Jakobsen, 1997:148, ISBN 82-471-0189-0, ISSN 0802-3271.

"A numerical study of flow about fixed and flexibly mounted circular cylinders",
Trond Stokka Meling, 1998:48, ISBN 82-471-0244-7, ISSN 0802-3271.

“Estimation of chloride penetration into concrete bridges in coastal areas”,
Per Egil Steen, 1998:89, ISBN 82-471-0290-0, ISSN 0802-3271.

“Stress-resultant material models for reinforced concrete plates and shells”,
Jan Arve Øverli, 1998:95, ISBN 82-471-0297-8, ISSN 0802-3271.

“Chloride binding in concrete. Effect of surrounding environment and concrete composition”,
Claus Kenneth Larsen, 1998:101, ISBN 82-471-0337-0, ISSN 0802-3271.

“Rotational capacity of aluminium alloy beams”,
Lars A. Moen, 1999:1, ISBN 82-471-0365-6, ISSN 0802-3271.

“Stretch Bending of Aluminium Extrusions”,
Arild H. Clausen, 1999:29, ISBN 82-471-0396-6, ISSN 0802-3271.

“Aluminium and Steel Beams under Concentrated Loading”,
Tore Tryland, 1999:30, ISBN 82-471-0397-4, ISSN 0802-3271.

"Engineering Models of Elastoplasticity and Fracture for Aluminium Alloys",
Odd-Geir Lademo, 1999:39, ISBN 82-471-0406-7, ISSN 0802-3271.

"Kapasitet og duktilitet av dybelforbindelser i trekonstruksjoner",
Jan Siem, 1999:46, ISBN 82-471-0414-8, ISSN 0802-3271.

“Etablering av distribuert ingeniørarbeid; Teknologiske og organisatoriske erfaringer fra en norsk ingeniørbedrift”,
Lars Line, 1999:52, ISBN 82-471-0420-2, ISSN 0802-3271.

“Estimation of Earthquake-Induced Response”,
Símon Ólafsson, 1999:73, ISBN 82-471-0443-1, ISSN 0802-3271.

“Coastal Concrete Bridges: Moisture State, Chloride Permeability and Aging Effects”
Ragnhild Holen Relling, 1999:74, ISBN 82-471-0445-8, ISSN 0802-3271.

”Capacity Assessment of Titanium Pipes Subjected to Bending and External Pressure”,
Arve Bjørset, 1999:100, ISBN 82-471-0473-3, ISSN 0802-3271.

“Validation of Numerical Collapse Behaviour of Thin-Walled Corrugated Panels”,
Håvar Ilstad, 1999:101, ISBN 82-471-0474-1, ISSN 0802-3271.

“Strength and Ductility of Welded Structures in Aluminium Alloys”,
Miroslaw Matusiak, 1999:113, ISBN 82-471-0487-3, ISSN 0802-3271.

“Thermal Dilation and Autogenous Deformation as Driving Forces to Self-Induced Stresses in High Performance Concrete”,
Øyvind Bjøntegaard, 1999:121, ISBN 82-7984-002-8, ISSN 0802-3271.

“Some Aspects of Ski Base Sliding Friction and Ski Base Structure”,
Dag Anders Moldestad, 1999:137, ISBN 82-7984-019-2, ISSN 0802-3271.

"Electrode reactions and corrosion resistance for steel in mortar and concrete",
Roy Antonsen, 2000:10, ISBN 82-7984-030-3, ISSN 0802-3271.

"Hydro-Physical Conditions in Kelp Forests and the Effect on Wave Damping and Dune Erosion. A case study on Laminaria Hyperborea",
Stig Magnar Løvås, 2000:28, ISBN 82-7984-050-8, ISSN 0802-3271.

"Random Vibration and the Path Integral Method",
Christian Skaug, 2000:39, ISBN 82-7984-061-3, ISSN 0802-3271.

"Buckling and geometrical nonlinear beam-type analyses of timber structures",
Trond Even Eggen, 2000:56, ISBN 82-7984-081-8, ISSN 0802-3271.

”Structural Crashworthiness of Aluminium Foam-Based Components”,
Arve Grønsund Hanssen, 2000:76, ISBN 82-7984-102-4, ISSN 0809-103X.

“Measurements and simulations of the consolidation in first-year sea ice ridges, and some aspects of mechanical behaviour”,
Knut V. Høyland, 2000:94, ISBN 82-7984-121-0, ISSN 0809-103X.

”Kinematics in Regular and Irregular Waves based on a Lagrangian Formulation”,
Svein Helge Gjøsund, 2000-86, ISBN 82-7984-112-1, ISSN 0809-103X.

”Self-Induced Cracking Problems in Hardening Concrete Structures”,
Daniela Bosnjak, 2000-121, ISBN 82-7984-151-2, ISSN 0809-103X.

"Ballistic Penetration and Perforation of Steel Plates",
Tore Børvik, 2000:124, ISBN 82-7984-154-7, ISSN 0809-103X.

"Freeze-Thaw resistance of Concrete. Effect of: Curing Conditions, Moisture Exchange and Materials",
Terje Finnerup Rønning, 2001:14, ISBN 82-7984-165-2, ISSN 0809-103X

"Structural behaviour of post tensioned concrete structures. Flat slab. Slabs on ground",
Steinar Trygstad, 2001:52, ISBN 82-471-5314-9, ISSN 0809-103X.

"Slipforming of Vertical Concrete Structures. Friction between concrete and slipform panel",
Kjell Tore Fosså, 2001:61, ISBN 82-471-5325-4, ISSN 0809-103X.

"Some numerical methods for the simulation of laminar and turbulent incompressible flows",
Jens Holmen, 2002:6, ISBN 82-471-5396-3, ISSN 0809-103X.

“Improved Fatigue Performance of Threaded Drillstring Connections by Cold Rolling”,
Steinar Kristoffersen, 2002:11, ISBN: 82-421-5402-1, ISSN 0809-103X.

"Deformations in Concrete Cantilever Bridges: Observations and Theoretical Modelling",
Peter F. Takâcs, 2002:23, ISBN 82-471-5415-3, ISSN 0809-103X.

"Stiffened aluminium plates subjected to impact loading",
Hilde Giæver Hildrum, 2002:69, ISBN 82-471-5467-6, ISSN 0809-103X.

"Full- and model scale study of wind effects on a medium-rise building in a built up area", Jónas Thór Snæbjørnsson, 2002:95, ISBN82-471-5495-1, ISSN 0809-103X.

“Evaluation of Concepts for Loading of Hydrocarbons in Ice-infested water”, Arnor Jensen, 2002:114, ISBN 82-417-5506-0, ISSN 0809-103X.

”Numerical and Physical Modelling of Oil Spreading in Broken Ice”, Janne K. Økland Gjøsteen, 2002:130, ISBN 82-471-5523-0, ISSN 0809-103X.

”Diagnosis and protection of corroding steel in concrete”, Franz Pruckner, 20002:140, ISBN 82-471-5555-4, ISSN 0809-103X.

“Tensile and Compressive Creep of Young Concrete: Testing and Modelling”, Dawood Atrushi, 2003:17, ISBN 82-471-5565-6, ISSN 0809-103X.

“Rheology of Particle Suspensions. Fresh Concrete, Mortar and Cement Paste with Various Types of Lignosulfonates”, Jon Elvar Wallevik, 2003:18, ISBN 82-471-5566-4, ISSN 0809-103X.

“Oblique Loading of Aluminium Crash Components”, Aase Reyes, 2003:15, ISBN 82-471-5562-1, ISSN 0809-103X.

“Utilization of Ethiopian Natural Pozzolans”, Surafel Ketema Desta, 2003:26, ISSN 82-471-5574-5, ISSN:0809-103X.

“Behaviour and strength prediction of reinforced concrete structures with discontinuity regions”, Helge Brå, 2004:11, ISBN 82-471-6222-9, ISSN 1503-8181.

“High-strength steel plates subjected to projectile impact. An experimental and numerical study”, Sumita Dey, 2004:38, ISBN 82-471-6282-2 (printed version), ISBN 82-471-6281-4 (electronic version), ISSN 1503-8181.

“Alkali-reactive and inert fillers in concrete. Rheology of fresh mixtures and expansive reactions.” Bård M. Pedersen, 2004:92, ISBN 82-471-6401-9 (printed version), ISBN 82-471-6400-0 (electronic version), ISSN 1503-8181.

“On the Shear Capacity of Steel Girders with Large Web Openings”. Nils Christian Hagen, 2005:9 ISBN 82-471-6878-2 (printed version), ISBN 82-471-6877-4 (electronic version), ISSN 1503-8181.

”Behaviour of aluminium extrusions subjected to axial loading”. Østen Jensen, 2005:7, ISBN 82-471-6873-1 (printed version), ISBN 82-471-6872-3 (electronic version), ISSN 1503-8181.

”Thermal Aspects of corrosion of Steel in Concrete”. Jan-Magnus Østvik, 2005:5, ISBN 82-471-6869-3 (printed version), ISBN 82-471-6868 (electronic version), ISSN 1503-8181.

”Mechanical and adaptive behaviour of bone in relation to hip replacement.” A study of bone remodelling and bone grafting.
Sébastien Muller, 2005:34, ISBN 82-471-6933-9 (printed version), ISBN 82-471-6932-0 (electronic version), ISSN 1503-8181.

“Analysis of geometrical nonlinearities with applications to timber structures”.
Lars Wollebæk, 2005:74, ISBN 82-471-7050-5 (printed version), ISBN 82-471-7019-1 (electronic version), ISSN 1503-8181.

“Pedestrian induced lateral vibrations of slender footbridges”,
Anders Rönnquist, 2005:102, ISBN 82-471-7082-5 (printed version), ISBN 82-471-7081-7 (electronic version), ISSN 1503-8181.

“Initial Strength Development of Fly Ash and Limestone Blended Cements at Various Temperatures Predicted by Ultrasonic Pulse Velocity”,
Tom Ivar Fredvik, 2005:112, ISBN 82-471-7105-8 (printed version), ISBN 82-471-7103-1 (electronic version), ISSN 1503-8181.

“Behaviour and modelling of thin-walled cast components”,
Cato Dørum, 2005:128, ISBN 82-471-7140-6 (printed version), ISBN 82-471-7139-2 (electronic version), ISSN 1503-8181.

“Behaviour and modelling of selfpiercing riveted connections”,
Raffaele Porcaro, 2005:165, ISBN 82-471-7219-4 (printed version), ISBN 82-471-7218-6 (electronic version), ISSN 1503-8181.

”Behaviour and Modelling og Aluminium Plates subjected to Compressive Load”,
Lars Rønning, 2005:154, ISBN 82-471-7169-1 (printed version), ISBN 82-471-7195-3 (electronic version), ISSN 1503-8181.

”Bumper beam-longitudinal system subjected to offset impact loading”,
Satyanarayana Kokkula, 2005:193, ISBN 82-471-7280-1 (printed version), ISBN 82-471-7279-8 (electronic version), ISSN 1503-8181.

“Control of Chloride Penetration into Concrete Structures at Early Age”,
Guofei Liu, 2006:46, ISBN 82-471-7838-9 (printed version), ISBN 82-471-7837-0 (electronic version), ISSN 1503-8181.

“Modelling of Welded Thin-Walled Aluminium Structures”,
Ting Wang, 2006:78, ISBN 82-471-7907-5 (printed version), ISBN 82-471-7906-7 (electronic version), ISSN 1503-8181.

”Time-variant reliability of dynamic systems by importance sampling and probabilistic analysis of ice loads”,
Anna Ivanova Olsen, 2006:139, ISBN 82-471-8041-3 (printed version), ISBN 82-471-8040-5 (electronic version), ISSN 1503-8181.

“Fatigue life prediction of an aluminium alloy automotive component using finite element analysis of surface topography”.

Sigmund Kyrre Ås, 2006:25, ISBN 82-471-7791-9 (printed version), ISBN 82-471-7791-9 (electronic version), ISSN 1503-8181.

”Constitutive models of elastoplasticity and fracture for aluminium alloys under strain path change”,
Dasharatha Achani, 2006:76, ISBN 82-471-7903-2 (printed version), ISBN 82-471-7902-4 (electronic version), ISSN 1503-8181.

“Simulations of 2D dynamic brittle fracture by the Element-free Galerkin method and linear fracture mechanics”,
Tommy Karlsson, 2006:125, ISBN 82-471-8011-1 (printed version), ISBN 82-471-8010-3 (electronic version), ISSN 1503-8181.

“Penetration and Perforation of Granite Targets by Hard Projectiles”,
Chong Chiang Seah, 2006:188, ISBN 82-471-8150-9 (printed version), ISBN 82-471-8149-5 (electronic version), ISSN 1503-8181.

“Deformations, strain capacity and cracking of concrete in plastic and early hardening phases”,
Tor Arne Hammer, 2007:234, ISBN 978-82-471-5191-4 (printed version), ISBN 978-82-471-5207-2 (electronic version), ISSN 1503-8181.

“Crashworthiness of dual-phase high-strength steel: Material and Component behaviour”,
Venkatapathi Tarigopula, 2007:230, ISBN 82-471-5076-4 (printed version), ISBN 82-471-5093-1 (electronic version), ISSN 1503-8181.

“Fibre reinforcement in load carrying concrete structures”,
Åse Lyslo Døssland, 2008:50, ISBN 978-82-471-6910-0 (printed version), ISBN 978-82-471-6924-7 (electronic version), ISSN 1503-8181.

“Low-velocity penetration of aluminium plates”,
Frode Grytten, 2008:46, ISBN 978-82-471-6826-4 (printed version), ISBN 978-82-471-6843-1 (electronic version), ISSN 1503-8181.

“Robustness studies of structures subjected to large deformations”,
Ørjan Fyllingen, 2008:24, ISBN 978-82-471-6339-9 (printed version), ISBN 978-82-471-6342-9 (electronic version), ISSN 1503-8181.

“Constitutive modelling of morsellised bone”,
Knut Birger Lunde, 2008:92, ISBN 978-82-471-7829-4 (printed version), ISBN 978-82-471-7832-4 (electronic version), ISSN 1503-8181.

“Experimental Investigations of Wind Loading on a Suspension Bridge Girder”,
Bjørn Isaksen, 2008:131, ISBN 978-82-471-8656-5 (printed version), ISBN 978-82-471-8673-2 (electronic version), ISSN 1503-8181.

“Cracking Risk of Concrete Structures in The Hardening Phase”,
Guomin Ji, 2008:198, ISBN 978-82-471-1079-9 (printed version), ISBN 978-82-471-1080-5 (electronic version), ISSN 1503-8181.

“Modelling and numerical analysis of the porcine and human mitral apparatus”,
Victorien Emile Prot, 2008:249, ISBN 978-82-471-1192-5 (printed version), ISBN 978-82-471-1193-2 (electronic version), ISSN 1503-8181.

“Strength analysis of net structures”,
Heidi Moe, 2009:48, ISBN 978-82-471-1468-1 (printed version), ISBN 978-82-471-1469-8 (electronic version), ISSN1503-8181.

“Numerical analysis of ductile fracture in surface cracked shells”,
Espen Berg, 2009:80, ISBN 978-82-471-1537-4 (printed version), ISBN 978-82-471-1538-1 (electronic version), ISSN 1503-8181.

“Subject specific finite element analysis of bone – for evaluation of the healing of a leg lengthening and evaluation of femoral stem design”,
Sune Hansborg Pettersen, 2009:99, ISBN 978-82-471-1579-4 (printed version), ISBN 978-82-471-1580-0 (electronic version), ISSN 1503-8181.

“Evaluation of fracture parameters for notched multi-layered structures”,
Lingyun Shang, 2009:137, ISBN 978-82-471-1662-3 (printed version), ISBN 978-82-471-1663-0 (electronic version), ISSN 1503-8181.

“Modelling of Dynamic Material Behaviour and Fracture of Aluminium Alloys for Structural Applications”
Yan Chen, 2009:69, ISBN 978-82-471-1515-2 (printed version), ISBN 978-82 471-1516-9 (electronic version), ISSN 1503-8181.

“Nanomechanics of polymer and composite particles”
Jianying He 2009:213, ISBN 978-82-471-1828-3 (printed version), ISBN 978-82-471-1829-0 (electronic version), ISSN 1503-8181.

“Mechanical properties of clear wood from Norway spruce”
Kristian Berbom Dahl 2009:250, ISBN 978-82-471-1911-2 (printed version) ISBN 978-82-471-1912-9 (electronic version), ISSN 1503-8181.

“Modeling of the degradation of TiB_2 mechanical properties by residual stresses and liquid Al penetration along grain boundaries”
Micol Pezzotta 2009:254, ISBN 978-82-471-1923-5 (printed version) ISBN 978-82-471-1924-2 (electronic version) ISSN 1503-8181.

“Effect of welding residual stress on fracture”
Xiabo Ren 2010:77, ISBN 978-82-471-2115-3 (printed version) ISBN 978-82-471-2116-0 (electronic version), ISSN 1503-8181.

“Pan-based carbon fiber as anode material in cathodic protection system for concrete structures”
Mahdi Chini 2010:122, ISBN 978-82-471-2210-5 (printed version) ISBN 978-82-471-2213-6 (electronic version), ISSN 1503-8181.

“Structural Behaviour of deteriorated and retrofitted concrete structures”
Irina Vasililjeva Sæther 2010:171, ISBN 978-82-471-2315-7 (printed version) ISBN 978-82-471-2316-4 (electronic version) ISSN 1503-8181.

“Prediction of local snow loads on roofs”
Vivian Meløysund 2010:247, ISBN 978-82-471-2490-1 (printed version) ISBN 978-82-471-2491-8 (electronic version) ISSN 1503-8181.

“Behaviour and modelling of polymers for crash applications”
Virgile Delhaye 2010:251, ISBN 978-82-471-2501-4 (printed version) ISBN 978-82-471-2502-1 (electronic version) ISSN 1503-8181.
“Blended cement with reducted CO_2 emission – Utilizing the Fly Ash-Limestone Synergy”,
Klaartje De Weerdt 2011:32, ISBN 978-82-471-2584-7 (printed version) ISBN 978-82-471-2584-4 (electronic version) ISSN 1503-8181.

“Chloride induced reinforcement corrosion in concrete” Concept of critical chloride content – methods and mechanisms.
Ueli Angst 2011:113, ISBN 978-82-471-2769-9 (printed version) ISBN 978-82-471-2763-6 (electronic version) ISSN 1503-8181.

“A thermo-electric-Mechanical study of the carbon anode and contact interface for Energy savings in the production of aluminium”.
Dag Herman Andersen 2011:157, ISBN 978-82-471-2859-6 (printed version) ISBN 978-82-471-2860-2 (electronic version) ISSN 1503-8181.

“Structural Capacity of Anchorage Ties in Masonry Veneer Walls Subjected to Earthquake”. The implications of Eurocode 8 and Eurocode 6 on a typical Norwegain veneer wall.
Ahmed Mohamed Yousry Hamed 2011:181, ISBN 978-82-471-2911-1 (printed version) ISBN 978-82-471-2912-8 (electronic ver.) ISSN 1503-8181.

“Work-hardening behaviour in age-hardenable Al-Zn-Mg(-Cu) alloys”.
Ida Westermann , 2011:247, ISBN 978-82-471-3056-8 (printed ver.) ISBN 978-82-471-3057-5 (electronic ver.) ISSN 1503-8181.

“Behaviour and modelling of selfpiercing riveted connections using aluminium rivets”.
Nguyen-Hieu Hoang, 2011:266, ISBN 978-82-471-3097-1 (printed ver.) ISBN 978-82-471-3099-5 (electronic ver.) ISSN 1503-8181.

“Fibre reinforced concrete”.
Sindre Sandbakk, 2011:297, ISBN 978-82-471-3167-1 (printed ver.) ISBN 978-82-471-3168-8 (electronic ver) ISSN 1503:8181.

“Dynamic behaviour of cablesupported bridges subjected to strong natural wind”.
Ole Andre Øiseth, 2011:315, ISBN 978-82-471-3209-8 (printed ver.) ISBN 978-82-471-3210-4 (electronic ver.) ISSN 1503-8181.

“Constitutive modeling of solargrade silicon materials”
Julien Cochard, 2011:307, ISBN 978-82-471-3189-3 (printed ver). ISBN 978-82-471-3190-9 (electronic ver.) ISSN 1503-8181.

“Constitutive behavior and fracture of shape memory alloys”
Jim Stian Olsen, 2012:57, ISBN 978-82-471-3382-8 (printed ver.) ISBN 978-82-471-3383-5 (electronic ver.) ISSN 1503-8181.

“Field measurements in mechanical testing using close-range photogrammetry and digital image analysis”
Egil Fagerholt, 2012:95, ISBN 978-82-471-3466-5 (printed ver.) ISBN 978-82-471-3467-2 (electronic ver.) ISSN 1503-8181.

“Towards a better under standing of the ultimate behaviour of lightweight aggregate concrete in compression and bending”,
Håvard Nedrelid, 2012:123, ISBN 978-82-471-3527-3 (printed ver.) ISBN 978-82-471-3528-0 (electronic ver.) ISSN 1503-8181.

“Numerical simulations of blood flow in the left side of the heart”
Sigrid Kaarstad Dahl, 2012:135, ISBN 978-82-471-3553-2 (printed ver.) ISBN 978-82-471-3555-6 (electronic ver.) ISSN 1503-8181.

“Moisture induced stresses in glulam”
Vanessa Angst-Nicollier, 2012:139, ISBN 978-82-471-3562-4 (printed ver.) ISBN 978-82-471-3563-1 (electronic ver.) ISSN 1503-8181.

“Biomechanical aspects of distraction osteogensis”
Valentina La Russa, 2012:250, ISBN 978-82-471-3807-6 (printed ver.) ISBN 978-82-471-3808-3 (electronic ver.) ISSN 1503-8181.

“Ductile fracture in dual-phase steel. Theoretical, experimental and numerical study”
Gaute Gruben, 2012:257, ISBN 978-82-471-3822-9 (printed ver.) ISBN 978-82-471-3823-6 (electronic ver.) ISSN 1503-8181.

“Damping in Timber Structures”
Nathalie Labonnote, 2012:263, ISBN 978-82-471-3836-6 (printed ver.) ISBN 978-82-471-3837-3 (electronic ver.) ISSN 1503-8181.

“Biomechanical modeling of fetal veins: The umbilical vein and ductus venosus bifurcation”
Paul Roger Leinan, 2012:299, ISBN 978-82-471-3915-8 (printed ver.) ISBN 978-82-471-3916-5 (electronic ver.) ISSN 1503-8181.

“Large-Deformation behaviour of thermoplastics at various stress states”
Anne Serine Ognedal, 2012:298, ISBN 978-82-471-3913-4 (printed ver.) ISBN 978-82-471-3914-1 (electronic ver.) ISSN 1503-8181.

“Hardening accelerator for fly ash blended cement”
Kien Dinh Hoang, 2012:366, ISBN 978-82-471-4063-5 (printed ver.) ISBN 978-82-471-4064-2 (electronic ver.) ISSN 1503-8181.

“From molecular structure to mechanical properties”
Jianyang Wu, 2013:186, ISBN 978-82-471-4485-5 (printed ver.) ISBN 978-82-471-4486-2 (electronic ver.) ISSN 1503-8181.

“Experimental and numerical study of hybrid concrete structures”
Linn Grepstad Nes, 2013:259, ISBN 978-82-471-4644-6 (printed ver.) ISBN 978-82-471-4645-3 (electronic ver.) ISSN 1503-8181.

“Mechanics of ultra-thin multi crystalline silicon wafers”
Saber Saffar, 2013:199, ISBN 978-82-471-4511-1 (printed ver.) ISBN 978-82-471-4513-5 (electronic ver). ISSN 1503-8181.

“Through process modelling of welded aluminium structures”
Anizahyati Alisibramulisi, 2013:325, ISBN 978-82-471-4788-7 (printed ver.) ISBN 978-82-471-4789-4 (electronic ver.) ISSN 1503-8181.

“Combined blast and fragment loading on steel plates”
Knut Gaarder Rakvåg, 2013:361, ISBN978-82-471-4872-3 (printed ver.) ISBN 978-82-4873-0 (electronic ver.). ISSN 1503-8181.

“Characterization and modelling of the anisotropic behaviour of high-strength aluminium alloy”
Marion Fourmeau, 2014:37, ISBN 978-82-326-0008-3 (printed ver.) ISBN 978-82-326-0009-0 (electronic ver.) ISSN 1503-8181.

“Behaviour of threated steel fasteners at elevated deformation rates”
Henning Fransplass, 2014:65, ISBN 978-82-326-0054-0 (printed ver.) ISBN 978-82-326-0055-7 (electronic ver.) ISSN 1503-8181.

“Sedimentation and Bleeding”
Ya Peng, 2014:89, ISBN 978-82-326-0102-8 (printed ver.) ISBN 978-82-326-0103-5 (electric ver.) ISSN 1503-8181.

“Impact against X65 offshore pipelines”
Martin Kristoffersen, 2014:362, ISBN 978-82-326-0636-8 (printed ver.) ISBN 978-82-326-0637-5 (electronic ver.) ISSN 1503-8181.

“Formability of aluminium alloy subjected to prestrain by rolling”
Dmitry Vysochinskiy, 2014:363,, ISBN 978-82-326-0638-2 (printed ver.) ISBN 978-82-326-0639-9 (electronic ver.) ISSN 1503-8181.

“Experimental and numerical study of Yielding, Work-Hardening and anisotropy in textured AA6xxx alloys using crystal plasticity models”
Mikhail Khadyko, 2015:28, ISBN 978-82-326-0724-2 (printed ver.) ISBN 978-82-326-0725-9 (electronic ver.) ISSN 1503-8181.

“Behaviour and Modelling of AA6xxx Aluminium Alloys Under a Wide Range of Temperatures and Strain Rates”
Vincent Vilamosa, 2015:63, ISBN 978-82-326-0786-0 (printed ver.) ISBN 978-82-326-0787-7 (electronic ver.) ISSN 1503-8181.

“A Probabilistic Approach in Failure Modelling of Aluminium High Pressure Die-Castings”
Octavian Knoll, 2015:137, ISBN 978-82-326-0930-7 (printed ver.) ISBN 978-82-326-0931-4 (electronic ver.) ISSN 1503-8181.

“Ice Abrasion on Marine Concrete Structures”
Egil Møen, 2015:189, ISBN 978-82-326-1034-1 (printed ver.) ISBN 978-82-326-1035-8 (electronic ver.) ISSN 1503-8181.

“Fibre Orientation in Steel-Fibre-Reinforced Concrete”
Giedrius Zirgulis, 2015:229, ISBN 978-82-326-1114-0 (printed ver.) ISBN 978-82-326-1115-7 (electronic ver.) ISSN 1503-8181.

“Effect of spatial variation and possible interference of localised corrosion on the residual capacity of a reinforced concrete beam”
Mohammad Mahdi Kioumarsi, 2015:282, ISBN 978-82-326-1220-8 (printed ver.) ISBN 978-82-1221-5 (electronic ver.) ISSN 1503-8181.

“The role of concrete resistivity in chloride-induced macro-cell corrosion”
Karla Horbostel, 2015:324, ISBN 978-82-326-1304-5 (printed ver.) ISBN 978-82-326-1305-2 (electonic ver.) ISSN 1503-8181.

“Flowable fibre-reinforced concrete for structural applications”
Elena Vidal Sarmiento, 2015-335, ISBN 978-82-326-1324-3 (printed ver.) ISBN 978-82-326-1325-0 (electronic ver.) ISSN 1503-8181.

“Development of chushed sand for concrete production with microproportioning” Rolands Cepuritis, 2016:19, ISBN 978-82-326-1382-3 (printed ver.) ISBN 978-82-326-1383-0 (electronic ver.) ISSN 1503-8181.

“Withdrawal properties of threaded rods embedded in glued-laminated timer elements”
Haris Stamatopoulos, 2016:48, ISBN 978-82-326-1436-3 (printed ver.) ISBN 978-82-326-1437-0 (electronic ver.) ISSN 1503-8181.

“An Experimental and numerical study of thermoplastics at large deformation”
Marius Andersen, 2016:191, ISBN 978-82-326-1720-3 (printed ver.) ISBN 978-82-326-1721-0 (electronic ver.) ISSN 1503-8181.

“Modeling and Simulation of Ballistic Impact”
Jens Kristian Holmen, 2016:240, ISBN 978-82-326-1818-7 (printed ver). ISBN 978-82-326-1819-4 (electronic ver.) ISSN 1503-8181.

“Early age crack assessment of concrete structures”
Anja B. Estensen Klausen, 2016:256, ISBN 978-82-326-1850-7 (printed ver). ISBN 978-82-326-1851-4 (electronic ver.) ISSN 1503-8181.

“Uncertainty quantification and sensitivity analysis for cardiovascular models”
Vinzenz Gregor Eck, 2016:234, ISBN 978-82-326-1806-4 (printed ver.) ISBN 978-82-326-1807-1 (electronic ver.) ISSN 1503-8181.

“Dynamic behaviour of existing and new railway catenary systems under Norwegain conditions”
Petter Røe Nåvik, 2016:298, ISBN 978-82-326-1935-1 (printed ver.) ISBN 978-82-326-1934-4 (electronic ver.) ISSN 1503-8181.

“Mechanical behaviour of particle-filled elastomers at various temperatures”
Arne Ilseng, 2016-295, ISBN978-82-326-1928-3 (printed ver.) ISBN 978-82-326-1929-0 (electronic ver.) ISSN 1503-8181.

“Nanotechnology for Anti-Icing Application”
Zhiwei He, 2016:348, ISBN 978-82-326-2038-8 (printed ver.) ISBN 978-82-326-2019-5 (electronic ver.) ISSN 1503-8181.

“Conduction Mechanisms in Conductive Adhesives with Metal-Coated Polyer Spheres”
Sigurd Rolland Pettersen, 2016:349, ISBN 978-326-2040-1 (printed ver,) ISBN 978-82-326-2041-8 (electronic ver.) ISSN 1503-8181.

“The interaction between calcium lignosulfonate and cement”
Alessia Colombo, 2017:20, ISBN 978-82-326-2122-4 (printed ver.) ISBN 978-82-326-2123-1 (electronic ver.) ISSN 1503-8181.

“Behaviour and Modelling of Flexible Structures Subjected to Blast Loading”
Vegard Aune, 2017:101, ISBN 978-82-326-2274-0 (printed ver.) ISBN 978-82-326-2275-7 (electronic ver.) ISSN 1503-8181.

“Behaviour of steel connections under quasi-static and impact loading”
Erik Løhre Grimsmo, 2017:159, ISBN 978-82-326-2390-7 (printed ver.) ISBN 978-82-326-2391-4 (electronic ver.) ISSN 1503-8181.

“An experimental and numerical study of cortical bone at he macro and Nano-scale”
Masoud Ramenzanzadehkoldeh,, 2017:208, ISBN 978-82-326-2488-1 (printed ver.) ISBN 978-82-326-2489-8 (electronic ver.) ISSN 1503-8181.

“Optoelectrical Properties of a Novel Organic Semiconductor: 6,13-Dichloropentacene” Mao Wang, 2017:130, ISBN 978-82-326-2332-7 (printed ver.) ISBN 978-82-326-2333-4) (electronic ver.) ISSN 1503-8181.

“Core-shell structured microgels and their behavior at oil and water interface”
Yi Gong, 2017:182, ISBN 978-82-326-2436-2 (printed. ver.) ISBN 978-82-326-2437-9 (electronic ver.) ISSN 1503-8181.

“Aspects of design of reinforced concrete structures using nonliear finite element analyses”
Morten Engen, 2017:149, ISBN 978-82-326-2370-9 (printed ver.) ISBN 978-82-326-2371-6 (electronic ver.) ISSN 1503-8181.

“Numerical studies on ductile failure of aluminium alloys”
Lars Edvard Dæhli, 2017:284, ISBN 978-82-326-2636-6 (printed ver.) ISBN 978-82-326-2637-3 (electronic ver.) ISSN 1503-8181.

“Modelling and Assessment of Hydrogen Embrittlement in Steels and Nickel Alloys”
Haiyang Yu, 2017:278, ISBN 978-82-326-2624-3 (printed. ver.) ISBN 978-82-326-2625-0 (electronic ver.) ISSN 1503-8181.

“Network arch timber bridges with light timber deck on transverse crossbeams”
Anna Weronika Ostrycharczyk, 2017:318, ISBN 978-82-326-2704-2 (printed ver.) ISBN 978-82-326-2705-9 (electronic ver.) ISSN 1503-8181.

“Splicing of Large Glued Laminated Timber Elements by Use of Long Threated Rods”
Martin Cepelka, 2017:320, ISBN 978-82-326-2708-0 (printed ver.) ISBN 978-82-326-2709-7 (electronic ver.) ISSN 1503-8181.

“Thermomechanical behaviour of semi-crystalline polymers: experiments, modelling and simulation”
Joakim Johnsen, 2017-317, ISBN 978-82-326-2702-8 (printed ver.) ISBN 978-82-326-2703-5 (electronic ver.) ISSN 1503-8181.

“Small-Scale Plasiticity under Hydrogen Environment”
Kai Zhao, 2017:356, ISBN 978-82-326-2782-0 (printed ver.) ISBN 978-82-326-2783-7 (electronic er.) ISSN 1503-8181.

“Risk and Reliability Based Calibration of Structural Design Codes”
Michele Baravalle, 2017:342, ISBN 978-82-326-2752-3 (printed ver,) ISBN 978-82-326-2753-0 (electronic ver.) ISSN 1503-8181.

“Dynamic behaviour of floating bridges exposed to wave excitation”
Knut Andreas Kvåle, 2017:365, ISBN 978-82-326-2800-1 (printed ver.) ISBN 978-82-326-2801-8 (electronic ver.) ISSN 1503-8181.

“Dolomite calcined clay composite cement – hydration and durability”
Alisa Lydia Machner, 2018:39, ISBN 978-82-326-2872-8 (printed ver.). ISBN 978-82-326-2873-5 (electronic ver.) ISSN 1503-8181.

“Modelling of the self-excited forces for bridge decks subjected to random motions: an experimental study”
Bartosz Siedziako, 2018:52, ISBN 978-82-326-2896-4 (printed ver.). ISBN 978-82-326-2897-1 (electronic ver.) ISSN 1503-8181.

“A probabilistic-based methodology for evaluation of timber facade constructions”
Klodian Gradeci, 2018:69, ISBN 978-82-326-2928-2 (printed ver.) ISBN 978-82-326-2929-9 (electronic ver.) ISSN 1503-8181.

“Behaviour and modelling of flow-drill screw connections”
Johan Kolstø Sønstabø, 2018:73, ISBN 978-82-326-2936-7 (printed ver.) ISBN 978-82-326-2937-4 (electronic ver.) ISSN 1503-8181.

“Full-scale investigation of the effects of wind turbulence characteristics on dynamic behavior of long-span cable-supported bridges in complex terrain”
Aksel Fenerci, 2018 100, ISBN 9978-82-326-2990-9 (printed ver.) ISBN 978-82-326-2991-6 (electronic ver.) ISSN 1503-8181.

“Modeling and simulation of the soft palate for improved understanding of the obstructive sleep apnea syndrome”
Hongliang Liu, 2018:101, ISBN 978-82-326-2992-3 (printed ver.) ISBN 978-82-326-2993-0 (electronic ver.) ISSN 1503-8181.

“Long-term extreme response analysis of cable-supported bridges with floating pylons subjected to wind and wave loads”.
Yuwang Xu, 2018:229, ISBN 978-82-326-3248-0 (printed ver.) ISBN 978-82-326-3249-7 (electronic ver.) ISSN 1503-8181.

“Reinforcement corrosion in carbonated fly ash concrete”
Andres Belda Revert, 2018:230, ISBN 978-82-326-3250-3 (printed ver.) ISBN 978-82-326-3251-0 (electronic ver.) ISSN 1503-8181.

“Direct finite element method for nonliear earthquake analysis of concrete dams including dam-water-foundation rock interaction”
Arnkjell Løkke, 2018:252, ISBN 978-82-326-3294-7 (printed ver.) ISBN 978-82-326-3295-4 (electronic ver.) ISSN 1503-8181.

“Electromechanical characterization of metal-coated polymer spheres for conductive adhesives”
Molly Strimbeck Bazilchuk, 2018:295, ISBN 978-82-326-3380-7 (printed. ver.) ISBN 978-82-326-3381-4 (electrical ver.) ISSN 1503-8181.

“Determining the tensile properties of Artic materials and modelling their effects on fracture”
Shengwen Tu, 2018:269, ISBN 978-82-326-3328-9 (printed ver.) ISBN 978-82-326-3329-6 (electronic ver.) ISSN 1503-8181.

“Atomistic Insigth into Tranportation of Nanofluid in Ultra-confined Channel”
Xiao Wang, 2018:334, ISBN978-82-326-3456-9 (printed ver.) ISBN 978-82-326-3457-6 (electronic ver.) ISSN 1503-8181.

“An experimental and numerical study of the mechanical behaviour of short glass-fibre reinforced thermoplastics”.
Jens Petter Henrik Holmstrøm, 2019:79, ISBN 978-82-326-3760-7 (printed ver.) ISBN 978-82-326-3761-4 (electronic ver.) ISSN 1503-8181.

“Uncertainty quantification and sensitivity analysis informed modeling of physical systems”
Jacob Sturdy, 2019:115, ISBN 978-82-326-3828-4 (printed ver.) ISBN 978-82-326-3829-1 (electric ver.) ISSN 1503-8181.

“Load model of historic traffic for fatigue life estimation of Norwegian railway bridges”
Gunnstein T. Frøseth, 2019:73, ISBN 978-82-326-3748-5 (printed ver.) ISBN 978-82-326-3749-2 (electronic ver.) ISSN 1503-8181.

“Force identification and response estimation in floating and suspension bridges using measured dynamic response”
Øyvind Wiig Petersen, 2019:88, ISBN 978-82-326-3778-2 (printed ver.) ISBN 978-82-326-377-9 (electronic ver.) ISSN 1503-8181.

“Consistent crack width calculation methods for reinforced concrete elements subjected to 1D and 2D stress states”
Reignard Tan, 2019:147, ISBN 978-82-326-3892-5 (printed ver.) ISBN 978-82-326-3893-2 (electronic ver.) ISSN 1503-8181.

“Nonlinear static and dynamic isogeometric analysis of slender spatial and beam type structures”
Siv Bente Raknes, 2019:181, ISBN 978-82-326-3958-8 (printed ver.) ISBN 978-82-326-3959-5 (electronic ver.) ISSN 1503-8181.

“Experimental study of concrete-ice abrasion and concrete surface topography modification”
Guzel Shamsutdinova, 2019:182, ISBN978-82-326-3960-1 (printed ver.) ISBN 978-82-326-3961-8 (electronic ver.) ISSN 1503-8181.

“Wind forces on bridge decks using state-of-the art FSI methods”
Tore Andreas Helgedagsrud, 2019:180, ISBN 978-82-326-3956-4 (printed ver.) ISBN 978-82-326-3957-1 (electronic ver.) ISSN 1503-8181.

“Numerical Study on Ductile-to-Brittle Transition of Steel and its Behavior under Residual Stresses”
Yang Li, 2019:227, ISBN 978-82-326-4050-8 (printed ver.) ISBN 978-82-326-4015-5 (electronic ver.) ISSN 1503-8181.

“Micromechanical modelling of ductile fracture in aluminium alloys”
Bjørn Håkon Frodal, 2019:253, ISBN 978-82-326-4102-4 (printed ver.) ISBN 978-82-326-4103-1 (electronic ver.) ISSN 1503-8181.

“Monolithic and laminated glass under extreme loading: Experiments, modelling and simulations”
Karoline Osnes, 2019:304, ISBN 978-82-326-4204-5 (printed ver.) ISBN 978-82-326-4205-2 (electronic ver.) ISSN 1503-8181.

“Plastic flow and fracture of isotropic and anisotropic 6000-series aluminium alloys: Experiments and numerical simulations “
Susanne Thomesen, 2019:312, ISBN 978-82-326-4220-5 (printed ver.), ISBN 978-82-326-4221-2 (electriniv ver.) ISSN 1503-8181

“Stress-laminated timber decks in bridges”
Francesco Mirko Massaro, 2019:346, ISBN 978-82-326-4288-5 (printed ver.), ISBN 978-82-326-4289-2 (electronic ver.) ISSN 1503-8181

“Connections between steel and aluminium using adhesive bonding combined with self-piercing riveting: Testing, modelling and analysis”
Matthias Reil, 2019:319, ISBN 978-82-326-4234-2 (printed ver.), ISBN 978-82-326-4235-9 (electronic ver.) ISSN 1503-8181

“Designing Polymeric Icephobic Materials”
Yizhi Zhuo, 2019:345, ISBN 978-82-326-4286-1 (printed ver.), ISBN 978-82-326-4287-8 (electronic ver.) ISSN 1503-8181

“Fundamental Mechanisms of Ice Adhesion”
Rønneberg, Sigrid 2020:87, ISBN 978-82-326-4527-8 (printed version) ISBN 978-82- 326-4524-5 (electronic version) ISSN 1503-8181

“Mechanical modeling of the polymeric coating on a subsea pipeline” Vestrum, Ole 2020:105, ISBN 978-82-326-4562-6 (printed version) ISBN 978-82- 4563-3 (electronic version ISSN 1503-8181

“Conceptual form-finding in structural engineering” Marcin Luczkowski 2020: “Self-assembled superstructures of magnetic nanoparticles: advanced nanofabrication and enhanced mechanical properties”

“Self-assembled superstructures of magnetic nanoparticles: advanced nanofabrication and enhanced mechanical properties” Verner Håkonsen 2020:271, ISBN 978-82-326-4890-0 (printed version) ISBN 978-82- 326-4891-7 (electronic version) ISSN 1503-8181

“Micromechanical modelling of fracture in ductile alloys with applications to high-strength steel” Sondre Bergo 2020:313, ISBN 978-82-326-4974-7 (printed version) ISBN 978-82-326- 4975-4 (electronic version) ISSN 1503-8181

“Fracture in wood of Norway spruce - Experimental and numerical study”
Katarzyna Ostapska 2020:314, ISBN 978-82-326-4976-1 (printed version) ISBN 978- 82-326-4977-8 (electronic version) ISSN 1503-8181

“Dynamic anti-icing surfaces (DAIS)” Feng Wang 2020:330 ISBN 978-82-326-5006-4 (printed version) ISBN 978-82-326-5007-1 (electronic version) ISSN 1503-8181

“«Multiaxial Fatigue analysis of offshore mooring chains, considering the effects of residual stresses and corrosion pits» Ershad P. Zarandi 2020:337 ISBN 978-82-326-5020-0 (printed version) ISBN 978-82-326-5021-7 (electronic version) ISSN 1503-8181

“Production and documentation of frost durable high-volume fly ash concrete: air entrainment, cracking and scaling in performance testing” Andrei Shpak 2020:366 ISBN 978-82-326-5078-1 (printed version) ISBN 978-82-326-5079-8 (electronic version) ISSN 1503-8181

“Physics-based and data-driven reduced-order blood flow models: Applications to coronary artery disease diagnostics” Fredrik Eikeland Fossan 2020:362 ISBN 978-82-326-5070-5 (printed version) ISBN 978-82-326-5071-2 (electronic version) ISSN 1503-8181

“Multi-scale modelling and simulation of ductile failure in aluminium structures” Henrik Granum 2020:374 ISBN 978-82-326-5094-1 (printed version) ISBN 978-82-326-5095-8 (electronic version) ISSN 1503-8181

“Testing and modelling of multi-material joints” Jon Fredrick Berntsen 2020:368 ISBN 978-82-326-5082-8 (printed version) ISBN 978-82-326-5083-5 ISSN 1503-8181

“Heuristic models for wear prediction and dynamic-based condition monitoring techniques in pantograph-catenary interaction” Stefano Derosa 2020:381 ISBN 978-82-326-5108-5 (printed version) ISBN 978-82-326-5109-2 (electronic version) ISSN 1503-8181

“Experimental and numerical study of dilation in mineral filled PVC” Sindre Nordmark Olufsen 2020:388 ISBN 978-82-326-5122-1 (printed version) ISBN 978-82-326-5123-8 (electronic version) ISSN 1503-8181

“Residual stresses and dimensional deviation in metal additive manufacturing: prediction and mitigation methods” Li Sun 2020:411 ISBN 978-82-471-9600-7 (printed version) ISBN 978-82-471-9581-9 (electronic version) ISSN 1503-8181 (printed version) ISSN 2703-8084 (online version)

“Moment-resisting timber frames with semi-rigid connections” Aivars Vilguts 2021:88 ISBN 978-82-326-6987 (printed version) ISBN 978-82-326-5737-7 (electronic version) ISSN 2703-8084 (online version)

“Thermal transport in metal-polymer systems” Susanne Sandell 2021:63 ISBN 978-82-326-5304-1 (printed version) ISBN 978-82-326-6278-4 (electronic version) ISSN 2703-8084 (online version)
“Competitive timber floors” Sveinung Ørjan Nesheim 2021:134 ISBN 978-82-326-6481-8 (printed version) ISBN 978-82-326-5399-7 (electronic version) ISSN 2703-8084

“Thermodynamics of Nanoscale Films and Fluid Volumes” Bjørn Andre Strøm 2021:166 ISBN 978-82-326-6778-9 (printed version) ISBN 978-82-326-5900-5 (electronic version) ISSN 2703-8084 (online version)

“Characterization and modeling of the mechanical behavior of polymer foam” Daniel Thor Morton 2021:173 ISBN 978-82-326-6245-6 (printed version) ISBN 978-82-326-5699-8 (electronic version) ISSN 2703-8084 (online version)

“Atomistic Insights to Interfacial Dynamics” Yuequn Fu 2021:233 ISBN 978-82-326-5530-4 (printed version) ISBN 978-82-326-6894-6 (electronic version) ISSN 2703-8084 (online version)

“Mechanisms and enhancement of CO2 condensation heat transfer” Ingrid Snustad 2021:236 ISBN 978-82-326-5606-6 ISBN 978-82-236-6715-4 (electronic version) ISSN 2703-8084

“Experimental study of reinforced concrete slabs subjected to fire exposure and blast loading” Assis Arano Barenys 2021:239 ISBN 978-82-326-5289-1 ISBN 978-82-326-5876-3 (electronic version) ISSN 2703-8084 (online version)

“Long-term extreme buffeting response investigations for long-span bridges considering uncertain turbulence parameters based on field measurements” Tor Martin Lystad 2021:216 ISBN 978-82-326-5797-1 (printed version) ISBN 978-82-326-6154-1 (electronic version) ISSN 2703-8084 (online version)

“Development and Application of a Vision-Based System for Structural Monitoring of Railway Catenary System” Tengjiao Jiang 2021:280 ISBN 978-82-326-6866-3 (printed ver.) ISBN 978-82-326-5778-0 (electronic ver.) ISSN 1503-8181 (online ver.)

“Integrated design and maintenance of deteriorating structral systems” Jorge Mendoza Espinosa 2021:351 ISBN 978-82-326-6608-9 (printed ver.) ISBN 978-82-326-6954-7 (electronic ver.) ISSN 2703-8084 (online ver.)

“Numerical and experimental studies for damage detection and structural helath monitoring of steel bridges” Bjørn T. Svendsen 2021:382 ISBN 978-82-326-6327-9 (printed ver.) ISBN 978-82-326-5895-4 (electronic ver.) ISSN 2703-8084 (online ver.)

“Uncertainty quantification for multiphase flow” Andreas Strand 2021:410 ISBN 978-82-326-6519-8 (printed ver.) ISBN 978-82-326-6928-8 (electronic ver.) ISSN 2703-8084 (online ver.)

“Prediction of rheological properties of filler modified cement paste from constituent properties, flow measurements and modelling” Elisabeth Leite Skare 2022:38 ISBN 978-82-326-5753-7 (printed ver.) ISBN 978-82-326-6958-5 (electronic ver.) ISSN 2703-8084 (online ver.)

“Nanomechanical characterization of additively manufactured metallic alloys” Siqi Liu 2022:96 ISBN 978-82-326-5457-4 (printed ver.) ISBN 978-82-326-5481-9 (electronic ver.) ISSN 2703-8084 (online ver.)

“Modeling and experiments in transient potenial drop meausurements for nondestructive evaluation” Øyvind Othar Aunet Persvik 2022:146 ISBN 978-82326-5682-0 (printed ver.) ISBN 978-82-326-5365-2 (electronic ver.) ISSN 2703-8084 (online ver.)

“Ductile fracture of aluminium alloys in the low to moderate stress triaxiality range” Asle Joachim Tomstad 2022:150 ISBN 978-82-326-6681-2 (printed ver.) ISBN 978-82-326-5506-9 (electronic ver.) ISSN 2703-8084 (online ver.)

“Application of marine field data for prediction of chloride ingress in concrete” Simon Fjendbo 2022:173 ISBN 978-82-326-6071-1 (printed ver.) ISBN 978-82-326-6659-1 (electronic ver.) ISSN 1503-8181 (online ver.)

“On the use of a virtual laboratory for aluminum alloys: application to large-scale analyses of extruded profiles” Marcos Fernandez Garcia 2022:199 ISBN 978-82-326-5527-4 (printed ver.) ISBN 978-82-326-6036-0 (electronic ver.) ISSN 2703-8084 (online ver.)

“Energy absorption and failure in aluminum alloys: An experimental and numerical study” Kristin Qvale 2022:213 ISBN 978-82-326-5172-6 (printed ver.) ISBN 978-82-326-5208-2 (electronic ver.) ISSN 2703-8084 (online ver.)

“Probabilistic modelling of wind induced load effects for suspension bridges with emphasis on long-term extreme value analysis” Dario Rafael Fernandez Castellon 2022:218 ISBN 978-82-326-5343-0 (printed ver.) ISBN 978-82-326-5401-7 (electronic ver.) ISSN 2703-8084 (online ver.)

“Fatigue crack initiation in corroded offshore mooring chains” Paul Qvale 2022:296 ISBN 978-82-326-5720-9 (printed er.) ISBN 978-82-326-5943-2 (electronic ver.) ISSN 2703-8084 (online ver.)

“Durability and structural performance of pretensioned concrete girders in coastal climate bridges” Magdalena Jadwiga Osmolska 2022:372 ISBN 978-82-326-5806-0 (printed ver.) ISBN 978-82-326-5555-7 (electronic ver). ISSN 2703-8084 (electronic ver.)

“The impact of curing temperatures on Portland composite cements – hydrate assemblage, porosity, and compressive strength” Pamela Zuschlag 2022:374 ISBN 978-82-326-6521-1 (printed ver.) ISBN 978-82-326-6793-2 (electronic ver.) ISSN 2703-8084 (online ver.)

“Behaviour, modelling and simulation of thin steel plates subjected to combined blast and impact loading” Benjamin Stavnar Elveli 2022:392 ISBN 978-82-326-5179-5 (printed ver.) ISBN 978-82-326-5383-6 (electronic ver.) ISSN2703-8084 (electronic ver.)

«Load effects of alkali-silica reaction in reinforced concrete beam bridges - Material testing, Constitutive modelling and Numerical simulation» Simen Sørgaard Kongshaug 2023:20 ISBN 978-82-326-6952-3 (printed ver.) ISBN 978-82-326-5497-0 (electronic ver.) ISSN 2703-8084 (online ver.)

«Field investigations of crosswinds and vehicle-driver response on bridges» Sebastian Reymert 2023:41 ISBN 978-82-326-6227-2 (printed ver.) ISBN 978-82-326-6117-6 (electronic ver.) ISSN 2703-8084 (online ver.)

«Atomistic insight into nanofluid enabled enhanced oil recovery» Yuanhao Chang 2023:72 ISBN 978-82-326-5971-5 (printed ver.) ISBN 978-82-326-6817-5 (electronic ver.) ISSN 2703-8084 (electronic ver.)

ISBN 978-82-326-5886-2 (printed ver.)
ISBN 978-82-326-5314-0 (electronic ver.)
ISSN 1503-8181 (printed ver.)
ISSN 2703-8084 (online ver.)

NTNU
Norwegian University of
Science and Technology